

Diplomarbeit  
zur Erlangung des akademischen Grades Diplom-Ingenieur der Biotechnologie

# On-Chip Monitoring of Fungal Biofilms Using a Lab-on-a-Chip

eingereicht von  
Lukas Richter

durchgeführt in der Abteilung für Nano-Systemtechnologien der  
Austrian Research Centers (ARC)

eingereicht am  
05.06.2008

Betreuer:

Dr. phil. Peter Ertl (ARC)

Privatdozent Dr. nat. techn. Johannes Grillari (Universität für Bodenkultur)

# Acknowledgment / Danksagung

First of all I want to thank my supervisor Peter Ertl at ARC for his faith in my person and efforts. He well supported me in writing this thesis and also gave good advises how to prepare my future scientific carrier. Also thanks to my supervisor Johannes Grillari at the University of Applied Life Science Vienna to take over the universal supervision. Further I want to thank my colleagues, mainly being physicists, at Tech gate in the section Nano-System-Technolgies for helping me, as a student of biotechnologies, to be well integrated into the highly technical scientific area of mirco- and nanotechnologies.

Außerdem möchte ich meiner Verlobten für ihre Unterstützung und Geduld danken, wenn die Arbeit mal wieder meine vollste Aufmerksamkeit forderte. An dieser Stelle möchte ich auch meinen Eltern danken, die mir ein höheres Studium überhaupt ermöglicht haben. Ihre Unterstützung und ihr Vertrauen haben mich Durststrecken während des Studiums stets überstehen lassen.

# Summary

We have developed a microfabricated biochip capable of continuously monitoring cell population dynamics in a non-invasive manner. In the presented work we describe the novel combination of contact-less dielectric microsensors and microfluidics that promote biofilm formation for quantitative cell analysis. The developed cell chip consists of a polymeric fluidic (PDMS) system bonded to a glass wafer containing the electrodes while temperature and flow profile are controlled by external heating and pumping stations. The application of high-density interdigitated electrode structures ( $\mu IDES$ ) as dielectric sensors are ideal for cell analysis due to their flexible geometry and ability to tune electric field distribution. The  $\mu IDES$  are isolated by a 300 nm multi-passivation layer of defined dielectric property and provide stable, robust and non-drifting measurement conditions. The performance of this detector is evaluated using various bacterial and yeast strains. The high sensitivity of the developed dielectric microsensors allows direct identification of microbial strains based on morphological differences and biological composition. The novel biofilm analysis platform is used to continuously monitor the dynamic responses of *C. albicans* and *P. pastoris* biofilms to increased shear stress and antimicrobial agent concentration. While the presence of shear stress triggers significant changes in yeast growth profiles, the addition of  $0.5 \mu g mL^{-1}$  Amphotericin B revealed two distinct dynamic behaviors of the *C. albicans* biofilm. Initially, impedance spectra increased linearly at  $30 \Omega h^{-1}$  for two hours followed by  $10 \Omega h^{-1}$  (at 50 kHz) over 10 hours while cell viability remained above 95% during fungicide administration. These results demonstrate the ability to directly monitor dielectric changes of sub-cellular components within a living cell population.

# Zusammenfassung

Wir haben einen Mikrochip entwickelt, der das dynamische Verhalten von Zellpopulationen kontinuierlich und nicht invasiv verfolgen kann. Im Rahmen dieser Arbeit wird die neuartige Kombination aus isolierten dielektrischen Sensoren und Mikrofluidik, welche das Wachstum von Biofilmen und deren quantitative Analyse ermöglicht, beschrieben. Der entwickelte Mikrochip setzt sich zusammen aus einer polymeren Fluidik (PDMS), welche kovalent mit einem Mikrochip verbunden ist, während Temperatur und mikrofluidischer Fluss von externen Geräten gesteuert werden. Die Anwendung von mikrofabrizierten Interdigital-Kondensatoren ( $\mu IDK$ ) als dielektrische Sensoren hat sich als günstig erwiesen, da diese in ihrer Geometrie sehr flexibel sind und so die Verteilung elektrischer Feldlinien gut kontrollierbar wird. Die ( $\mu IDK$ ) sind durch eine Mehrfachpassivierung isoliert, wodurch stabile und robuste Messbedingungen ohne Drift ermöglicht werden. Die Leistung dieses neuartigen Sensors wird durch seine Anwendung an unterschiedlichen Bakterien- und Hefestämmen beurteilt. Die hohe Sensitivität dieses dielektrischen Sensors ermöglicht die Identifizierung von Mikroorganismen aufgrund ihrer morphologischen Unterschiede und ihrer biologischen Zusammensetzung. Die neue Plattform wird im Rahmen dieser Arbeit zur Charakterisierung des dynamischen Verhaltens von *Candida albicans* und *Pichia pastoris* gebildeten Biofilmen gegenüber erhöhten Scherstress und dem Einfluss von Antibiotika verwendet. Während Scherstress das Wachstumsprofil von Hefen signifikant beeinflusst, zeigen *Candida albicans* Biofilme ein zweistufiges dynamisches Verhalten gegenüber dem Antibiotikum Amphotericin B mit einer Konzentration von  $0.5 \mu g L^{-1}$ . Anfänglich steigen die Impedanzsignale linear um  $30 \Omega h^{-1}$  für zwei Stunden an, gefolgt von einer Steigung

von  $10 \Omega h^{-1}$  für weitere 10 Stunden, während die Viabilität der Zellen von 95% erhalten bleibt. Diese Ergebnisse demonstrieren die Möglichkeit dieses Sensors Veränderungen sub-zellulärer Strukturen in lebenden Zellen über lange Zeit zu beobachten.

# Contents

List of Figures	10
List of Tables	13
<b>1 Introduction</b>	<b>14</b>
1.1 Aims . . . . .	14
1.2 Lab-on-a-chip systems . . . . .	15
1.2.1 Microfluidic biochips . . . . .	17
1.3 Fundamentals of microfluidics . . . . .	19
1.4 Cells on-chip . . . . .	21
1.4.1 Manipulation and treatment of cells in microfluidic biochips . . . . .	22
1.4.2 Cell analysis . . . . .	25
1.5 Microbial biofilm analysis on-chip . . . . .	30
1.5.1 Definition of microbial biofilms . . . . .	30
1.5.2 Medical importance of <i>Candida</i> biofilms . . . . .	31
1.5.3 Mechanisms of biofilm-related resistance to biocides . . . . .	33
1.5.4 State of the art of biofilm analysis . . . . .	33
<b>2 Design of a cell chip</b>	<b>36</b>
2.1 Bio micro-electro-mechanical systems (bio-MEMS) technologies . . . . .	36
2.2 Chip design . . . . .	36
2.2.1 Microfabrication of chips . . . . .	39
2.2.2 Simulation of flow profiles . . . . .	41

## Contents

2.3	Sensor design . . . . .	43
2.3.1	Simulation of electric field distribution . . . . .	45
<b>3</b>	<b>Materials and Methods</b>	<b>47</b>
3.1	Materials . . . . .	47
3.1.1	Solutions and media . . . . .	47
3.1.2	Equipment . . . . .	48
3.1.3	Strains . . . . .	48
3.2	Methods . . . . .	49
3.2.1	Microfabrication of chips . . . . .	49
3.2.2	Formation of the microfluidics and chip assembly . . . . .	51
3.2.3	Bonding by oxygen plasma ashing . . . . .	51
3.2.4	Sensor characterization using LCR Unit . . . . .	52
3.2.5	Atomic force microscope (AFM) imaging . . . . .	54
3.2.6	Surface modification with APTS . . . . .	54
3.2.7	Contact angle measurement . . . . .	55
3.2.8	Cultivation of microorganisms . . . . .	56
3.2.9	Dielectric spectroscopy . . . . .	56
3.2.10	Principle component analysis (PCA) . . . . .	57
3.2.11	Conformal mapping technique . . . . .	57
<b>4</b>	<b>Results</b>	<b>58</b>
4.1	Characterization of the microfluidic biofilm chip . . . . .	58
4.1.1	Physical characterization of dielectric sensor using LCR meter, AFM and CV . . . . .	58
4.1.2	Sensor performance . . . . .	62
4.2	On-chip cultivation of yeasts . . . . .	72
4.2.1	On-chip cultivation . . . . .	78
4.3	On chip monitoring of <i>Candida</i> biofilms . . . . .	86
4.4	Normalization of obtained impedance data . . . . .	91
<b>5</b>	<b>Discussion</b>	<b>94</b>

# List of Figures

1.1	Principles of Lab-on-a-chip systems and Miniaturization . . . . .	16
1.2	Microfluidic devices and their applications. . . . .	18
1.3	Parabolic flow profile in a rectangular channel . . . . .	21
1.4	Manipulation technologies of living cells on microfabricated biochips . .	23
1.5	Theory of cyclic voltammetry . . . . .	27
1.6	Representation of the complex impedance plane . . . . .	28
1.7	Monitoring fermentation broth using contactless ring electrodes . . . .	29
1.8	Biofilm of <i>Candida albicans</i> . . . . .	31
1.9	Biofilm formation . . . . .	32
1.10	Schematic representation of a modified Robinson device (MRD) . . . .	34
2.1	Experimental setup . . . . .	37
2.2	Design of the microfluidic system . . . . .	39
2.3	Principle of positive UV-Lithography and lift-off . . . . .	40
2.4	Pressure and velocity profiles in the proliferation chamber . . . . .	42
2.5	Picture of the proliferation chamber containing contactless electrode structures . . . . .	43
2.6	Simulation of electric field distribution . . . . .	45
3.1	Scheme of the Lithographic process during the fabrication of the cell chip	50
3.2	LCR meter setup . . . . .	53
3.3	Principle of atomic force microscopy (AFM) . . . . .	54
3.4	Scheme of contact angle measurement . . . . .	55

## LIST OF FIGURES

4.1	LCR-Meter setup during $\mu IDES$ capacitance measurements . . . . .	59
4.2	AFM images of passivation layer surfaces . . . . .	60
4.3	Cyclic voltammetry traces using $\mu IDES$ . . . . .	61
4.4	Nyquist plot of air and different solutions . . . . .	62
4.5	Stability measurement using passivated $\mu IDES$ . . . . .	63
4.6	Signal change with change of temperature, salt concentration and pH .	65
4.7	Measuring background effects . . . . .	66
4.8	Sensor response to different microorganisms . . . . .	67
4.9	Pattern recognition plot of dielectric spectra of microbial strains . . . .	69
4.10	Chemical structure of the polyene Amphotericin B . . . . .	70
4.11	Sensor response to morphological changes . . . . .	71
4.12	Corresponding flow rates to turning velocity with a peristaltic pump . .	73
4.13	AgCl precipitation in a complex microfluidic system . . . . .	74
4.14	Particle transportation in a complex microfluidic channel system . . .	75
4.15	Observed damages to epoxy . . . . .	75
4.16	AFM image of an SOG surface after modification of an PDMS channel with APTS . . . . .	77
4.17	AFM image of an APTS layer and its height . . . . .	77
4.18	Contact angle measurements . . . . .	78
4.19	<i>Candida albicans</i> growing on chip not forming a biofilm . . . . .	79
4.20	<i>Candida albicans</i> growing on chip forming a biofilm . . . . .	80
4.21	Time laps microscopy . . . . .	81
4.22	<i>C. albicans</i> microcolonies selected for time laps microscopy at the ab- sence of fluid flow . . . . .	82
4.23	<i>C. albicans</i> microcolonies selected for time laps microscopy at the pres- ence of fluid flow ( $0.12 \mu L/min$ ) . . . . .	83
4.24	Growing profile of <i>P. pastoris</i> at alternating shear stress ( $0.12 \mu L/min$ to $0.5 \mu L/min$ flow rate) monitored with bioimpedance using contactless microelectrodes . . . . .	84

## LIST OF FIGURES

4.25 Growing profile of <i>C. albicans</i> at alternating shear stress (0.12 $\mu\text{L}/\text{min}$ to 0.5 $\mu\text{L}/\text{min}$ flow rate) monitored with bioimpedance using contactless micro electrodes . . . . .	85
4.26 <i>P. pastoris</i> and <i>C. albicans</i> growing on chip . . . . .	86
4.27 Determination of antifungal susceptibility of <i>C. albicans</i> to Amphotericin B . . . . .	88
4.28 <i>Candida</i> growth curves and cell viabilities under standard cultivation conditions in the absence and presence of AmpB . . . . .	90
4.29 <i>C. albicans</i> cell population grown on chip under antibiotic pressure . . . . .	91
4.30 <i>Candida</i> biofilm response to AmpB on chip . . . . .	92
4.31 3D plot of obtained data over a wide range of frequencies . . . . .	93

# List of Tables

1.1	Changes of system parameters by miniaturization . . . . .	15
1.2	on-chip optical detection methods for analysis of microbial cells . . . . .	26
4.1	Average background subtracted impedance values at 50 kHz and tripli- cate measurements . . . . .	66
4.2	Background subtracted impedance signals and corresponding phase an- gle values ( $\theta$ ) at 50 kHz . . . . .	70
4.3	Calculation of flow rates of the peristaltic pump . . . . .	72
4.4	AS of <i>C. albicans</i> to different concentrations of Amphotericin B . . . . .	87

# 1 Introduction

## 1.1 Aims

Many studies have demonstrated that cellular phenotypes are controlled by the complex interaction between genome, proteome and the external environment. Cells regularly change by altering their output of matter and energy which, depending on its genetic make up and environmental context, can lead to either a pathological (disease) or a normal phenotype. It is also important to consider that a living cell is not a single static entity and that every cell has the capacity to change in minutes [1]. In fact, a cell constantly senses its environment and adapts to changes by altering its gene-expression pattern, protein content, membrane constitution, surface receptors and etc. [2]. Investigating these changes is essential because cellular phenotypes are the expression of genotypes and therefore reveal gene function. Although various studies have shown that phenotypes are best studied using single cells analysis [3], the study of multi-cellular systems is of higher medical relevance when analyzing biofilms. As an example, cell-cell communication has a considerable influence on the cellular life cycle where the interplay of cells is known to significantly alter their behavior. For instance, unicellular *Candida* is known to form pseudohyphae (biofilm) and becomes a highly invasive pathogen persistent to many medical treatments like the application of antibiotic agents. The genus *Candida* is distributed worldwide and is recognized as a a major source of hospital-acquired infections causing superficial and deep-seated mycoses. Furthermore, the phenotypic switching from uni-cellular to the filamentous form of *C. albicans* may play a role in its virulence and multi-drug resistance [4]. Since increased resistance of *C. albicans* biofilms has been reported, the application of standard antimicrobial susceptibility assays performed with plactonic cells may be

particularly misleading [5]. Therefore the newly developed biofilm chip is applied to assess the dynamic response of invasive *C. albicans* infections at relevant clinical peak serum concentrations of Amphotericin B.

Consequently the aim of this work is to develop a fungal biofilm analysis platform using microchip technology. The newly developed microfluidic biochip is applied to yeast cells under different culture conditions, as antibiotic pressure or shear stress. *Candida albicans* is used as a model organism because of the particular interest of this genus in health care. The ability to continuously monitor fungal biofilms using contactless dielectric microsensors promises to present new and innovative applications in medicine.

## 1.2 Lab-on-a-chip systems

The term "*Lab-on-a-chip*" (LOC) also called micro total analysis system ( $\mu T A S$ ) is widely used for devices that allow to miniaturize chemical or biological processes or the integration of sample preparation and analysis. Overall, LOC includes microfluidic chips as well as non-fluidic miniaturized systems such as sensors and arrays which are also called biochips [6].

Since the introduction of  $\mu T A S$  a decade ago the miniaturization of reaction systems offered a variety of new opportunities to research shown in the scheme of Figure 1.1 and Table 1.1. For instance by scaling down a reaction system not only the dimension

Parameter	Macroscopic	factor change	Microscopic
length of edge	1 mm	$d$	1 $\mu m$
surface	1 mm <sup>2</sup>	$d^2$	1 $\mu m^2$
volume	1 $\mu L$	$d^3$	1 fL
number of molecules	10 <sup>9</sup>	$d^3$	1
diffusion time over d	15 min	$d^2$	1 ms

Table 1.1: Changes of system parameters by miniaturization

of the system itself but also the reaction parameters are significantly altered [7]. In a down scaled system transport times of mass and heat are shortened [8] resulting in

## 1 Introduction

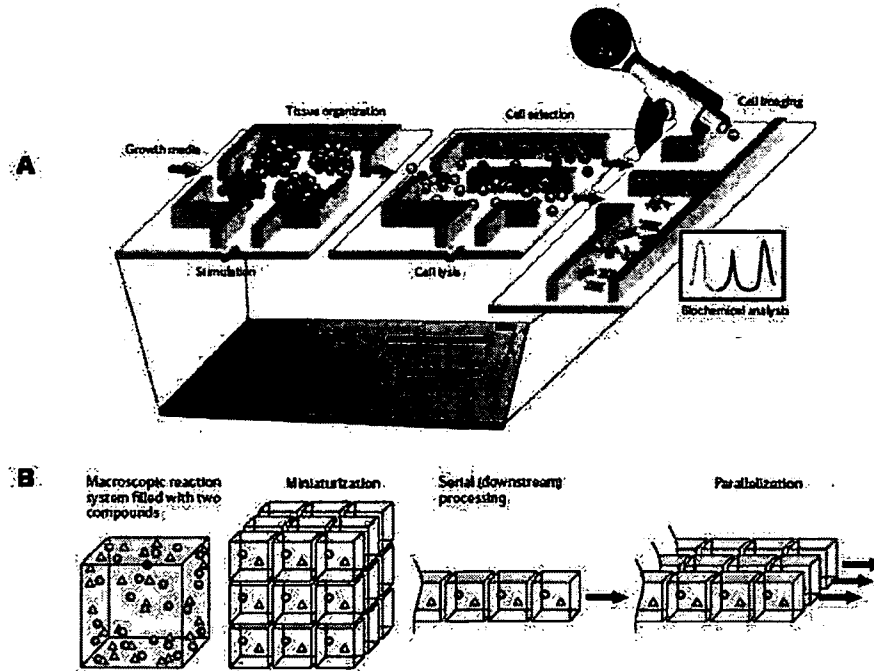


Figure 1.1: *Principles of Lab-on-a-chip systems and Miniaturization* [6]. A schematic application of a Lab-on-a-chip is shown, where the cultivation, separation, lysis and microscopical analysis are introduced into one single chip.

better control over these parameters due to the high surface to volume ratios found in such designs. Important reaction parameters of chemical processes, such as compound concentration and temperature, can be precisely regulated while analytical compounds pass the reaction area in a serial matter, what further results in a higher sensor performance and sensitivity. Because space for the devices becomes very small, massive parallelization is also possible [9]. Furthermore, microfluidic networks can supply integrated biosensors with small volumes in a continuous and serial matter. In addition adequate channel design allows for the handling of fluid volumes far smaller than a microliter resulting in better control of biological molecules and cells [10].

The term "*Microfluidic biochips*" in general describes a multifunctional platform containing a network of microchannels with widths in the micrometer range connected to small volume tubing systems which are in turn linked to external reservoirs [6]. Microchip technologies were already used to solve chemical or biological problems some decades ago. The following paragraph presents some selected historical aspects of  $\mu$ TAS including the first miniaturized devices and further their application in bio-

chemistry and biology.

The first analytical miniaturized device, developed in 1975, was a gas chromatographic analyzer, that was able to separate a simple mixture of compounds within a few seconds. The device included an injection valve and a separation column located on a single silicon wafer [11]. About fifteen years later, in 1990, the concept of  $\mu TAS$  was proposed by Manz et al. [7]. Though the main intention of miniaturization was to enhance the analytical performance of the device the reduction of size enabled smaller consumption of expensive carrier, reagent and mobile phase [8]. In the following years aspects of fluid transportation in the micro- and nanoliter range were intensively studied, where special attention was directed to electroosmotic flow (EOF) [7], pressure driven flow [12, 13] and also sample injection [14, 15]. As an example electrophoresis in planar chips was successfully integrated [16, 17], where injection, separation and detection within the same device was successfully demonstrated [8]. In addition to the pure chemical applications the handling of biomolecules and cells in microfabricated chambers started to emerge. DNA amplification by means of polymerase chain reaction (PCR) [18], the measurement of cellular metabolism [19] and flow cytometry [20] on-chip was performed. In 1994 the separation of oligonucleotides [21], DNA [22], amino acids [23] and cell manipulation by electric fields [24] were introduced.

Today, LOC technologies are envisioned to have an enormous potential to also improve health in developing countries [25]. Developing as well as developed countries have an urgent need of new technologies for health diagnostics in order to accelerated and cheapen diagnostic measurements. Therefore LOC systems can automate complex diagnostic procedures in a microfluidic chip that are normally performed in centralized laboratories. This capacity of new diagnostic instruments enables health-care workers and patients to get important health-related information in even the most secluded regions of a country [25] and an adequate time range.

### 1.2.1 Microfluidic biochips

"Microfluidics" is the science and technology of systems that transport volumes of fluids that vary from microliters to femtoliters using channels with dimensions of tens to hundreds of micrometers embossed in the surface of polymers or glass. The origins of

## 1 Introduction

microfluidics can be found in microanalytical methods such as high-pressure liquid chromatography (HPLC), gas-phase chromatography (GPC) and capillary electrophoresis. Due to the success of these technologies more compact and versatile formats were developed to enlarge the application sector [26]. Low requirement of sample volumes and reagents, low production of waste, short analysis times, cheap technology and reduced dimensions compared to commercial analysis systems [16] have attracted scientists in the fields of biology, chemistry, engineering and medicine. These characteristics make microfluidics and microchip technology particularly useful for studying biomedicine and biology [27]. Figure 1.2 shows some examples of microfluidic designs and features. Although today many analytical methods for detecting DNA, pathogens, proteins and

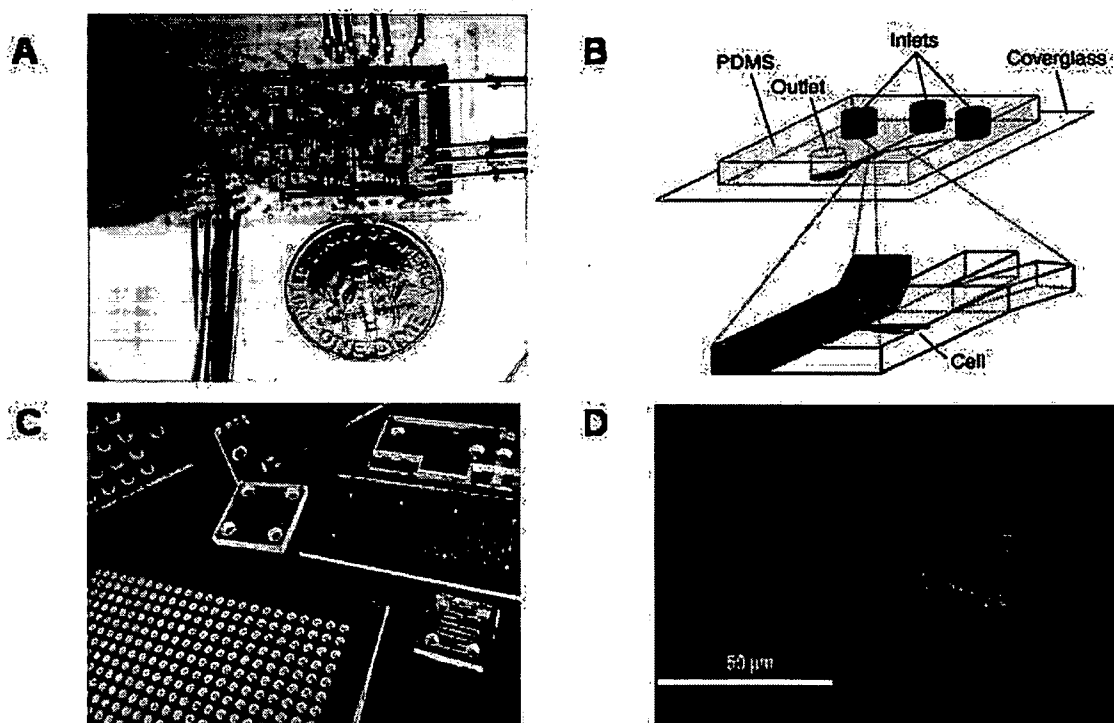


Figure 1.2: *Microfluidic devices and their applications.* A) is a microfluidic chemostat with an intricate plumbing system used for studying bacteria [27]. In B) a scheme of a microfluidic biochip for mammalian cell lines is figured. Due to the adjacent laminar streams the cell can be addressed with different fluorescent dyes at the same time and on different regions (D) [27]. C) shows some microfluidic devices made out of glass.

## 1 Introduction

small organic molecules are conventionally available, miniaturization and integration into single microfabricated devices, i.e.  $\mu TAS$ , provides higher detection sensitivity and signal-to-noise ratios, shorter reaction times and spare of space and sample volume. The resulting devices find essential application in the field of clinical diagnostics, where the loss-free sample preparation and the proper analysis are still fundamental challenges. The broad range of applications of miniaturized analytical methods are thoroughly reviewed in the papers of Manz *et al.* [8,28–30].

For instance microfabricated and microfluidic devices have been developed to detect pathogens by reverse transcription-PCR (RT-PCR), electrophoresis, ELISA or toxins by electrophoresis based immunoassays, electrokinetically controlled immunoassays and surface plasmon resonance, just to mention some applications. In addition DNA analysis assays have been developed to determine restriction sites with high accuracy in nano-channels, the number of bounding proteins onto DNA by optical methods, to perform hybridization experiments on small devices, to detect single base pair mismatch, to perform DNA sequencing, high resolution separation and many more. Furthermore, protein separation techniques on-chip like electric field gradient focusing and chromatography have resulted in higher performances in separation. Fully automated on-chip mixing operations to generate thousands complex mixtures in a single day have been performed. Also miniaturized protein digestion or crystallization experiments have shown a 100-fold decrease of analysis time. Microfluidic devices have been developed to be coupled to MALDI-TOF and ESI-MS to perform sample preparation and analysis of proteins in one step.

All these techniques make use of the new phenomena of miniaturized systems and bring new opportunities to the sciences of genomics, proteomics and metabolomics.

### 1.3 Fundamentals of microfluidics

A special feature of microfluidic systems is the establishment of laminar flows. The "kind" of flow is in general characterized by calculating the dimensionless *Reynold number*,  $Re$ . The Reynold number gives information about the relationship between magnitudes of the inertial and viscous forces of a fluid in a particular channel, as shown

## 1 Introduction

in the following equation (1.1):

$$Re = \frac{\rho d \nu}{\eta} \quad (1.1)$$

In the above equation  $d$  is the diameter of the channel,  $\rho$  the density,  $\eta$  the viscosity of the fluid and  $\nu$  the average velocity. Reynold numbers over 2300 describe *turbulent flow*, what means that inertial forces are dominant, whereas numbers below 2300 describe *laminar flow*, where viscous forces dominate. With average dimensions of microfluidic systems in the range of 100 micrometers Reynold numbers are calculated to around 1 and therefore describe laminar flows. In other words only diffusive mixing occurs in microfluidic devices as shown in Figure 1.2 b and d. Consequently, this effect allows for controllable mixing and results in exact adjustment of compound concentrations. This phenomenon has been used to generate linear concentration gradients and barrier free supplement of reagents.

In many cases and also in this work the channels do not feature cylindric geometries required to calculate Re numbers. Consequently the concept of the hydraulic diameter  $D$  was introduced to calculate Reynold numbers in channels of differing geometries:

$$D = \frac{4A}{P_{wet}} \quad (1.2)$$

$A$  is the cross sectional area, while  $P_{wet}$  is the perimeter, which is in contact with the liquid. Corresponding to a channel of rectangular geometry  $P_{wet}$  is twice the width plus twice the height.

In order to describe dynamics of liquids in more detail, Navier-Stokes equation (equation 1.3) is used for flow profile simulations [31].

$$\rho \frac{Dv_i}{Dt} = \rho g_i - \frac{\partial P}{\partial i} + \frac{\partial}{\partial i} \left( \frac{2}{3} \eta \nabla v \right) + \nabla \left( \eta \frac{\partial v}{\partial i} \right) + \nabla (\eta \nabla v_i), i = x, y, z \quad (1.3)$$

The Navier-Stoke formalism is built on the fundamental laws of conservation (energy, momentum, mass), combining them with constitutive equations for fluids (thermal conductivity and governing viscosity) and describes interaction in a fluid as a many-body problem. However only with assumptions and simplifications a fluid system is mathematically solvable. Assumptions for the microfluidic system used in the presented work are neglect of gravitation and using incompressible fluids. According to these assumptions the Navier-Stokes equation is reduced to:

$$\rho \frac{Dv}{Dt} = \eta \nabla^2 v - \nabla P \quad (1.4)$$

## 1 Introduction

Additionally the *Hagen-Poiseuille equation*(equation 1.5) has been used to describe flows in capillaries driven by pressure gradients. The volume flow,  $Q$ , for a rectangular channel is described in the below equation:

$$Q = \frac{\Delta V}{t} = \frac{\Delta P}{R} = \frac{wh^3}{12\eta L} \Delta P \quad (1.5)$$

where  $w$  is the width,  $h$  the height and  $L$  the length of the channel.  $\Delta P$  is the pressure drop along this length. The term  $\frac{wh^3}{12\eta L}$  is the inverted fluidic resistance,  $\frac{1}{R}$ , specially described for channels with rectangular geometry [31]. The high flow resistance at the channel walls leads to a parabolic flow profile where the velocity drops to zero along the walls (Figure 1.3). Consequently, the position of a particle rectangular to flow direction in a microchannel is dependend of its mass. In other words, particles of high mass are concentrated in the center of a fluid flow in a micro channel.

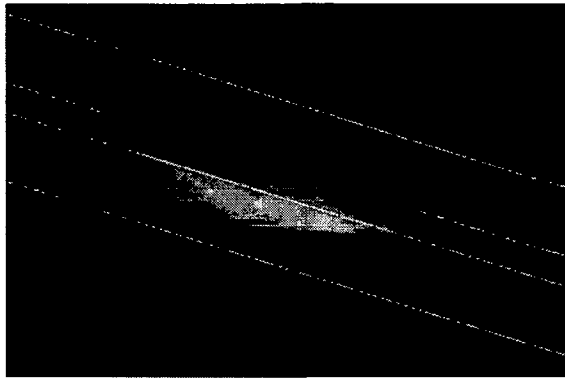


Figure 1.3: *Parabolic flow profile in a rectangular channel.* Fluid velocities increase from blue to red within the colour code. [32]

### 1.4 Cells on-chip

A more recent development of microfluidic biochip is their application to cell analysis. Microfabricated systems can present opportunities to control the external cues and the environment (thus tissue engineering) of cell populations to reproducibly analyze their behavior [33]. Many assays, like optical or electrochemical methods, and standard operations, like PCR, lysing of cells and DNA hybridizations performed in macroscopic dimensions have already been miniaturized, especially to serve the science of systems

biology. Overall, cell analysis composes and involves the analysis of single cells and their manipulation in microfluidic biochips.

### 1.4.1 Manipulation and treatment of cells in microfluidic biochips

Manipulation and treatment of cells in microfluidic devices has been an intensively examined topic of the past few years with an enormous output. In this chapter some examples and general methods of manipulating and treating cells in microfluidic devices are presented.

#### Manipulation

Manipulation of cells can be broadly categorized by the kind of applied forces, i.e. magnetic, optical, mechanical, electrical and others.

*Magnetic manipulation.* Here magnetic nanoparticles with sizes ranging from 10 to 100 nm in diameter are selectively attached to cells manipulated through external magnetic fields. Figure 1.4 a) shows an example, where cells are "navigated" by a magnetic field. Cells are forced to move along the magnetic wires, because a high magnetic field gradient at the edge of each wire imposes a force on the magnetic beads at an specific angle to the hydrodynamic flow [34].

*Optical manipulation.* Optical manipulation technologies are a means of non-contact and contamination-less manipulation. In most cases optical tweezers are used that direct biological molecules to dielectric spheres and then capture the spheres at the focal point of an electric field gradient as seen in Figure 1.4b [35].

*Mechanical manipulation.* The main application of mechanical manipulation methodologies on microfluidic chips is the separation of target cells for culture or analysis. Many structures have been developed including micro filters (see Figure 1.4 c)) [36], microwells, microgrippers, dam structures and also reactive coatings [10].

*Electrical manipulation.* Dielectrophoresis (DEP) as the electronic analogue to optical tweezers is defined as the lateral motion imparted on uncharged particles as a result of polarization induced by non-uniform electric fields. This principle is widely used to

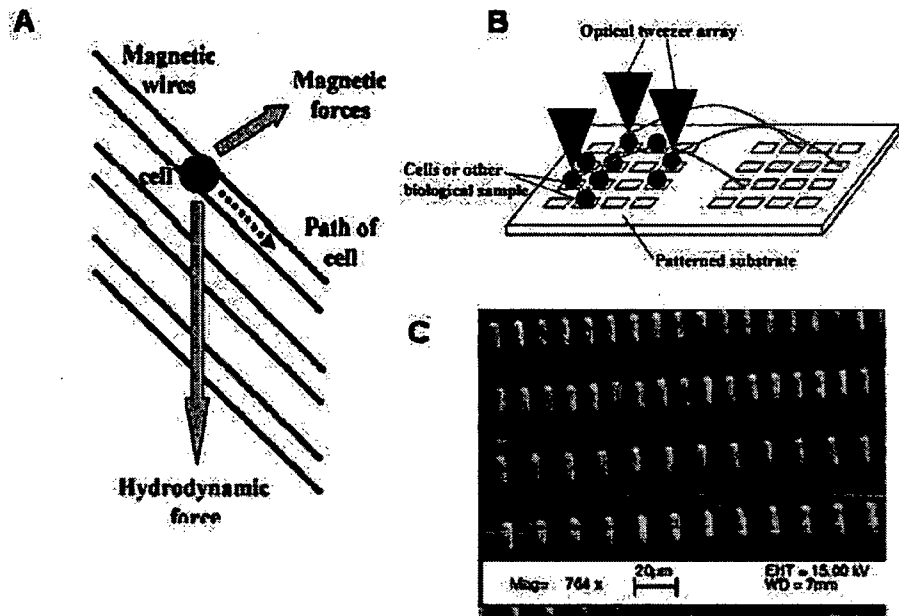


Figure 1.4: *Manipulation technologies of living cells on microfabricated biochips.* The scheme in A) Schematic representation of biological cells, labeled with magnetic nanoparticles for indirectly navigate them in microfluidic channel networks [34]. B) Vertical cavity surface emitting lasers (VCSEL) system used for optical manipulation of living cells [35]. In C) Microfabricated filter system for specific collection of various cell types can be seen [36].

transport cells or particles to specific locations, e.g. in a microcytometer [10]. There are two categories of DEP, free floating electrodes (DEP) and insulated electrodes or electrodeless DEP (EDEP), where electrical fields are squeezed into a conducting liquid. EDEP provides various advantages over DEP, since very high electric fields can be applied without gas evolution or electrode fouling [37].

### Treatment

The treatment of cells on-chip are in general miniaturized protocols of standard operations, like cell cultivation, cell lysis, electroporation, optoporation and fusion of cells, which were adapted to microfluidics technology.

*Cell culture.* Cells cultured in microfluidic devices provides various advantages over standard culture technologies. In microfluidic devices the cellular microenvironment and the media composition can be controlled more precisely while using relatively small numbers of cells. Small cell populations can better maintain their micro environment than in macroscale flask cultures. In addition cells grow significantly slower in microdevices [38] indicating a different cell behaviour than in large scale culture systems. Furthermore a variety of substrates such as PDMS and also other polymers has been used for cell culture in microfabricated devices. In recent years 3D-scaffolds have been introduced as new opportunities for tissue engineering [39–41].

*Electroporation and electrofusion.* Electroporation is a technique which provides the possibility to deliver DNA molecules into cells, which is relevant for various cell-based assays. Due to the new features in microfluidic systems it is possible to increase the efficiency of such experiments. Electrofusion provides cell fusion by applying electrical impulses. These electrical pulses provide a short destabilization of cellular membranes. After application of the pulses membranes randomly fuse together. This technique is essential for hybridoma technology, where monoclonal antibodies are produced. Both techniques, electroporation and electrofusion have been adopted to microfabricated devices, with the result that lower voltages are required due to the rapid heat dissipation in microfluidic environments (large surface to volume ratio). Additionally, the lower applied potentials significantly reduce the risks associated with high voltage [10]. Additionally the number of target cells can be reduced using flow-type electroporation or

electrofusion microfluidic chips exploiting their highly controllable environment.

*Chemical and mechanical cell lysis.* The ability to integrate cell lysis techniques on-chip has shown to increase the application of microfluidic devices systems biology, because sample loss due to handling can be avoided. Mechanical-based lysis makes use of nanostructured filter-like contractions in microfluidic channels in the present of a pressure-driven cell flow [42]. Chemical lysis uses denaturing detergents delivered to target cells. However, it is still a complicate process to effectively deliver reagents for chemical lysis or the integration of mechanical techniques on-chip [10].

### 1.4.2 Cell analysis

Overall, nearly all detection methods have been applied to chip based systems, including optical and electrochemical detection methods. Optical methods are commonly used, because they are well accessible and because of the commercially available microfluidic-detector interfaces. Additionally they are highly compatible with microfluidics. Electrochemical methods, such as amperometry, potentiometry and conductometry have been integrated into microfluidic systems, because of their good detection limits for various analytes and their cheap fabrication [43].

#### Optical methods

Fluorescence detection is the most frequently optical detection method used due to its high sensitivity and broad application in cell biology. This optical principle has been exploited for on-chip measurments of ionophore-mediated intracellular  $Ca^{2+}$  flux, cell viability, cell lysis, intracellular enzyme reactions, while also continuous monitoring of gene expression was performed to picture dynamic cellular responses to external stimuli, just to mention some applications. Other optical methods, like universal absorbance detection, have to struggle with poor detection limits due to small amount of sample in microfluidic channels at a particular point in time and short optical path length [43]. However the length of the optical pathway through microfluidic channels can be enlarged by using small integrated mirrows to reflect the incident light within the channel, without changing its geometry [44].

As mentioned above, fluorescence techniques are widely employed in microfabricated

## 1 Introduction

devices. In brief fluorescence is a relaxation process where an excited electron returns to its ground state. During this process the electron emits light, called fluorescence.

Chemi-, bioluminescence and scanning thermal lens microscope imaging have been performed on microfluidic chips. Chemiluminescence is the generation of light due to the release of energy during a chemical reaction [45], where the emission intensity is a function of the compound concentration. When this energy is released in biological samples it is called bioluminescence [46]. Also thermal lens microscopy (TLM) is used

Table 1.2: on-chip optical detection methods for analysis of cells.

Application	Method	Reference
Monitoring intracellular fluorescein diacetat metabolism and calcium mobilization in yeast	Fluorescence	[47]
Separating and detecting $\beta$ -galactosidase in <i>E. coli</i>	Fluorescence	[48]
Real-time monitoring of glucose and ethanol release and production in yeast	Chemiluminescence	[45]
Sensing mutagenicity using <i>E. coli</i>	Bioluminescence	[46]
Monitoring cytochrome <i>c</i> distribution in a neuroblastoma-glioma hybrid cell	TLM	[49]

for label-free measurements of low concentration compounds in microfluidic channels with an extremely high sensitivity. The TLM technique employs a light beam to excite the sample in order to measure the refractive index change, induced by the temperature rise and the resulting production of a lens-like optical element at the sample. With this technique e.g. the amount of cytochrome *c*, produced by neuroblastoma glioma hybrid cells in a microfluidic system, was estimated to be as low as  $10^{-20}$  mol [49]. Some chosen applications of optical measurements in microfluidic systems are presented in Table 1.2.

### Electrochemical methods

Electrochemical detection techniques like amperometry, potentiometry and conductometry have been employed in microfluidic devices to measure metabolic activity at

the extracellular and the single-cell level by detecting the electrical properties of analyte species undergoing redox reactions. Because of the relevance to this work further details of cyclic voltammetry and bioimpedance are presented in the sections below.

### Cyclic voltammetry

Cyclic voltammetry (CV) is the measurement of current over applied potentials and is the most widely used technique for acquiring qualitative information about electrochemical reactions, especially for redox processes, heterogeneous electron-transfer reactions and adsorption processes [50]. CV has been applied in this work to characterize the electrochemical behavior of interdigitated electrode structures in the absence and presence of various passivations.

The cyclic voltammogram presents a current response as a function of the applied potential. A redox couple in which both species exchange electrons with the working

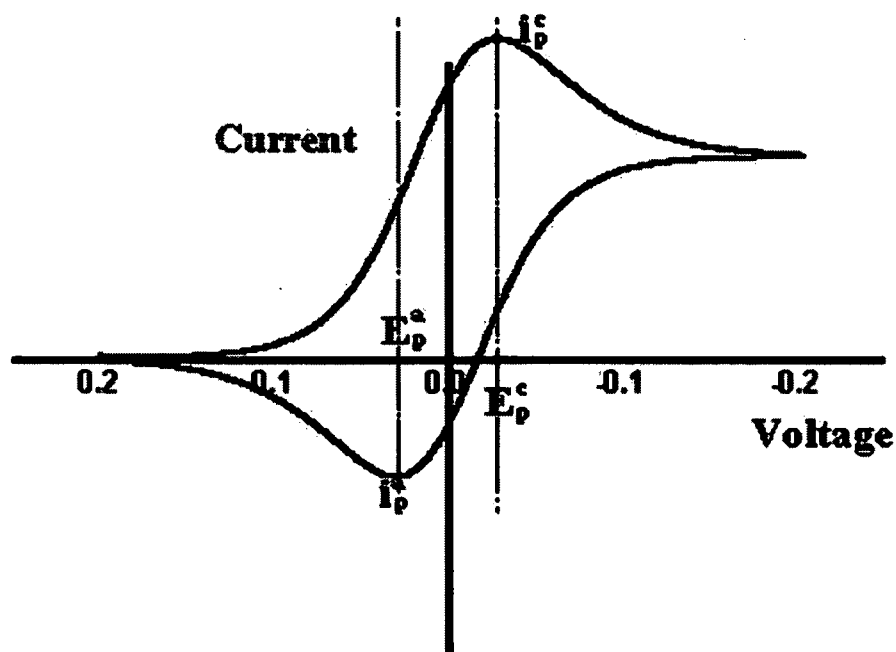


Figure 1.5: *Theory of cyclic voltammetry.* The graph shows a cyclic voltammogram of a perfectly reversible one electron redox system.

electrode is termed an electrochemically reversible redox couple. A redox active compound can be identified through characteristic peak potentials. The difference between two peak potentials of a perfectly reversible redox system is described by the following

equation:

$$\Delta E_p = E_p^a - E_p^c \approx \frac{0.058}{n} \quad (1.6)$$

where  $n$  is the number of transferred electrons and  $E_p^a$ ,  $E_p^c$  are the anodic and the cathodic peak potentials in volts [51].

### Bioimpedance spectroscopy

Impedance sensors measure the impedance of an interface in alternating current (AC) steady state by imposing a small sinusoidal voltage over a particular frequency range and measuring the resulting current. So is electrical impedance defined as the ratio of an incremental change in voltage to the resulting change in current.

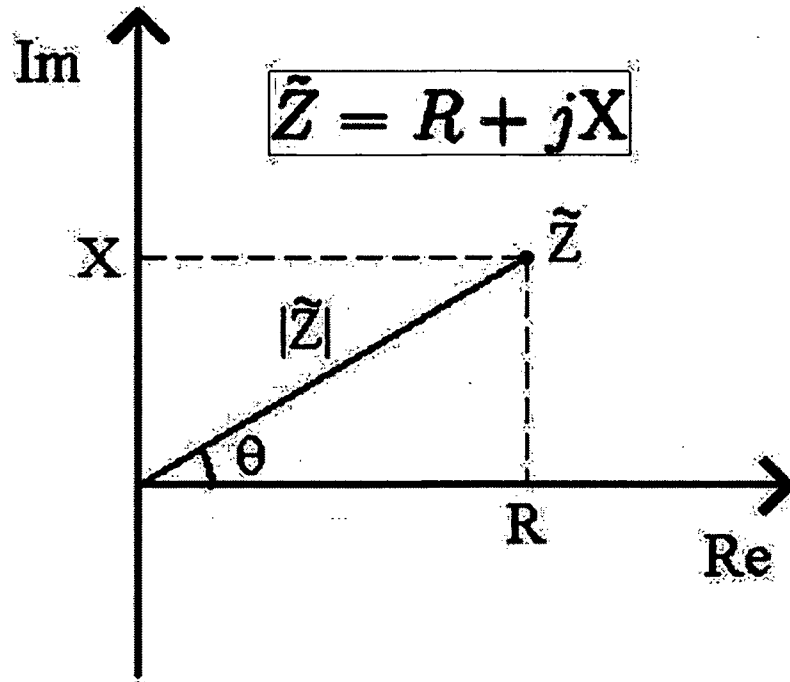


Figure 1.6: Representation of the complex impedance plane. Inset shows the complex impedance equation.  $Re$ ...real part;  $Im$ ...imaginary part;  $R$ ,  $X$ ...resistance;  $\theta$ ...phase difference between voltage and current;  $Z$ ...impedance.

$$Z(\omega) = \frac{V_m}{I_m} e^{(-\theta_m)i} = \frac{V_m}{I_m} (\cos(\theta_m) - i \sin(\theta_m)) = Z_{real} - i Z_{im} \quad (1.7)$$

Either an AC test voltage or AC test current is imposed while the other variable is measured. When impedance measurements are applied to biological systems it is called

## 1 Introduction

bioimpedance. Figure 1.6 shows a graphical representation of the complex impedance plane. The inset represents the complex impedance equation. In this work we measure the dielectric behavior of biological systems and therefore apply dielectric spectroscopy. Dielectric spectroscopy, sometimes called impedance spectroscopy, is a non-invasive and therefore a suitable technique for the characterization of living cells [52], where the impedance electrodes are isolated from the system to be analyzed. In general it measures the dielectric properties or the permittivity of a medium as a function of frequency. Permittivity describes how an electric field is affected by a dielectric medium (living cell). Dielectric spectroscopy was already applied in fermentation in

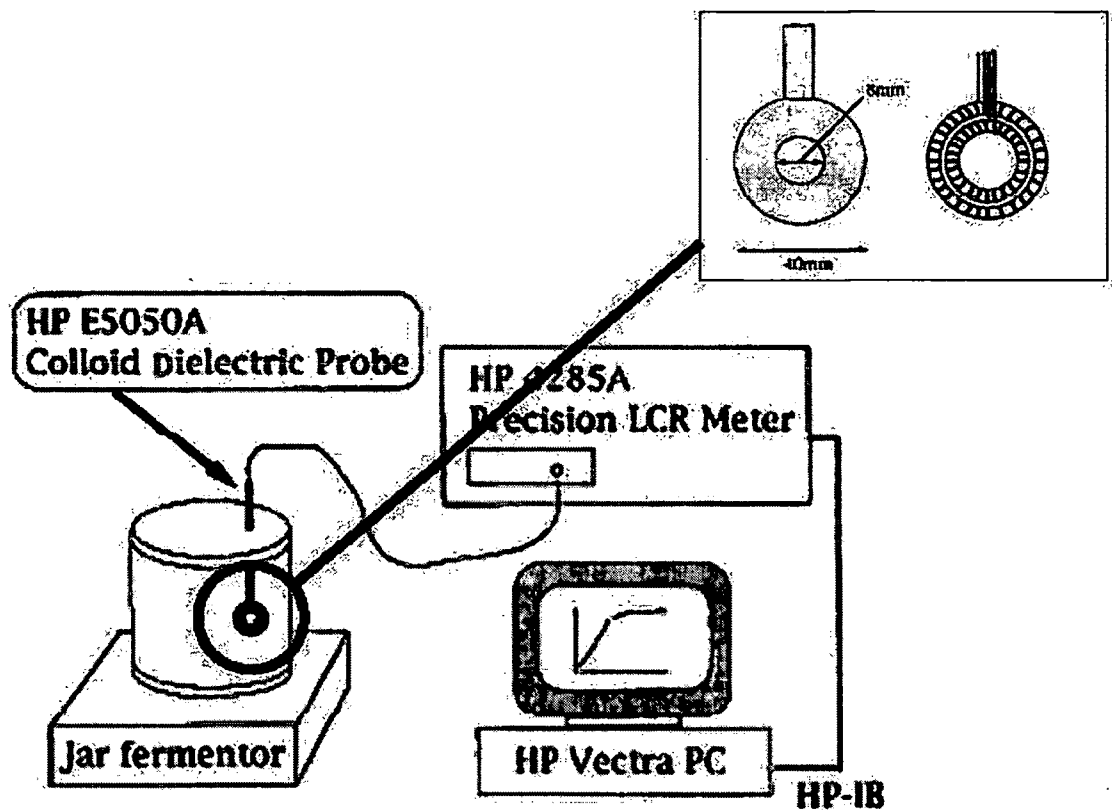


Figure 1.7: Schematic representation of a system monitoring fermentation broth using contactless ring electrodes.

order to measure biomass. This method performed good relationship between biomass and permittivity but did not come over signal falsifying problems including electrode polarization, bubble formation and significant background effects due to the growing media. Asami *et al.* presented a contactless method (see Figure 1.7) to measure

microbial biomass in fermentation broths using contactless ring electrodes [53].

It was then our intention to adopt the above presented principle for cell suspensions to microchip technology using sensors built out of  $\mu IDES$  in order to monitor the dielectric behavior of microbial biofilms on surfaces.

## 1.5 Microbial biofilm analysis on-chip

### 1.5.1 Definition of microbial biofilms

The first definition of biofilms was introduced in 1978 stating that the majority of bacteria grow in matrix-enclosed biofilms adherent to surfaces in all nutrient-sufficient aquatic ecosystems. In addition sessile bacterial cells differ profoundly from their planktonic (floating) counterparts [54]. However in addition to observable morphological differences of irreversibly adhered cells embedded in extracellular polymeric substances also physiological and genetical differences need to be considered [55]. Consequently recent definitions of biofilms also include the expression of certain genes that are inactive in planktonic cells [55, 56]. It has further been demonstrated that biofilms formed by the same species differ from each other because of surface-induced gene expression [57]. Microbial biofilms are preferentially established in high shear environments and once they are formed they behave like rubber materials [58] and persist despite strong mechanical influences [55]. It is also observed that cells within a biofilm are more resistant to medical treatment than cells growing in suspensions [59–61]. Cells in microbial biofilms are up to 10-1000 times more resistant to antibiotic therapy than their planktonic counterparts. In recent years high resolution methods like scanning electron microscopy (SEM) or confocal laser scanning microscopy (CLMS) brought interesting insights into the three dimensional (3D) ultrastructure of microbial biofilms as shown in Figure 1.8.

Overall biofilm formation proceeds in four stages during its development. Figure 1.9 [57] shows a schematic representation of these four stages of biofilm establishment using *Candida albicans* as a model. As mentioned previously the ultrastructure of biofilms is highly dependent on types of surface, where fungal biofilms predominantly form on plastic substrates as PVC. Initially host proteins are adsorbed to the surface of PVC catheter. Next cells adhere individually to the surface forming micro colonies.

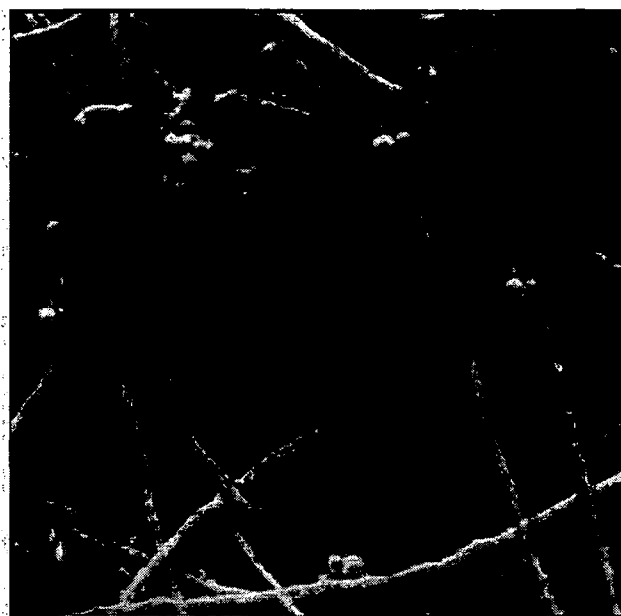


Figure 1.8: *SEM picture of a biofilm formed by Candida albicans on a PVC catheter disc. Growing surface is not seen. Reprinted from reference [57].*

In the next stage some cells start to switch into the hyphal phenotype and secrete the components of the biofilm matrix.

### 1.5.2 Medical importance of *Candida* biofilms

Although bacterial biofilms have been studied extensively, little is known about fungal biofilms and their role in disease. A rather small number of *Candida* species are pathogenic for humans but the species of most interest to medicine is *Candida albicans*. In general yeasts of the genus *Candida* are opportunistic pathogens and attack immunocompromised hosts, whereas *Candida albicans* are the most important *Candida* species involved in hospital-acquired infection. *Candida* are known to form biofilms on medical devices, such as implants, intravascular or urinary catheters and endotracheal tubes [62–64]. *Candida* spp. also colonize the gastrointestinal tract and are able to penetrate the intestinal mucosa and invade the bloodstream. In particular cancer patients, who receive chemotherapeutic regimes, often have serious damages on the intestinal mucosa and are more susceptible to *Candida* infections. Additionally non-device-related infections and biofilm formation can occur e.g. on damaged endothelium of native

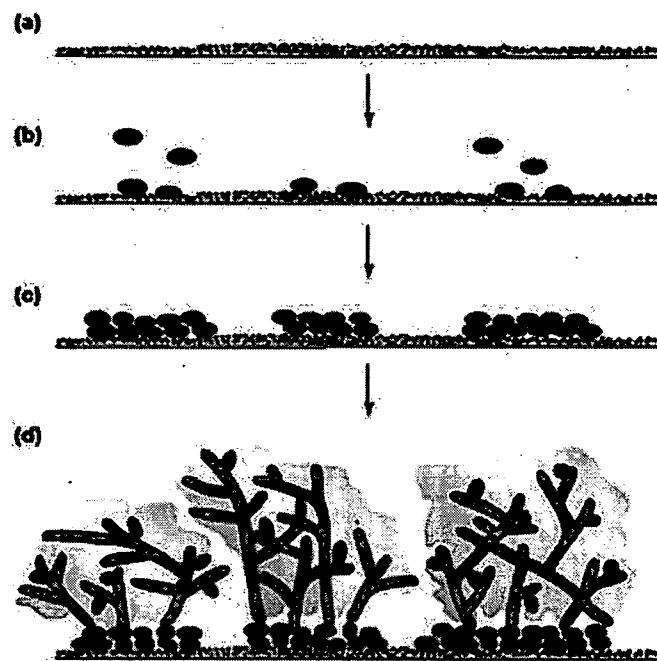


Figure 1.9: *Biofilm formation by Candida albicans on a PVC surface.* A) First host proteins adsorb to a surface. B) Adherence of individual cells. C) Formation of microcolonies. D) Cells switch into hyphal phenotype.

heart valves, where the establishment of a thrombus support biofilm formation of *Candida* [55]. *Candida* spp. are also involved in vaginitis, where mixed biofilms consisting of fungal and bacterial species of the vaginal flora are formed. These biofilms have shown a persistent recalcitrance against antifungal therapies and therefore remain in the vaginal lumen to continuous infections.

*Candida* species are ranked as the fourth most common cause of bloodstream infections, behind coagulase-negative staphylococci, *Staphylococcus aureus* and enterococci [57]. In 2004, 115 *C. albicans* strains from different sources (the oral cavity, the vagina, the environment) were examined in order to determine heterogeneity between biofilm formation. The outcome of the study showed significant differences in biofilm formation within clones and clones lineages but not between the three sources.

### 1.5.3 Mechanisms of biofilm-related resistance to biocides

Due to the complex structure of microbial biofilms various antibiotic resistance mechanisms have been proposed. For instance, biocides adsorb to matrix components, which by themselves also form penetration barriers [65]. Additionally, growth rate reduction can lead to persistence, because direct correlations have been observed between slow growth rates and resistance to antimicrobial agents [66, 67]. In general biofilms are highly heterogeneous systems. Individual cells differ in protein synthesis profiles and respiratory activities, because of the high heterogeneity of micro environments within a biofilm [68]. Consequently, the resistance to antimicrobial agents is different within one and the same biofilm, as it was observed for *Candida albicans* [69].

As a result determination of antimicrobial resistance has remained challenge. Studying biofilms under controlled environmental conditions may provide new opportunities in understanding resistance mechanisms.

### 1.5.4 State of the art of biofilm analysis

Although various procedures and techniques measuring biofilm formation under static conditions have been reported, so far the perfused biofilm fermenter has remained one of the few systems that allows accurate control over biofilm growth rates [70]. The tech-

## 1 Introduction

nology was initially developed to demonstrate that growth rates of adherent bacterial biomass is proportional to applied medium flow rates and limiting nutrient concentrations [71]. Here, cells are grown in a fermenter, collected by pressure filtration onto a cellulose acetate membrane and, following inversion into a modified base, membrane and microorganisms are perfused with fresh medium. Another system widely used to study biofilm growth under continuous flow is the modified Robinson Device (MRD), a laminar flow colonization chamber, which is comprised of a multiport sample catheter connected via tubing to a peristaltic pump, reservoirs and wastes. A schematic diagram of the experimental setup with a MRD is shown in Figure 1.10. Initially a cell

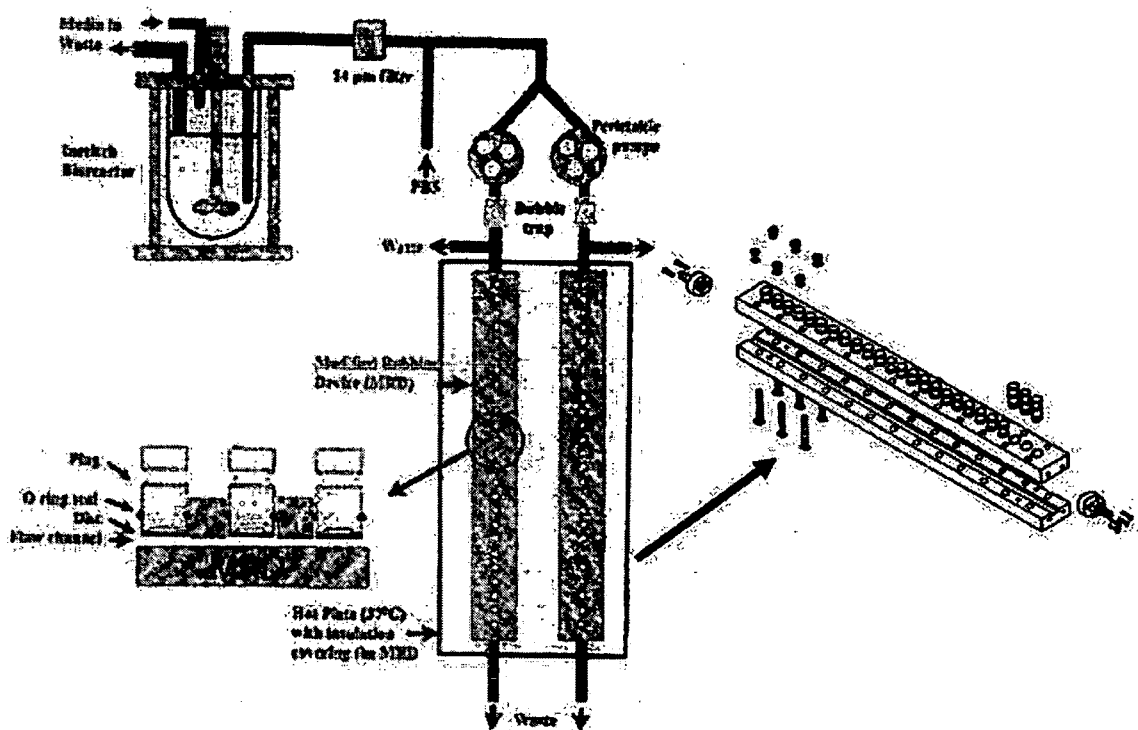


Figure 1.10: *Schematic representation of a modified Robinson device (MRD)*. The MRD comprises of 25 sampling catheters connected via tubing to peristaltic pump, reservoirs and waste. A cell suspension is pumped out of a fermentation process into the device to allow cell attachment on each sampling port.

suspension is pumped through the catheter to allow cell attachment on each of the 25 sampling ports. Fresh medium is subsequently pumped to control biofilm growth

## *1 Introduction*

rates [72]. The establishment of biofilms is optically monitored.

However, both existing biofilm analysis methods cannot monitor biofilm behaviour in real time, lacking the ability to study dynamic responses to external cues. Consequently, it is important to establish a continuous real-time phenotypic analysis platform to monitor morphological and phenotypic heterogeneous biological systems such as fungal biofilms. To gain a deeper biological understanding of cellular dynamic behaviour, such as found in biofilms, it is necessary to first make progress in experimental devices, software, and analytical methods.

## 2 Design of a cell chip

### 2.1 Bio micro-electro-mechanical systems (bio-MEMS) technologies

The term "*bio-MEMS*" includes the fabrication and the integration of mechanical units, sensors, actuators and electronics on microchips for biological and biomedical purposes. This technology initially developed for the electronic sector has revolutionized the LOC systems, where it is often combined with microfluidic technology.

### 2.2 Chip design

We have developed a microfluidic biochip that is capable of continuous monitoring cells in a non-invasive manner. Figure 2.2 shows the basic design of the microchip comprising of a glass bottom and the polymer polydimethoxsilan (PDMS) cover housing the various sensors and microfluidics, respectively. Corresponding inputs (1-3) are connected via tubing to liquid reservoirs and pumps, as well as proliferation chambers, detection channels and wastes. The LOC is designed to continuously assess cell viability, reproduction and metabolic activity over long periods of time. The fluidic and heating systems allow controlled manipulation of living cells adherent to modified, respectively activated chip surfaces that are comparable to biological niches. Furthermore, the chip contains an integrated reference arm providing a low-noise detection environment by eliminating background signals and interferences. The experimental setup consists of seven parts (see Figure 2.1 a), the chip, a fixture for the chip, a water pump, a syringe pump, a potentiostat and a microscope both connected to a PC. Figure 2.1 B) shows the chip assembly. The gray colored part at the bottom of the assembly is an

## 2 Design of a cell chip

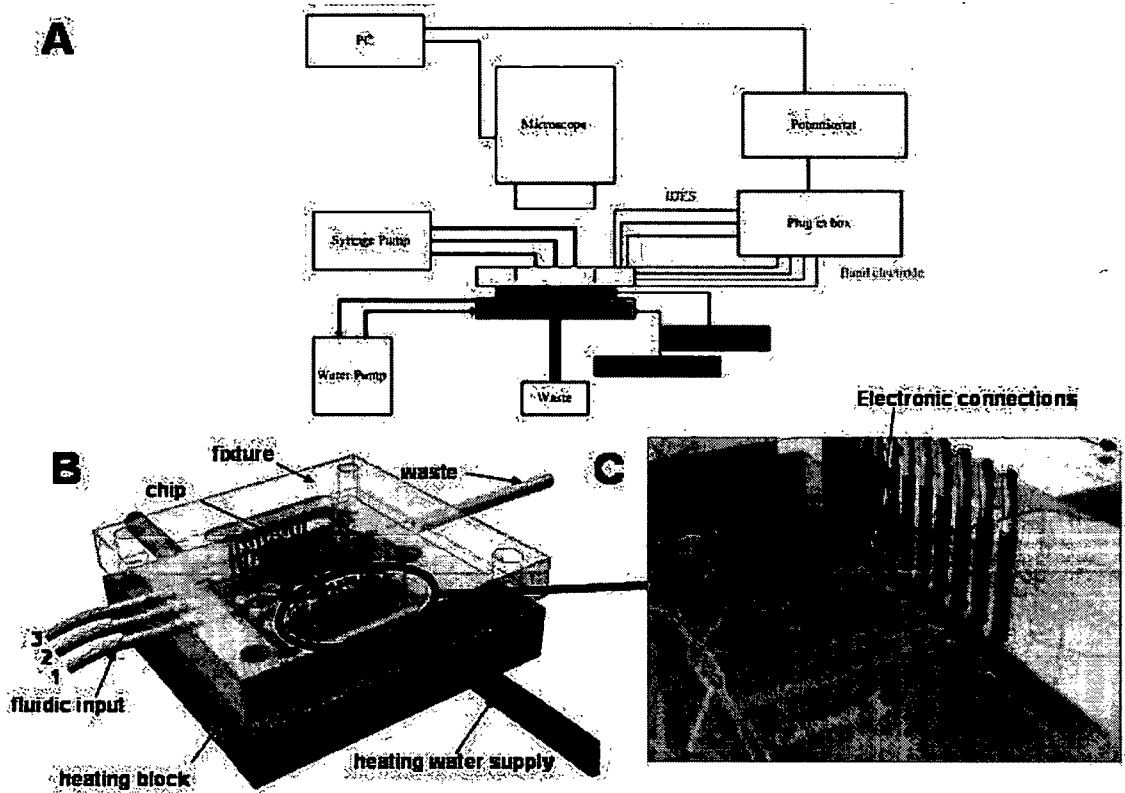


Figure 2.1: *Design of the chip and the experimental setup.* A) shows schematic measurement setup. B) shows the chip assembly including fluidics and the fixture, the chip and a heating block. C) shows the electronic connections to the chip.

## 2 Design of a cell chip

aluminium block connected to a water pump by silicon tubes (brown). The chip is situated right in the middle of the block and fixed by pressing down the top part of the fixture (transparent). The top part is connected to a pump by tubes and provides the solution supply into the microfluidic system and also out of the system by a single tube situated on the other side. The top part also possess gold tips, which touch the platinum pads of the chip to form an electrical connection to the potentiostat (shown in C).

The fixture of the chip (see Figure 2.1 b) houses the connections to a multichannel potentiostat, a water pump and to a syringe pump. An integrated optical window allows online visualizing cells. An external water bath circulates water through the aluminum block. The top fixture is made out of polycarbonate, a transparent and chemical inert material. Media, buffers and other solutions can be induced into the three ports located on the back side of the top fixture. The top part of the fixture also provides the electrical connection to the multichannel potentiostat (see Figure 2.1 c).

Solutions, buffers and other solutions are handled by a complex microfluidic system, which is connected to a syringe pump providing these fluids. The microfluidic system (see Figure 2.2) consists of three inlets, which connect two proliferation chambers through microchannels to wastes and cell seeding ports. In A) the gold pads are surrounded by a red marked area, which indicates that here no passivation can be found, gray areas are passivated. Brown marked microfluidic areas are channels where cells are inserted into the chip. B shows a three dimensional model of the microfluidic system.

### Microfluidics and PDMS

PDMS is a bulk polymer consisting of repeated units of  $-OSi(CH_3)_2O-$ . PDMS is highly hydrophobic what makes it difficult to wet its surface with aqueous solution. This polymer has become the most used material in the microfluidic sector for biological applications, because of its biocompatibility, low toxicity, high oxidative and thermal stability, gas permeability (i.e.  $CO_2$  and  $O_2$ ) as well as the easy fabrication by using soft lithography [27]. PDMS has also some disadvantages according to its ability of absorbing small organic molecules and also proteins, which are essential when performing cell culture [73]. The hydrophobic nature of PDMS is a major problem when

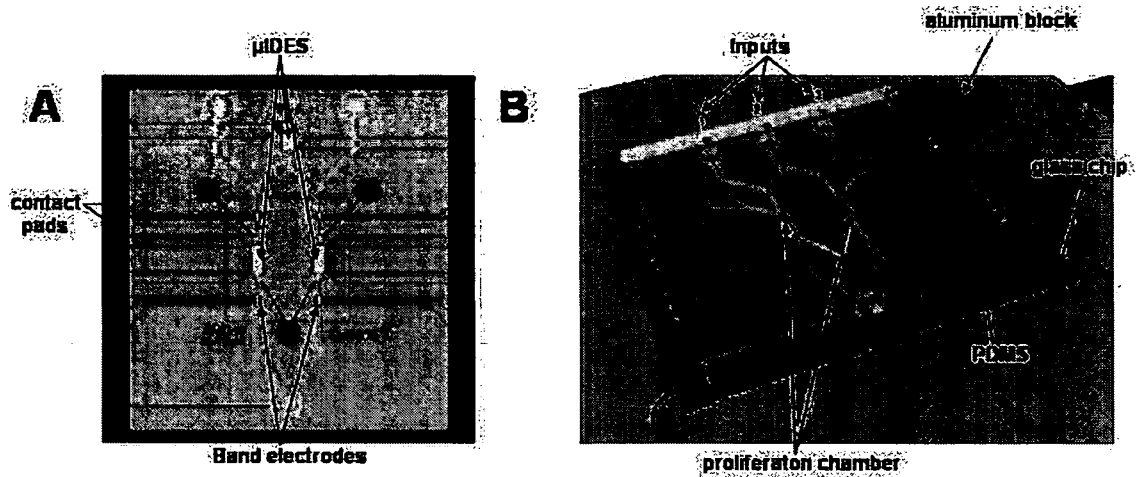


Figure 2.2: *Chip layout.* A) shows a schematic drawing of the chip layout containing microfluidics and sensors. B) shows a 3D model of the chip.

aqueous solution like cell growing media are handled. PDMS can be made hydrophilic through oxygen plasma treatment and various chemical surface modifications e.g. with aminopropyltrimethoxysilan (APTS). Despite oxygen plasma treatment and chemical modification PDMS does not keep this hydrophilicity because of aging effects [74]. On one hand the high gas permeability of PDMS, i.e. oxygen and carbondioxide, is a big advantage when working with cell-based microfluidic chips made out of this material, because the viability of cultured cells can be maintained over a long period of time. On the other hand PDMS also allows evaporation of water through its rigid structure, what results in the change of osmolarity of the fluid in the channels. Several cell types are very sensitive to such changes and alter their behaviour, in the worst case they die [73].

### 2.2.1 Microfabrication of chips

Our chips are fabricated in a clean room facility at the *Institute of Solid-State-Physics* at the *Technical University Vienna* by standard microfabrication techniques. In the following section the relevant applied techniques for the microchip fabrication is being explained in more detail including UV-lithography, sputtering, lift-off and chemical vapor deposition needed for chip fabrication as well as wet etching, soft lithography and oxygen plasma ashing required for the microfluidic system. Detailed protocols for

the fabrication can be read in the materials and methods section.

### UV-Lithography

Here, a film of photoresist is applied to a substrate radiation subsequently exposed to UV through a photolithographic mask containing a pattern. A photoresist is a photosensitive polymer, that can after light exposure become either more soluble in a solvent, then it is called positive tone, or less soluble, then it is called negative tone. Figure 2.3 a) shows the fabrication process using a positive tone photoresist. After light exposure the photoresist is developed to transfer the pattern of the mask onto the polymer. In other words the structures not protected by the mask are dissolved in a solvent and removed. Next, the integrated metallic structures such as electronic leads, electrodes etc. are fabricated using sputtering and a lift off process. Sputtering

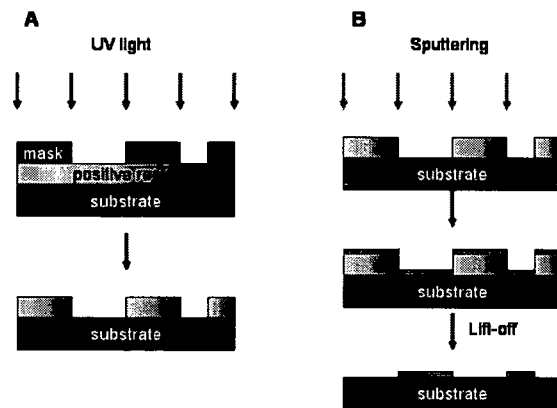


Figure 2.3: **A)** shows the principle of positive UV-Lithography. **B)** shows schematic the process of sputtering and lift-off.

is a physical vapor deposition process, where e.g. metal atoms of a solid material, called target, are transferred into the gas phase by a positive plasma bombardment. Of course the plasma ions need a sufficient energy to knock out target molecules. This energy is provided by acceleration of the ions in an electrical field. The resulting free metal atoms are deposited onto the nearby adjusted substrate.

After the metal deposition a lift-off is performed to remove the patterned photoresist as seen in Figure 2.3 b).

### Plasma enhanced chemical vapor deposition

Another important process is called Plasma enhanced chemical vapor deposition (PECVD) used to deposit thin layers of  $SiN_2$ ,  $SiO_2$  or other materials onto a substrate. At PECVD a plasma is used to dissociate the reaction molecules (gas phase), that finally form the passivation layer.

### Wet etching and soft lithography

In order to form channels in a microfluidic system made out of PDMS you need a mold, called master, with the negative structure of the channels. The mold for our microfluidic system is made out of silicon, by photolithography and wet etching processes. Wet etching is a commonly used method, where first a patterned photoresist is used as a mask due to remove the silicon oxide layer ( $SiO_2$ ) from the wafer surface, by using HF acid. HF perfectly meets requirements for this wet etching process, because it etches  $SiO_2$  but not the photoresist. The overall etching reaction of  $SiO_2$  by HF is shown in equation 2.1. After stripping the photoresist the patterned  $SiO_2$  acts as etching mask for a subsequently KOH etching step.



To finally form the microfluidic system, PDMS polymer is casted onto the patterned silicon wafer and cured by baking.

### 2.2.2 Simulation of flow profiles

Simulation of profiles were performed with a FemLab software in order to calculate velocity and pressure profiles within in the proliferaton chamber. Water was taken as fluid because all needed parameters, such as viscosity density *etc.*, were already known. Figure 2.4 shows a pressure and a velocity profile, where the pressure decreases with the colours from red to blue.

## 2 Design of a cell chip

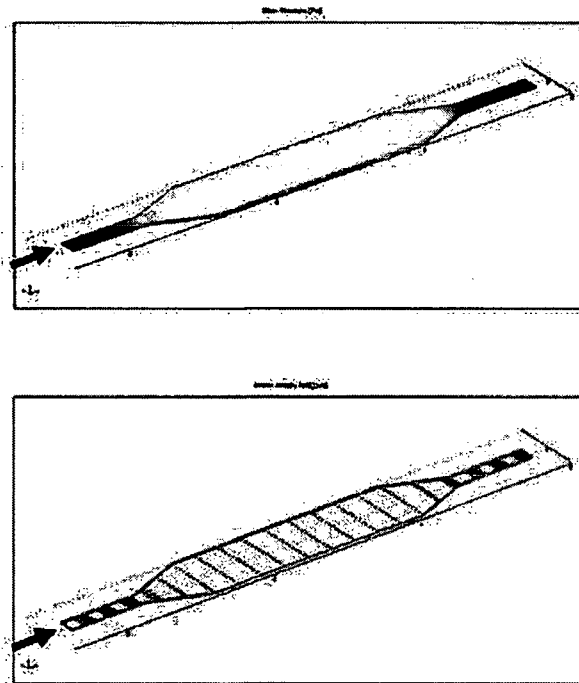


Figure 2.4: *Pressure and velocity profiles in the proliferation chamber.* The upper graph shows a pressure flow profile in the proliferation chamber, where pressure decreases with the colours from red to blue. The graph below presents a velocity profile.

## 2.3 Sensor design

As it was our intention to develop a biosensor capable of non-invasively monitoring cellular dynamics CDS was integrated into the microfluidic biochip using micro fabricated interdigitated electrode structures ( $\mu IDES$ ), shown in Figure 2.5. Interdigitated electrode structures are known to exhibit improved performance over standard two electrode systems. One benefit of interdigitated electrode structures is their ability to adopt the electric field distribution ( $H$ ) by controlling the ratio between space ( $G$ ) and width ( $w$ ) of the individual finger electrodes using the following equation:  $H = w + G$  [75]. This is particular important in measuring cellular behavior, because of differing height between different cell types. The current  $\mu IDES$  design consists of 200 fingers each  $5 \mu m$  in width and  $1000 \mu m$  in length that are separated by a  $5 \mu m$  gap ( $\lambda = 5 \mu m$ ) from each other. This means that the generated electric field reaches up to  $10 \mu m$  in the half spaces above and below the  $\mu IDES$ . Precise control over sensor geometry is therefore crucial for the development of a high performance sensor and achieved using MEMS technology [17, 28, 30, 76, 77]. In contrast to existing bioimpedance methods

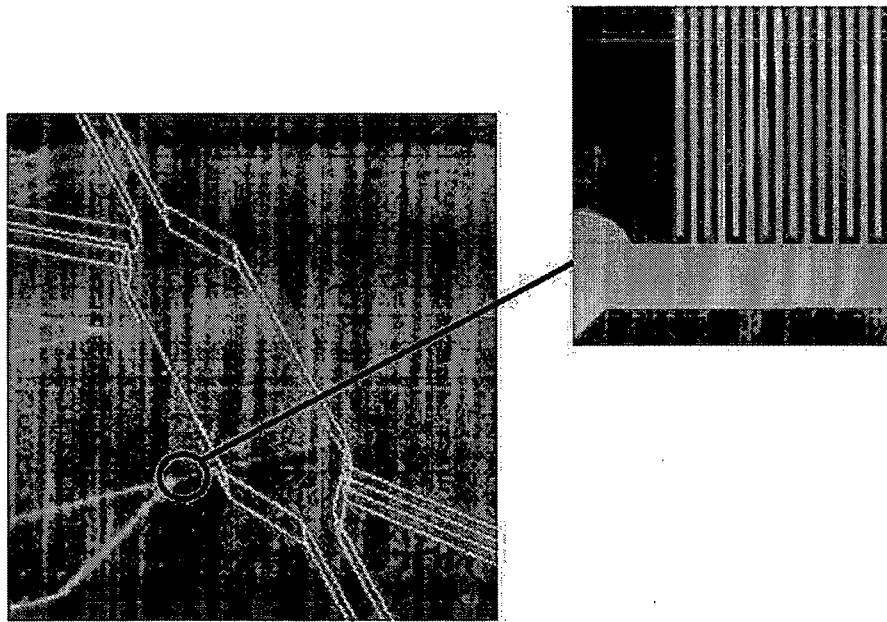


Figure 2.5: Picture of the proliferation chamber containing contactless electrode structures

implemented for cell analysis [78–80], the dielectric microsensors applied in this study

are completely insulated and physically removed from the liquid sensing environment using defined multi-passivation layers of distinct size and composition. Complete sensor isolation results not only in the absence of omic currents or faradaic contributions, but also eliminates electrode polarization events, fouling and bubble formation. Furthermore an intrinsic capacitance (offset) within the glass substrate and passivation layers has to be considered [81]. The actual multi-layer passivation consists of 100 nm silicon nitrite, 100 nm spin-on-glass and as a top layer 350 nm epoxy, since polymeric surfaces promote fungal biofilm formation [82]. Deposition of silicon nitrate and spin-on-glass was used to increase passivation and sensor stability.

### **Bioimpedance using contactless electrodes**

The technique employed to continuously measure cell viability and morphology changes is bioimpedance using insulated electrodes. If this technique is applied to living cells it is also called cellular dielectric spectroscopy (CDS). CDS makes use of the electric properties of cells exposed to a small magnitude ( $\pm 15$  mV) radio-frequency electrical field [83]. Dielectric spectroscopy has proven useful for analyzing biological cell suspensions to study cell sedimentation, cell aggregation, cell division and growth rates of low density liquid cultures (volume fraction below 0.15) [52, 84–87]. The main advantage of dielectric spectroscopy is its ability to perform non-invasive measurements with high precision over a wide time and frequency range [50, 83, 88]. Over a wide frequency range the reorientation of the dielectric dipoles and the polarization of the surface charge accumulated on the cell membranes (membrane potential) can be continuously monitored, thus allowing the investigation of cell structure and electrical properties of cellular components [85, 89].

Further more dielectrometry, thus dielectric measurements using fringing quasi-static electric fields above interdigitated electrodes, have been extensively described in industrial applications (*e.g.* curing processes, electrical insulation, moisture sensing *etc.*) as a non-destructive means of measuring dielectric changes induced by alterations of physical, chemical, and structural properties of polymeric materials [75].

In the context of cell analysis, high-density interdigital capacitors are ideal dielectric sensors due to their large active surface area and ability to tune electric field distri-

bution [90]. It is known that the penetration depth of the generated periodic electric field is proportional to the spacing between the sensing and driving electrodes and is independent of frequency [75].

### 2.3.1 Simulation of electric field distribution

In order to estimate the percentage of electric field distribution over the distance from the passivation surface, the capacity of the interdigitated electrode structures were calculated using the conformal mapping technique described in methods section 3.2.11. In brief the total capacitance of a  $\mu IDES$  sandwiched between arbitrary multi-layers

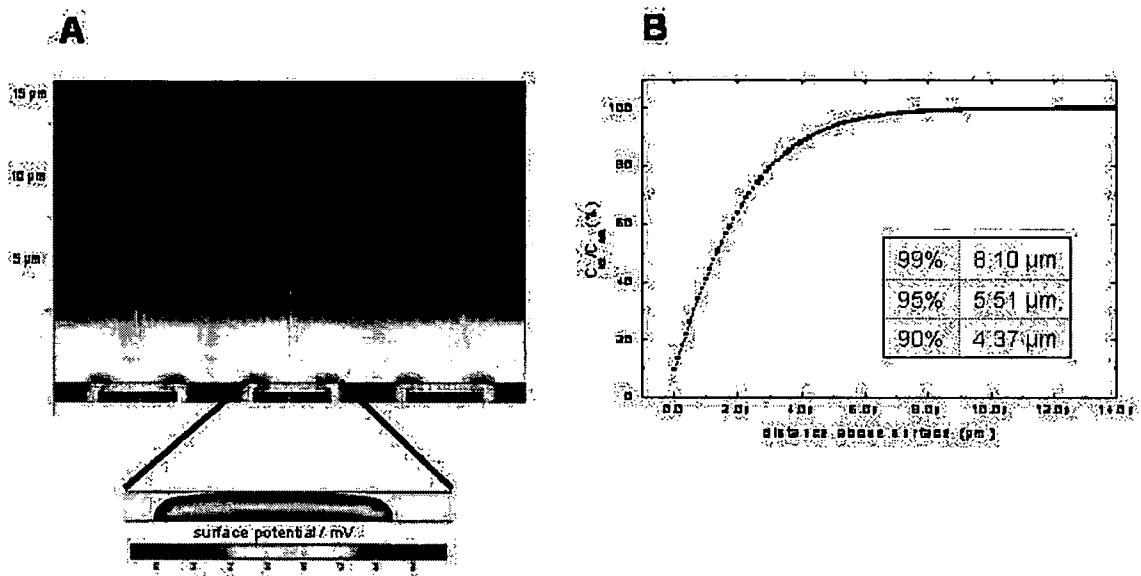


Figure 2.6: Simulation of electric field distribution performed in FemLab.

is evaluated analytically by conformal transformations using the partial capacitance method. In the first step, the planar comb-shaped electrodes are replaced by an equivalent circuit consisting of partial capacitances individually mapped onto parallel plate capacitor geometry for which capacitance values are calculated. Figure 2.6 a) shows the simulated field profile above the passivated electrodes. Furthermore, calculations using an electromagnetic finite element method software (Comsol Multiphysics 3.3a) in the presence of water ( $\epsilon_r=80$ ) above a 550nm passivation layer ( $\epsilon_r=8.7$ ) has shown that two thirds of the voltage drop off in the passivation region directly above the

## 2 Design of a cell chip

electrodes. 99% of the field are located in the first  $8.1 \mu m$  above the sensor region as shown in the graph of Figure 2.6 b). This means that dielectric changes occurring at  $8.1 \mu m$  distance from the passivation surface, for example, contribute only 1% to the overall signal, while the  $550 nm$  thick multipassivation layer is responsible for a 9% sensitivity loss.

## 3 Materials and Methods

### 3.1 Materials

#### 3.1.1 Solutions and media

- *APTS modification solution.* The modification solution consists of 2% APTS (Sigma), 94% methanol and 1% acidic acid for APTS stabilization. An initial stock solution of 0,85% acidic acid in methanol is prepared by adding 170  $\mu\text{L}$  acidic acid into 19,83  $\text{mL}$  of methanol. 18,8  $\text{mL}$  of this solution is combined with 800  $\mu\text{L}$  DI water and 400  $\mu\text{L}$  APTS (99%).
- *Preparation of Candida albicans medium and agar plates: Worthbroth (WB).* WB (Sifn) medium for a flask culture is prepared by dissolving 6.6 g in 200  $\text{mL}$  DI water. The mixture is stirred for 10 *min* at room temperature in a 500  $\text{mL}$  beacher and then transferred into a 300  $\text{mL}$  bottle to be sterilized in an autoclave at 121°C and 2 *bar* for 20 *min*. Agar plates are prepared by adding 3 g Agar-Agar to WB prior to sterilization. After the autoclaving step the medium is cooling down at room temperature to around 50°C casting the plates to prevent syneresis effects. The plates are casted under aseptic conditions by filling 15 to 20  $\text{mL}$  into each plate. The agar is allowed polymerizing at room temperature and the plates are either used immediately or stored at 4°C.
- *Dilution series of AmpB in WB.* A stock solution of AmpB in DMSO of 1  $\text{mgmL}^{-1}$  is prepared. Aliquods of 10  $\mu\text{L}$  of this are transferred into 1990  $\mu\text{L}$  of WB to obtain a solution of 5  $\mu\text{gmL}^{-1}$  AmpB. Next, series of dilutions are prepared to finally reach the concentration of 0,02  $\mu\text{gmL}^{-1}$ .

### 3 Materials and Methods

- *Preparation of Pichia pastoris medium and agar plates: Yeast extract Peptone Dextrose medium.* Yeast extract Peptone Dextrose medium (YPD) for flask culture is prepared by dissolving 2 g of yeast extract (Merck), 4 g of pepton (Merck) and 4 g of Dextrose (Merck) in 200 mL DI water. The mixture is stirred for 10 min at room temperature using a 500 mL beacher and then transferred into an 300 mL bottle to be sterilized in an autoclave at 121°C and 2 bar for 20 min. Agar plates are prepared by adding 3 g Agar-Agar to YPD prior to sterilization.
- *Preparation of Mueller Hinton medium and agar plates:* Mueller Hinton medium (MH) for a flask culture is prepared by dissolving 21 g in 1 L DI water. The mixture is stirred for 10 min at room temperature in a 2 L beecher and then transferred into two 500 mL bottles to be sterilized in an autoclave at 121°C and 2 bar for 20 min. To prepare agar plates containing MH to the prepared medium 15 g of Agar-Agar are added before the stirring step. Plates are similarly prepared as WB agar plates.

#### 3.1.2 Equipment

- Peristaltic pump: *Watson Marlow 205U*
- Heating circulation bath: *Haake C10-B3*
- Microscope: *Leica MZ16*
- Potentiostat: *Princeton Applied Research VMP3 Multi Potentiostat*
- Software for potentiostat: *EC-Lab V9.16*

#### 3.1.3 Strains

- *Escherichia coli* K12 ATCC 23716
- *Bacillus subtilis* ATCC 6501
- *Serratia fonticola* obtained from the University of applied Life Sciences in Vienna (BOKU)

- *Staphylococcus xylosus* (BOKU)
- *Pichia pastoris* ATCC 28485
- *Candida albicans* ATCC 10231

## 3.2 Methods

### 3.2.1 Microfabrication of chips

Fabrication of biochips commenced by using dry baked and primed (TI-Prime, MicroChemicals) glass substrates (170°C for 5 *min*). An initial resist layer is formed by spinning the nonphotosensitive resist (LOR 3A, MicroChem) on the wafer at 3000 *rpm* for 35 *s*. A second layer using the photo resist (positive resist AZ1MIR™ 701) is applied and soft baked at 110°C, 60 *s*. The resist is patterned using a MJB 3 mask aligner from SUESS Microtec (350 *W* mercury lamp, exposure time 6.35 *s*), developed for 25 *s* (AZ1MIF 726). Electrodes, leads, as well as contact pads, are fabricated by sputtering a 10 *nm* titanium seed layer and 200 *nm* gold onto the pre-patterned glass substrates and placing the glass substrates into a solution of NMP (1-methyl-2-pyrrolidinon) at a temperature of 70-80°C for at least 60 *min*.

The micro-dielectric sensors are further embedded underneath a multi passivation layer deposited on top of the interdigitated electrode structures ( $\mu IDES$ ). First a thin layer of silicon nitride (100 *nm*) is deposited via low temperature plasma enhanced chemical vapour deposition (PECVD, Oxford Plasmalab 80). A layer of spin-on-glass (SOG P84F, Filmtronics Inc.) is subsequently spun at 3000 *rpm* for 15 *s* (100 *nm*) onto the silicon nitride. After a soft bake, ramped from 80°C to 200°C on a hot plate, the chips are annealed for 1 hour at 70°C in a furnace. Curing of the layer takes place in a rapid thermal process (RTP) oven at 425°C for 1 hour under nitrogen atmosphere. A final 350 *nm* layer of SU-8 negative photoresist is used to cover the SOG surface thus creating a multi-passivation layer with a total thickness of 550 *nm*.

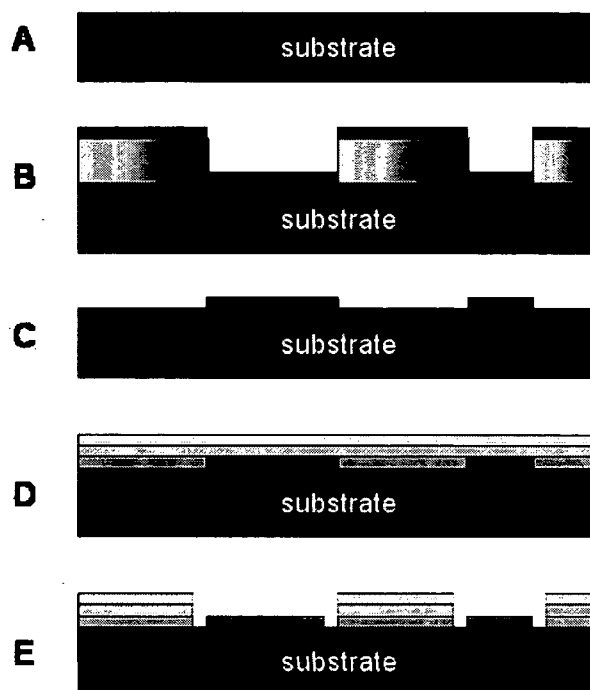


Figure 3.1: *Scheme of the Lithographic process during the fabrication of the cell chip.* A) figures the plane quartz glass substrate. B) models the lift off process for metal electrode (red) sputter deposition onto patterned resin (yellow). C) shows the resulting Ti/Pt electrode structures. D) figures the multi passivation layer consisting of SiN (green), SOG (bright blue) and SU8 (yellow). E) demonstrates the patterning of the passivation layer for the band electrodes and the pads.

#### 3.2.2 Formation of the microfluidics and chip assembly

The microfluidic channels were formed in a 2 – 3 mm thick PDMS (Polydimethylsiloxane) layer as an imprint of a silicon master mold. To fabricate the silicon master mould a 750 nm silicon oxide layer is deposited on a silicon wafer, by thermal oxidation. The thermal silicon oxide, used as hard mask for the subsequent KOH is patterned using buffered HF (BHF) for 14 min. After stripping the photo resist (MIR 701 positive photo resist) the substrate is etched using 40% KOH solution at 80°C for 25 min. The resulting etch depth was 20 μm. The remaining silicon oxide hard mask is then stripped by BHF etching.

The formation of fluidic channels is accomplished by placing the mold in a glass Petri dish and filling it with a 2 mm thick layer of liquid PDMS. The PDMS polymere consists of a base silicon elastomer and a curing agent (184 Kit Silicon Elastomer from Sylgard) mixed 10:1, respectively. About 16 mL of degased PDMS polymer has to be cast in the Petri dish to get the required thickness. After baking at 60°C for 6 h on a hot plate, to ensure complete polymerization, the PDMS with the fluidic channels is cut to the required dimensions to fit into the fixture. Holes for fluid access are plugged using metal tubes of different diameter.

Following extensive cleaning steps the PDMS scaffold is covalently bonded to the chip using oxygen plasma of 300 W and 0,7 torr for 30 sec. After a baking step of 120°C for 5 minutes on a hot plate a total covalent bonding is ensured.

#### 3.2.3 Bonding by oxygen plasma ashing

In this work oxygen plasma, established by an plasma asher, was applied to either activate the surface of the chip and the PDMS in order to establish a non-reversible bonding. Silicon based materials with  $Si - CH_3$  groups react to  $Si - OH$  groups after exposure to oxygen plasma.  $Si - OH$  groups form covalent bondings by a condensation reaction when brought into contact. Additionally the surfaces become more hydrophilic and therefore wettable. Because diffusion of molecules without  $SI - OH$  inside the PDMS network to the surface occurs the hydrophilicity does not last forever.

### 3.2.4 Sensor characterization using LCR Unit

After production in the clean room facilities the capacitance of the  $\mu IDES$  sensors is measured by a LCR unit. The following steps have to be performed:

- Rewiring to a 2 point measurement at the entrance of the black box: Plugs 1 and 4 (HCur and LCur) are connected to the Probes, 2 and 3 (HPot and LPot) are connected to 1 and 4 respectively.
- Execute the Open/Short correction at the Agilent 4285 and set the flag ON (with the short circuit bar made of gold in the cupboard). Open correction means that the needles do not have any contact. Short means that the needles have contact to the same electrode, so they are short-circuited. After this procedure the needles must be moved.
- Settings at the Agilent 4285:
  - cable length: 4 m
  - equivalent circuit (EC): Cp-G;
  - level: 50 mV
  - Bias: 0V/off
  - IntegTime: Long
- Measurement of the frequency spectra with the LabView program: hp4284sweep;
  - settings:
    - EC: CPG
    - Range: 1 kHz-1 MHz
    - Step: 10 kHz

When a measurement is controlled by the computer, the device is set to a remote state. By pressing LCL on the right hand side of the Agilent the device is set to the local mode but the trigger is still set to BUS waiting for commands from the PC. To change it and to measure values "from the panel" you have to change the trigger in the MEASUREMENT SETUP dialog menu.

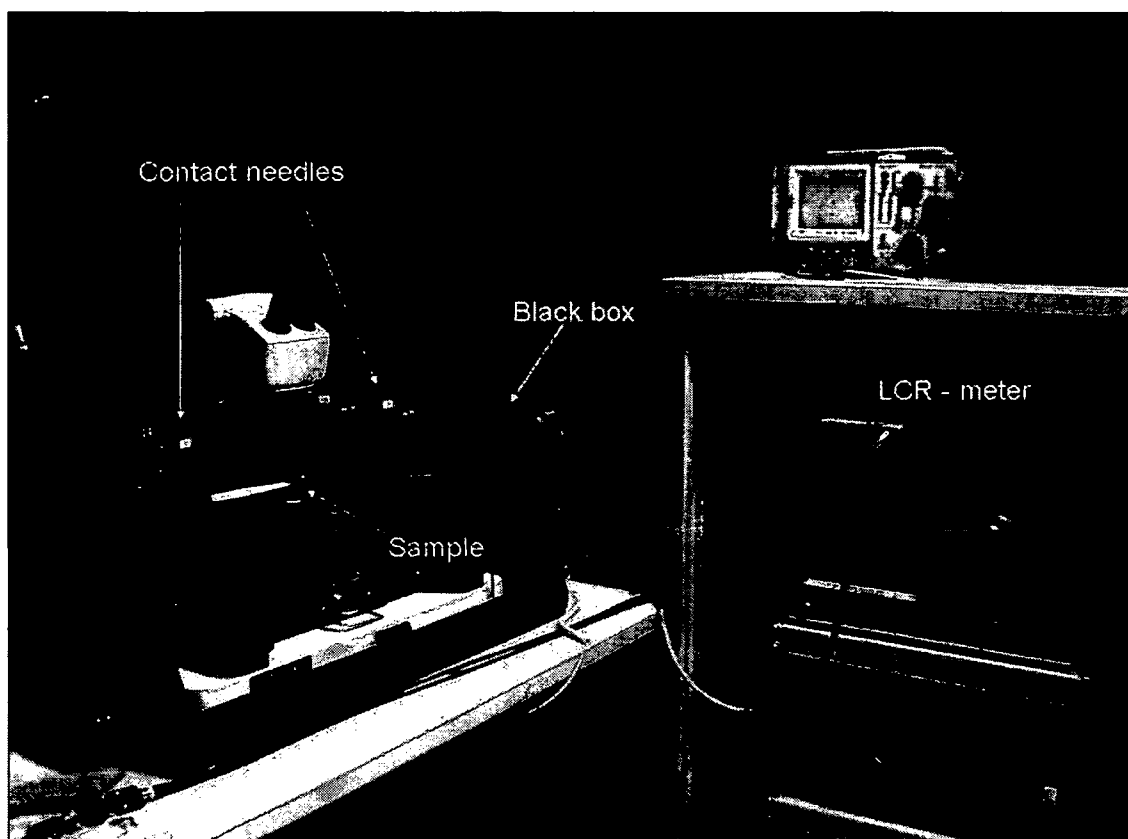


Figure 3.2: Setup of the LCR meter for measurement of  $\mu IDES$  capacitance

### 3.2.5 Atomic force microscope (AFM) imaging

An AFM consists of a microscaled cantilever with a sharp tip, also called probe, that is used to scan the specimen. When the probe is brought into proximity of the specimen surface occurring forces between each other lead to deflection of the probe and so of the whole cantilever. The rate of deflection is typically measured by a laser spot reflected from the back of the cantilever into an array of photodiodes, respectively the detector. In many cases the sample is mounted onto a piezoelectric tube, that can move the sample in the z direction for maintaining a constant force, and the x and y directions for scanning the sample.

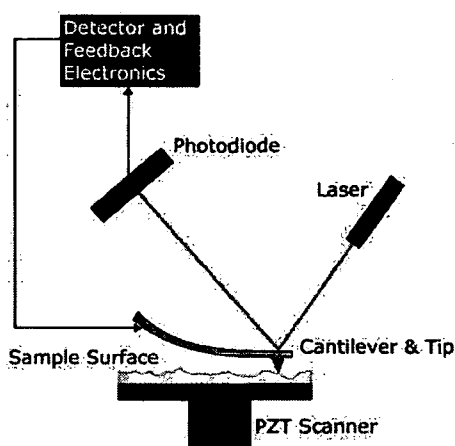


Figure 3.3: *Principle of atomic force microscopy (AFM)*. A cantilever is scanning a sample surface mounted onto a piezoelectric tube and deflected by the forces occurring between the the tip and the sample surface. The rate of deflection is measured by a laser reflected from the back of the cantilever into an array of photodiodes communicating with a detector.

### 3.2.6 Surface modification with APTS

*APTS modification of silicon oxide and glass after oxygen plasma treatment by dip coating.* Both the glass slide and the silicon oxide wafer are exposed to an 300 W oxygen plasma for 40 sec at 0.7 torr. The glass slide and the silicon oxide wafer are immediately transferred into the APTS modification solution for 10 min. Afterwords the samples are put onto an hot plate of 120°C for 30 min.

### 3 Materials and Methods

*APTS modification of microfluidic channels by wet chemistry.* First a PDMS and a chip are covalently bonded as described in Section 3.2.2. The modification is performed using a constant flow ( $1 \mu\text{L}/\text{min}$ ). In the first step the PDMS surface is hydrolyzed by adding a  $1 \text{ M}$  HCL solution for  $10 \text{ min}$ . Then the surface is deprotonated by adding a solution of  $1 \text{ M}$  NaOH solution for  $10 \text{ min}$ . When the microfluidic channels are rinsed with DI water for  $5 \text{ min}$ . The channels are then flushed with APTS modification for  $15 \text{ min}$  followed by methanol rinse  $10 \text{ min}$ . Finally a curing step at  $60^\circ\text{C}$  for  $30 \text{ min}$  is performed.

#### 3.2.7 Contact angle measurement

Contact angle measurement is a simple method for surface analysis related to surface energy and tension. The contact angle describes the shape of a liquid droplet resting on a solid surface. When drawing a tangent line from the droplet to the touch of the solid surface, the contact angle is the angle between the tangent line and the solid surface (see Figure 3.4). After placing a droplet of liquid ( $1 - 25 \mu\text{L}$ ) onto the surface, the

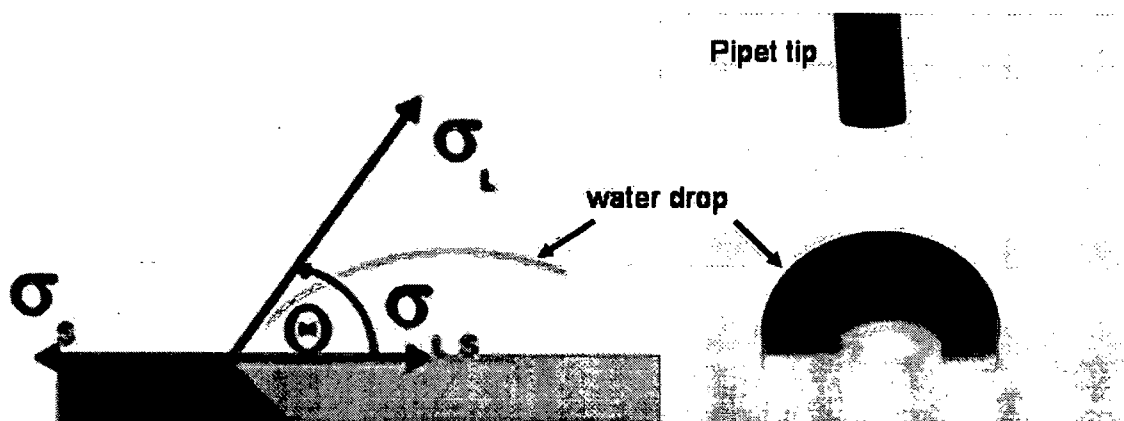


Figure 3.4: Scheme of contact angle measurement.  $\sigma_L$ ...surface tension of liquid;  $\sigma_s$ ...free surface energy of solid;  $\sigma_{LS}$ ...surface energy between fluid and solid.

outline of the droplet is studied through a magnifier. The operator positions a tangent line from the droplet to the touch of the surface. A protractor within the optics then provides a reading of the contact angle. A surface is perfectly wetted when the contact angle is under  $45^\circ$ . No surface wetting takes place when the contact angle is higher

than 90°.

#### 3.2.8 Cultivation of microorganisms

The bacterial strains *E. coli*, *B. subtilis*, *S. fonticola*, and *S. xylois* are cultivated aerobically in an incubation shaker at 37°C and 200 rpm using Miller Hinton media. The yeast strains *P. pastoris* and *C. albicans* are cultured at 30°C using YPD and WB, respectively. Optical density of buffered samples is measured at 600 nm using a UV-visible spectrophotometer (Thermo Electron Corporation, Nicolet evolution 100), while colony forming units ( $cfumL^{-1}$ ) are determined after biological samples are subjected to a series of 10-fold dilutions, and there aliquds of (100  $\mu L$ ),  $10^{-6}$ ,  $10^{-7}$  and  $10^{-8}$  dilutions of  $OD_{600}=1$ , are spread uniformly onto agar plates. The colony forming units are counted for each individual strain after over night incubation at 30°C.

*Culturing of Candida albicans and Pichia pastoris in flask culture.* 1 mL inoculum are transferred in 50 mL of medium and cultured at 30°C, 300 rpm. Cell growth is followed by measuring the optical density at a wave length of 600 nm ( $OD_{600}$ ) using 1 mL aliquods of the culture flask. Least samples are precipitated by centrifugation (5 min, 13000 rpm) and re-suspended in buffer prior measurement.

#### 3.2.9 Dielectric spectroscopy

Absolute impedance (IZI) and phase angle ( $\theta$ ) values are measured continuously over the frequency range of 5 to 500 kHz. Unless otherwise noted, 1  $\mu L$  of cell suspension ( $OD_{600} < 1.0$ ) is injected into the open fluidic access port (cell seeding) located in the center of the pre-filled biochip. Any excess fluid is carefully removed and the reservoir is sealed using a thin piece of PDMS. Activation of microfluidic flow through inputs A and/or C to the waste compartment causes cells to freely move into the proliferation chamber due to the establishment of a negative pressure within the cell proliferation chamber. Cell growth, viability and morphology changes are continuously measured and compared to signals obtained from the reference chamber also filled with media using a multichannel potentiostat (VMP3/P-01, Princeton Applied Research). The working and reference micro-dielectric sensors are addressed simultaneously by

continuously scanning 501 frequencies applying  $\pm 15\text{ mV}$  ( $V_{pp} 30\text{ mV}$ ) between the interdigitated electrode structures ( $\mu IDES$ ).

#### 3.2.10 Principle component analysis (PCA)

Dielectric spectroscopy data obtained for five replicate runs with each cell culture is used to generate the matrix for principle component analysis (PCA). Each column in the data matrix consists of 501 signals for one replicate measurement with each of the six microbial strains. The matrix was converted into a Lotus file for incorporation into MATLAB (Version 7.01). Factor analysis was performed using the Chemometric Toolbox for Matlab (Version 3.02), and involved the generation of reduced eigenvectors, examination of the resulting residual plots for randomness of noise, and the generation of scores for the first three principle components [91]. The obtained scores are plotted to determine qualitative groupings of individual data sets [92].

#### 3.2.11 Conformal mapping technique

To estimate the percentage of electric field distribution over the distance from the passivation surface, the capacity of the interdigitated electrode structures are calculated using the conformal mapping technique [93]. The total capacitance of a  $\mu IDES$  sandwiched between arbitrary multilayers is evaluated analytically by conformal transformations using the partial capacitance method. In the first step, the planar comb-shaped electrodes are replaced by an equivalent circuit consisting of partial capacitances individually mapped onto parallel plate capacitor geometry for which capacitance values are calculated.

## 4 Results

### 4.1 Characterization of the microfluidic biofilm chip

#### 4.1.1 Physical characterization of dielectric sensor using LCR meter, AFM and CV

The aim of this research is the development and characterization of technology capable of continuously monitoring cell growth, viability and morphology changes with high sensitivity. An important feature of the newly developed detection technology is the complete isolation of the  $\mu IDES$  to guarantee non-invasive monitoring conditions. Complete isolation is accomplished depositing various materials of defined dielectric properties. Consequently, single, bi- and multi-layer passivation strategies using epoxy, spin-on-glass, and silicon nitrite, and a combination thereof, were investigated.

Capacitance measurements of the  $\mu IDES$  sensors by a LCR unit confirmed the constancy of chip production within clean room facilities. The measurements are performed over many frequencies from 1  $kHz$  to 1  $MHz$  in 10  $kHz$  steps. Figure 4.1 shows the setup of the probe station (A) and a measurement with its settings (B). A passivated  $\mu IDES$  has a capacitance of around 8  $pF$  (300  $kHz$ ) when air is above the sensor.

In order to further confirm passivation quality and reproducibility of chip fabrication AFM is used. AFM studies showed the presence of passivation losses and pin holes caused by poor epoxy adhesion, uneven layer distribution and droplet formation along finger electrodes, see Figure 4.2. Inset shows an AFM image containing a multitude of 50 to 70 nm diameter holes (arrow) located throughout the SOG layer believed to originate by solvent evaporation during the curing process at 425°C of the precursor

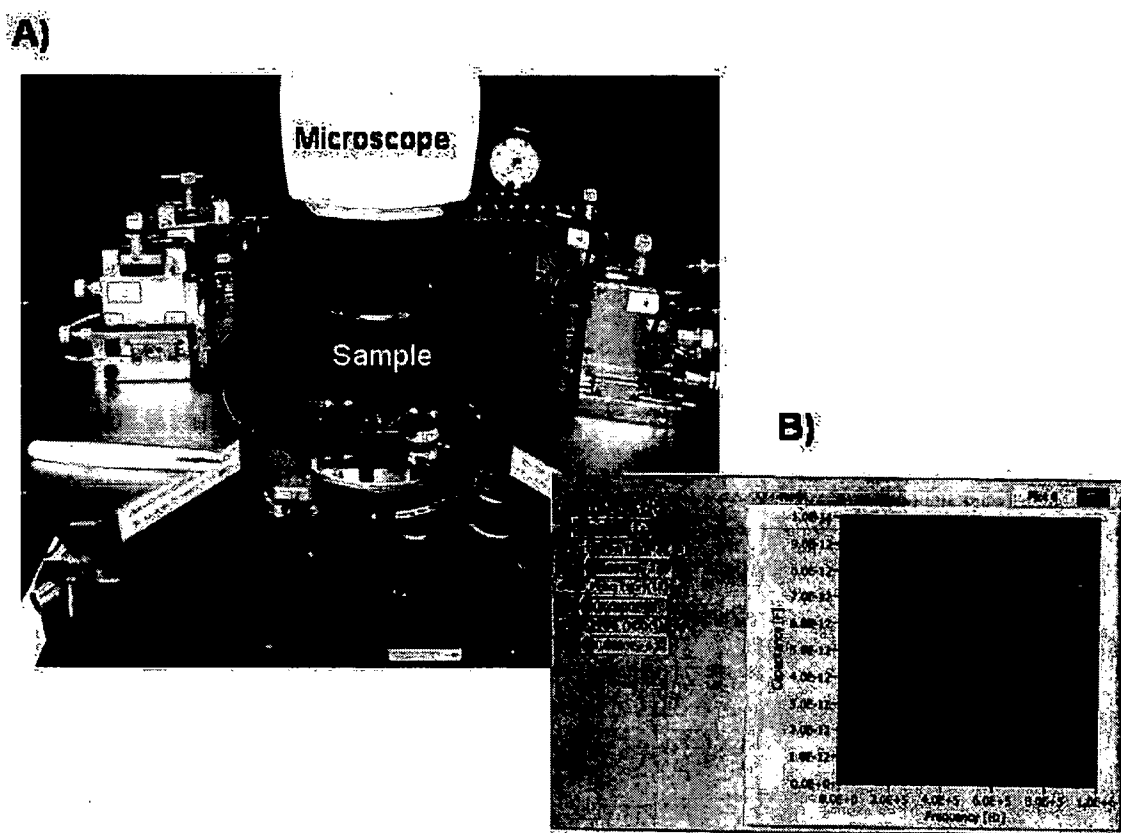


Figure 4.1: LCR-Meter setup during  $\mu IDES$  capacitance measurements

substrates.

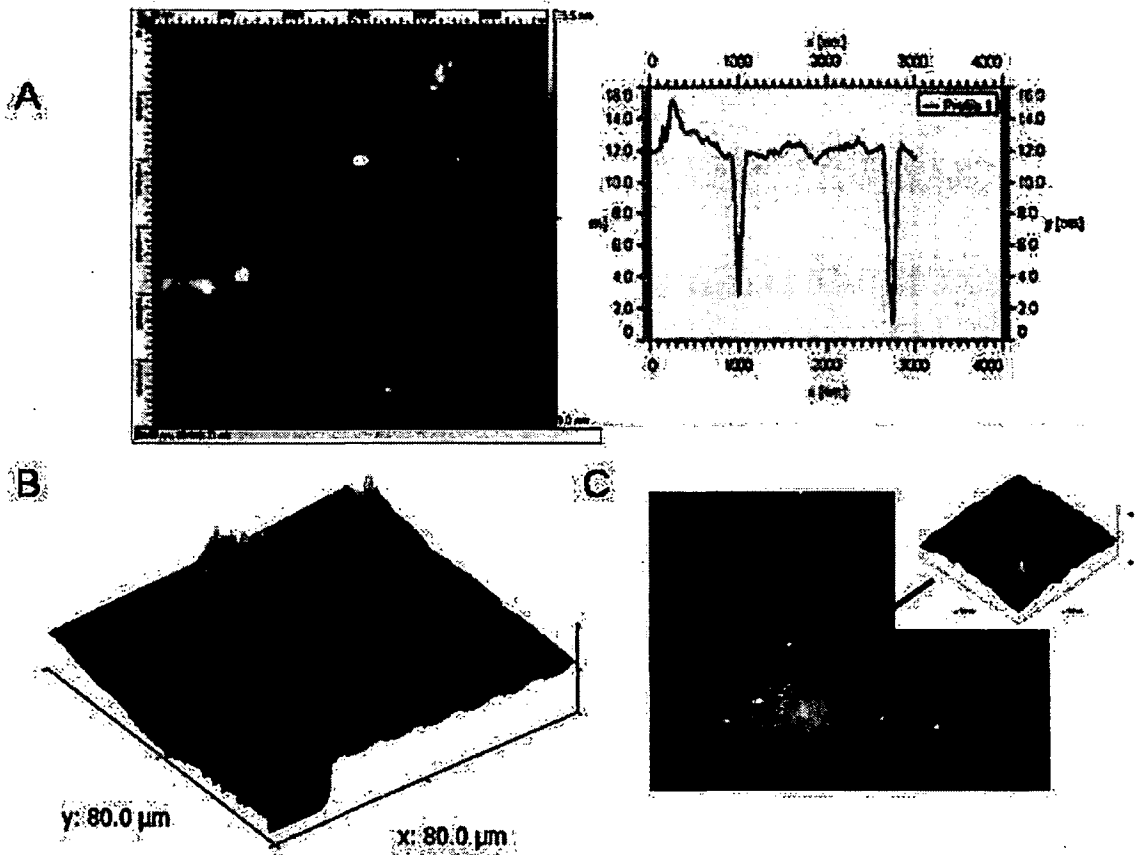


Figure 4.2: *AFM images of passivation layer surfaces. A) SOG surface containing 50 nm pinholes. B) SU8-coated  $\mu$ IDES. C) droplet formation of epoxy and contamination of SU8.*

Cyclic voltammetry was used to assess the electrical insulation quality. A comparison of oxidation currents using unpassivated sensors yielded  $-62 \mu A$ . In turn with single passivation layers using epoxy and SOG yielded  $-28 \mu A$  and  $-8 \mu A$  in the presence of the electro-active compound ferrocyanide ( $10 mM$ ). Figure 4.3 shows cyclic voltammetry (CV) traces of a single spin-on-glass (SOG) layer and SOG/epoxy resin bi-layer of  $100 nm$  and  $450 nm$  thickness, respectively. Although the application of bi-layers sufficiently insulated the dielectric sensors ( $-2 nA$ ) any degradation during chip cleaning, assembly or re-use resulted in massive drifts and also damages of the SU8 passivation layer (data not shown). In an effort to further increase sensor stability  $100 nm$  SiNx layer was added to the passivation strategy. Figure 4.4 shows a Nyquist

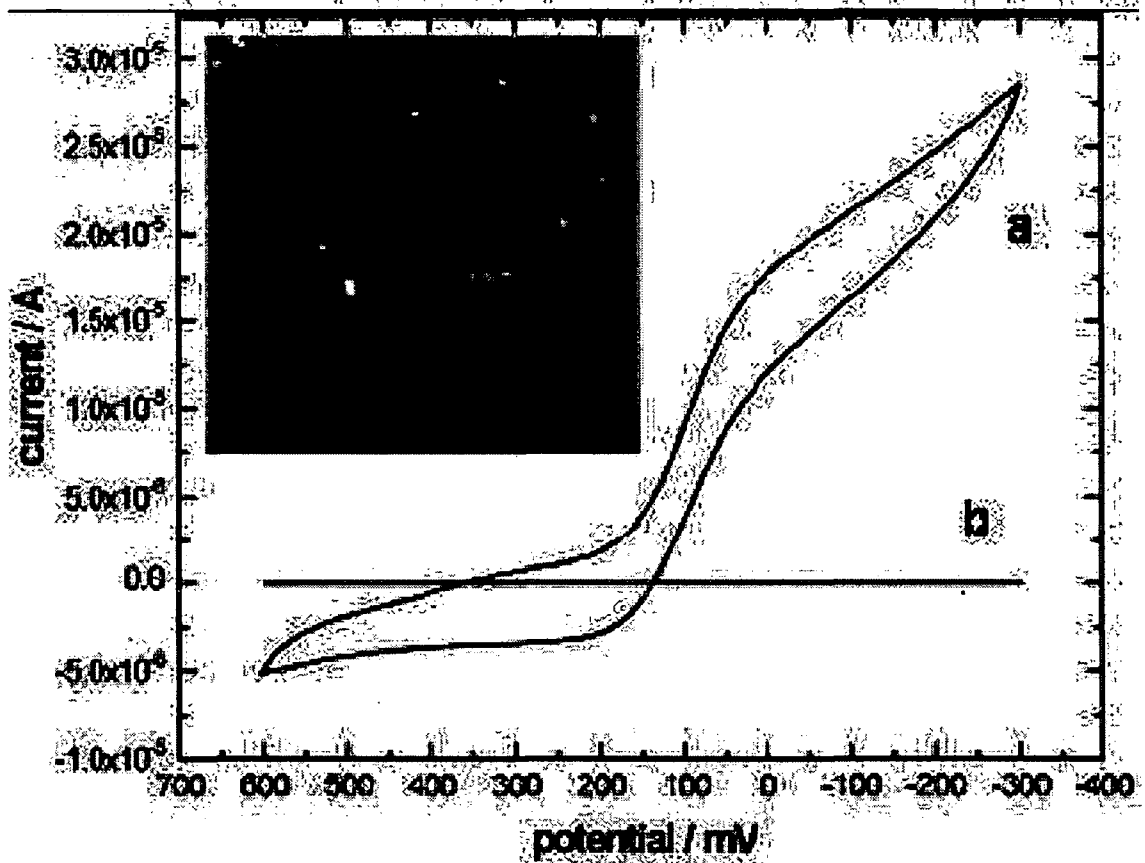


Figure 4.3: Cyclic voltammetry traces using  $\mu IDC$  passivated with SOG (a) or SOG plus SU-8 (b). CV traces of 10 mM ferrocyanide using platinum  $\mu IDC$  as working electrode and a silver wire as CE, / AgQRE in presence of SOG (a) and SOG/SU-8 (b) passivation layer. The inset shows an AFM image ( $1 \times 1 \mu m$ ) of SOG surface containing holes with diameters from 50 to 70 nm.

## 4 Results

plot using SiN<sub>x</sub>/SOG/SU-8 (550 nm) passivated dielectric sensors in the presence of air, DI water, 50 mM phosphate buffer and 10 mM ferricyanide (buffered), and it is evident that the contact less dielectric microsensors cannot detect an electro-active species (see Figure 4.4 c and d). Detection limit and baseline stability was determined over

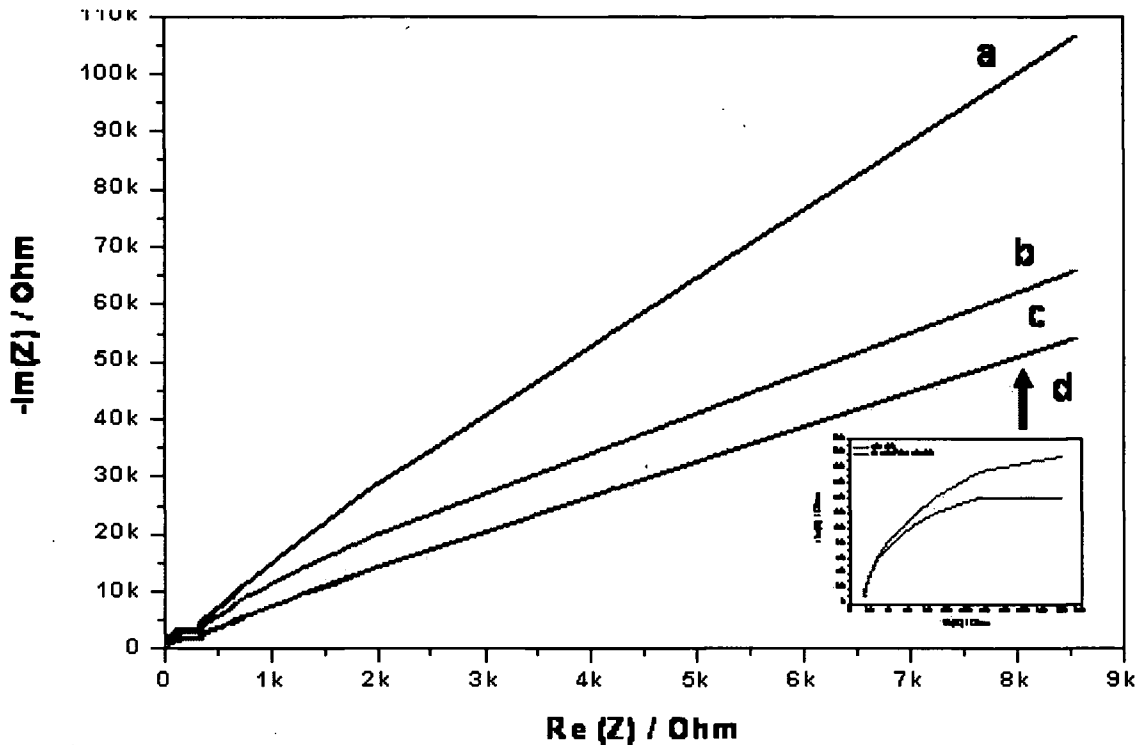


Figure 4.4: *Nyquist plot of air and diefferent solutions.* Nyquist plot of air (a), DI water (b), phosphate buffer (c) and 10 mM FCN using SOG/SU-8 passivated dielectric microsensors.

32 hours continuous flow measurement in saline buffer solution (flow rate 0.5  $\mu\text{L}/\text{min}$ ) and yielded a relative standard deviation of 1.5% or  $\pm 15 \text{ Ohm}$  at 100 kHz (see Figure 4.5).

### 4.1.2 Sensor performance

In an attempt to examine the sensor response in the presence of increasing temperature water was pumped through the microfluidic system while the temperature was up-regulated from RT to 28°C and then 37°C using an external water circulation system. As seen in Figure 4.6 A the sensor signals decrease linearly with increasing

## 4 Results

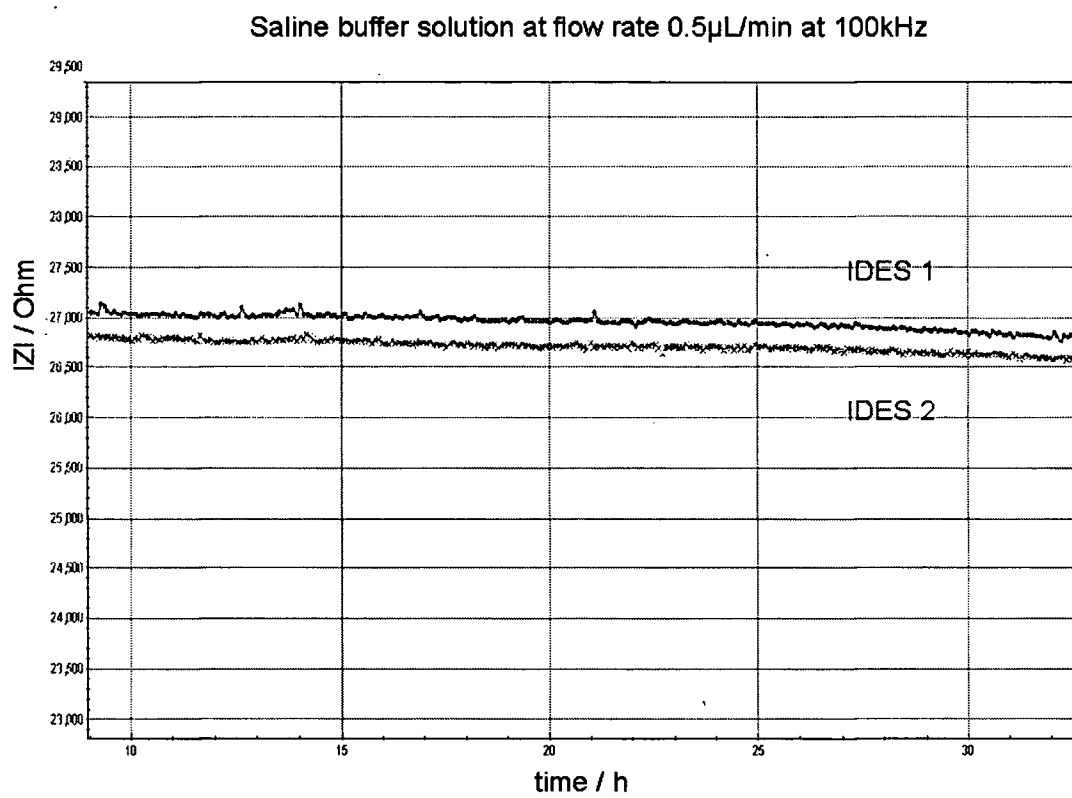


Figure 4.5: Measurement stability over a long period of time using passivated  $\mu$ IDES sensors.

## 4 Results

temperature. Observed variance at RT reflect to inconstant temperature conditions in the laboratory facilities caused by air ventilation. Because cells constantly change their surrounding microenvironment, we further wanted to examine sensor responses in the presence of increasing salt concentrations and pH. Figure 4.6 B shows impedance signals in the absence and presence of salt concentration (here 1 *MKCl* and 50 *mM PO<sub>4</sub>* buffer) and increasing pH. Only the addition of huge salt concentrations (1 *MKCl*) and application of extreme pH values significantly altered impedance signals. In an additional experiment we wanted to examine sensor response to altering media conditions. Therefore the cells (*Pichia pastoris*) were grown in a standard culture flask and samples were taken every hour. The cells were precipitated by centrifugation and re-suspended in phosphate buffer. Both the cells and the cell free media extract were measured with the  $\mu IDES$  sensor and photometer, respectively. As can be seen in Figure 4.7 the signal by the cells increased with increasing optical density while the cell free media extract does not cause a significant sensor response.

Next, sensor performance in the presence of biological samples was evaluated using two Gram-negative, two Gram-positive bacteria and two yeast strains. Microbial strains were selected based on their differences in size and morphological composition. For instance, Gram-negative bacterial cell walls consist of a second outer membrane of different complexities while yeast cells are 5 to 10 times bigger than bacteria. In a series of experiments, cells cultivated using incubator shaker were harvested in the exponential phase, centrifuged and re-suspended in saline buffer prior to use. Aliquots of 1  $\mu L$  buffered sample solutions were injected into the proliferation chamber (90 *nL* volume) and impedance data were recorded after cells were allowed to settle for 20 min prior to measurement. Figure 4.9 B shows impedance values from three microbial strains where absolute impedance signals changed rapidly as soon as cell concentrations reached a minimum detectable level and plateaued following complete coverage of the entire sensing volume.

In all cases microbial concentrations above 1000 *cfu*/ $\mu L$  showed significant signal changes, with decreasing impedance values for *E. coli* K12 (Gram-negative), *S. fonticola* (Gram-negative) and *C. albicans* (yeast) and increasing signals in the presence of *B. subtilis* (Gram-positive), *S. xylosus* (Gram-positive) and *P. pastoris* (yeast) strains.

#### 4 Results

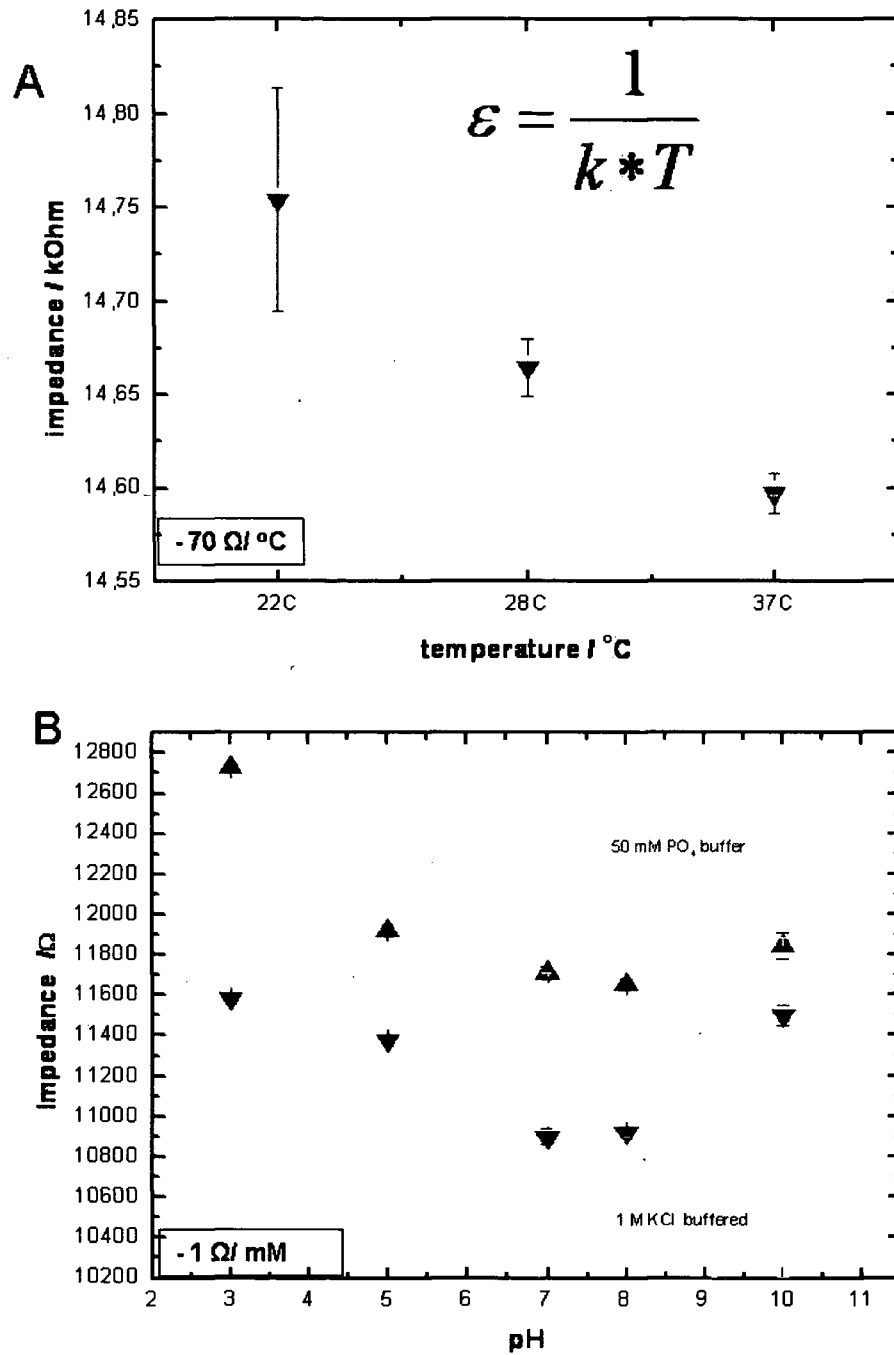


Figure 4.6: Signal change with change of temperature, salt concentration and pH. A) shows a linear signal decrease with a temperature increase, whereas the overall signal decreases with increasing salt concentrations as shown in B). In a pH region between 7 and 8 the signal remains constant, while it decreases before and increases after this pH area.

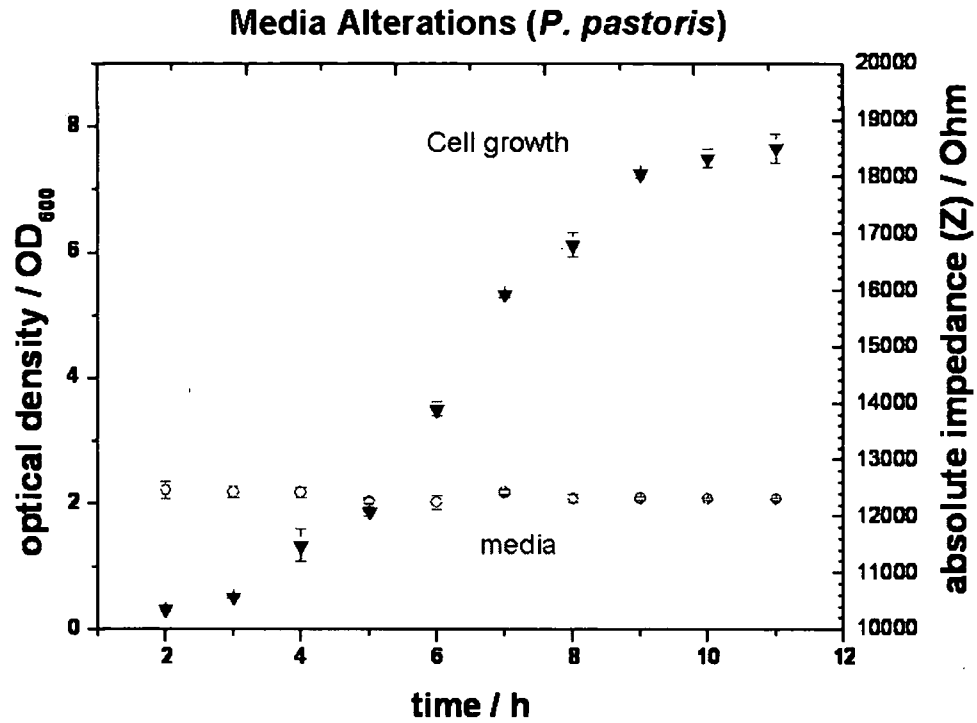


Figure 4.7: Measuring background effects caused by changes in growth media during cell culture of *P. pastoris*

Table 4.1: Average background subtracted impedance values at 50 kHz and triplicate measurements

Strain	at $10^4 cfumL^{-1}$	at $10^8 cfumL^{-1}$
<i>E. coli</i> K12 (Gram-negative)	$-25 \pm 10\Omega$	$-325 \pm 50\Omega$
<i>S. fonticola</i> (Gram-negative)	$-476 \pm 65\Omega$	$-1838 \pm 105\Omega$
<i>B. subtilis</i> (Gram-positive)	$72 \pm 22\Omega$	$6143 \pm 352\Omega$
<i>S. xylosus</i> (Gram-positive)	$900 \pm 110\Omega$	$12152 \pm 260\Omega$
<i>C. albicans</i> (yeast)	$-1150 \pm 145\Omega$	$-2368 \pm 378\Omega$
<i>P. pastoris</i> (yeast)	$1962 \pm 250\Omega$	$2653 \pm 350\Omega$

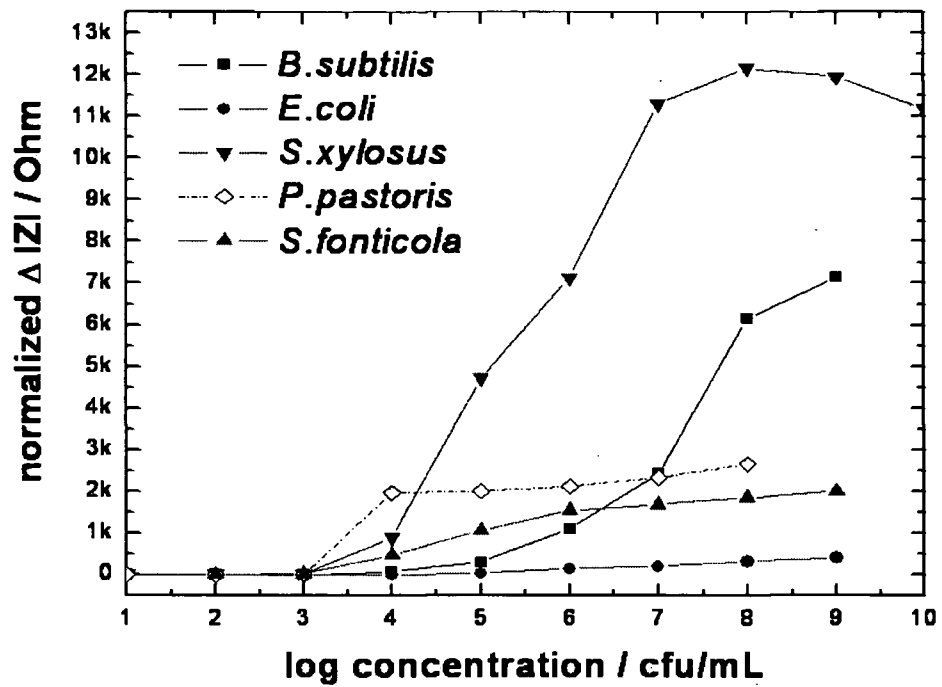


Figure 4.8: Sensor response to different microorganisms. Absolute Impedance values were normalized to  $0\text{ kHz}$  and positive values.

## 4 Results

Table 4.1 lists results of all six strains in the presence of low and high cell concentrations. Although the much larger yeast cells yielded measurable signals at low concentrations, highest signal changes are obtained with the smaller bacteria *S. xyloso* and *B. subtilis*. The above findings encouraged us to investigate the ability of the contact less dielectric microsensors to directly distinguish and identify individual strains in a nanovolume setting in the absence of any labels or indicators. In a series of experiments, five microbial strains were cultivated in shake flasks, harvested in the exponential phase and directly injected into the biochip. Next, chemometric PCA was applied to dielectric spectra of untreated samples in an attempt to apply pattern recognition methods to classify microbial strains. Figure 4.9 shows score plots using raw data (phase angle) of three to four replicate measurements of five microbial strains. Results show that variances between microorganisms appear high enough to allow classification, while replicate measurements possess enough similarities to cluster together. In comparison, generated pattern recognition plots of cell free media extracts showed only random distribution as seen in inset of Figure 4.9. These results clearly indicate that the identification of organisms is not affected by media components or metabolites generated during microbial cultivation. Overall, impedance signals and phase angle values of 501 frequencies were recorded during each measurement and used to generate pattern recognition plots.

In principle, not all frequencies are necessary for the clear distinction between microbial species. Analysis of impedance and phase angle data using bacterial strains show highest standard deviations between 72-75 kHz and 19-21 kHz, respectively. In turn, highest variances between *C. albicans* and *P. pastoris* are found at frequencies of 74 and 75 kHz using impedance signals and between 20-26 kHz, at 32 and 75 kHz using phase angle values. However, further investigation needs to be conducted to link the above listed frequencies to specific morphological components of microbial cells. The effects of cell morphology changes on sensor performance were further investigated using *C. albicans* and *P. pastoris*. Both strains were grown under standard conditions and harvested in the exponential phase. Aliquots of in-buffer re-suspended cell suspensions were either exposed to the plasma membrane disrupter Amphotericin B (AmpB) ( $5\mu\text{g mL}^{-1}$  for 4 hours at 37°C) or subjected to sonication treatment (2 hours). In brief

## 4 Results

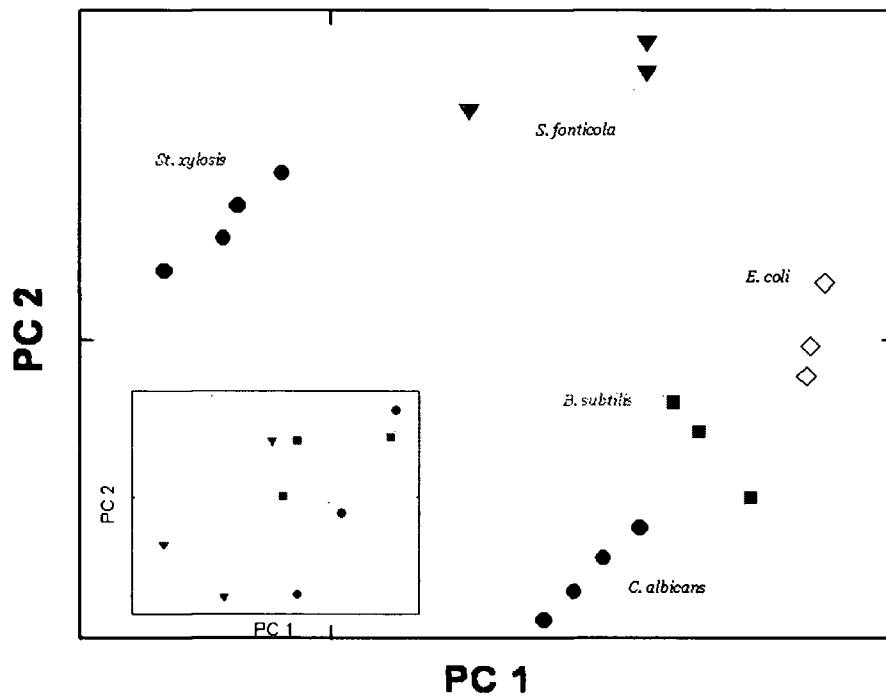


Figure 4.9: Pattern recognition plot generated from dielectric spectra obtained in the presence of different microbial strains

## 4 Results

Amphotericin B (Figure 4.10) is a polyene macrolide antibiotic that is widely used for its antifungal activity and acts by forming ion channels in the presence of sterols (cholesterol or ergosterol) in the membrane [94].

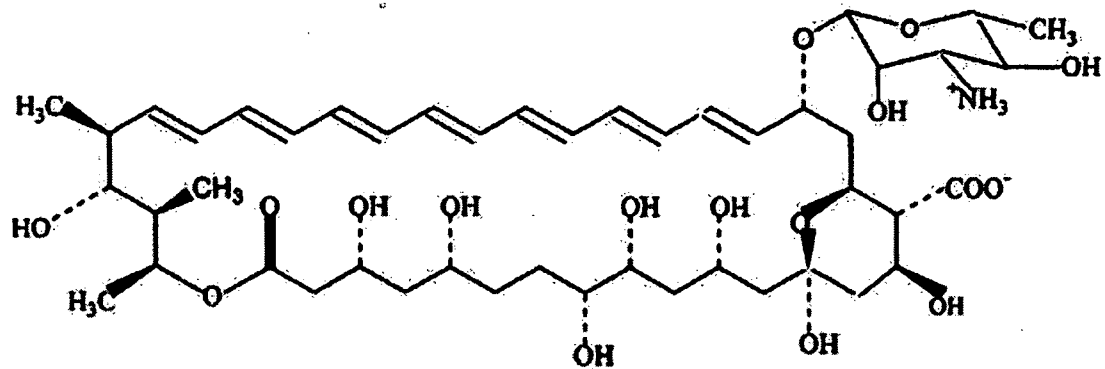


Figure 4.10: Chemical structure of the polyene Amphotericin B.

Table 4.2: Background subtracted impedance signals and corresponding phase angle values ( $\theta$ ) at 50 kHz

Treatment	<i>C. albicans</i>		<i>P. pastoris</i>	
	untreated	$-210 \pm 28\Omega$	$-74^\circ$	$-371 \pm 16\Omega$
AmpB ( $5\mu\text{gmL}^{-1}$ )	$1651 \pm 43\Omega$	$-80^\circ$	$1105 \pm 38\Omega$	$-78^\circ$
sonication	$2160 \pm 9\Omega$	$-81^\circ$	$2000 \pm 28\Omega$	$-82^\circ$

Results of this study are listed in Table 4.2 and Figure 4.11 including impedance and phase angle values of live, dead and plasma membrane disrupted cells. The results show that the living cells and the cells under AmpB influence are clearly distinguished by impedance signal whereas the by sonication disrupted cells exhibit similar impedance signals. It is evident that a brief exposure to the antimicrobial agent Amphotericin B can be readily detected using the present sensor geometry. Additionally, pretreated cell suspensions were also plated on agar plates confirming the high killing efficiency of the sonication treatment, while significant cell growth was observed with samples of Amphotericin B treated yeast samples (data not shown).

#### 4 Results

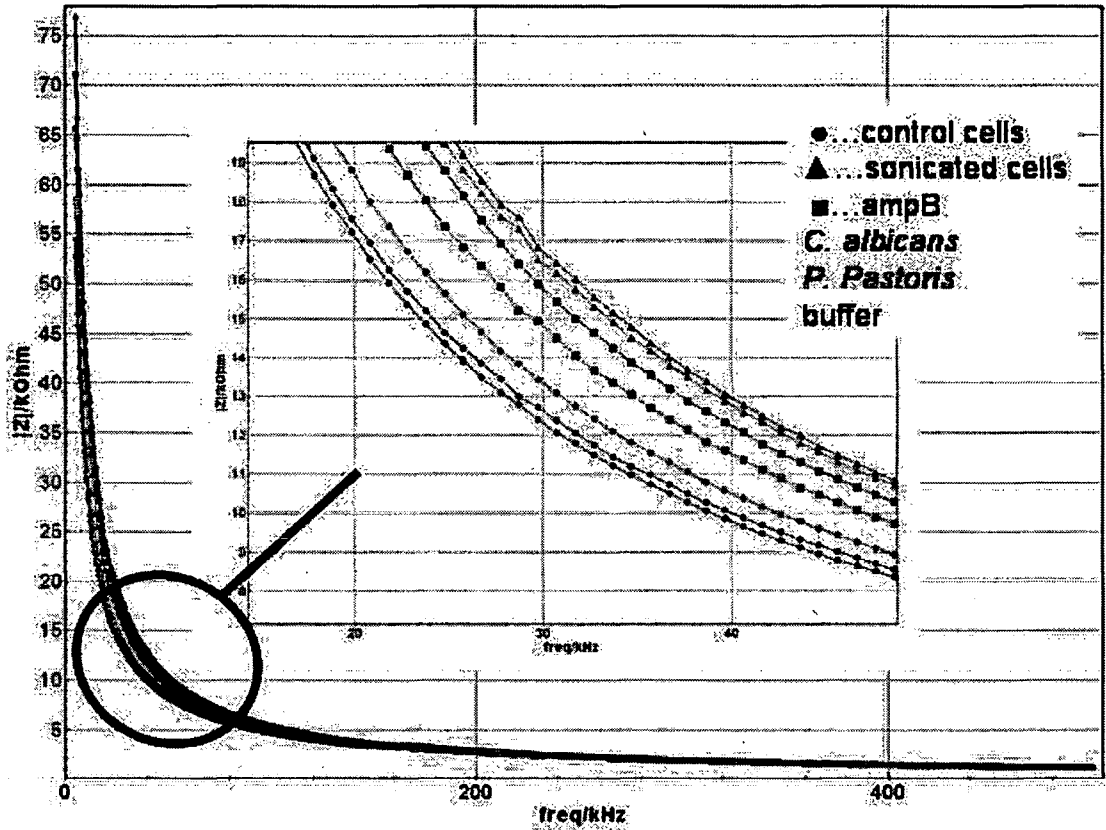


Figure 4.11: Sensor response to morphological changes over a wide range of frequencies (5 to 500  $kHz$ ). Cells were either sonicated or exposed to AmpB. Inset highlights the frequency range where sensor signals were mostly distinguishable.

## 4.2 On-chip cultivation of yeasts

### Characterization of the fluidic system

**Flow profile of the pump** When microorganisms are cultivated on chip a peristaltic pump is used. The pannel on the pump only shows the "rpm" instead of the real flow rate. Therefore the corresponding flow rates ( $\mu\text{L}/\text{min}$ ) to the rpm were calculated by measuring the weight difference of an eppendorf tube after a defined pumping time. In Table 4.3 only the settings "low" and 0.5 rpm are shown, because they are used during cultivation of fungal biofilms. Figure 4.12 shows corresponing flow rates of the peristaltic pump from "low" to 5 rpm. Using the peristaltic pump we are able to obtain linear flow rates over a wide pumping range.

Table 4.3: Calculation of flow rates of the peristaltic pump

velocity	"low" setting		0.5 rpm	
time in min	water in g	flow rate in mL/min	water in g	flow rate in mL/min
5	0.001	$2.00 \times 10^{-4}$	0.0046	$9.20 \times 10^{-4}$
10	0.0016	$1.60 \times 10^{-4}$	0.0095	$9.50 \times 10^{-4}$
15	0.0031	$2.07 \times 10^{-4}$	0.0144	$9.60 \times 10^{-4}$
20	0.0041	$2.05 \times 10^{-4}$	0.0195	$9.75 \times 10^{-4}$
25	0.0054	$2.16 \times 10^{-4}$	0.0242	$9.68 \times 10^{-4}$
	<i>Avg</i> = $0.2 \pm 0.02 \mu\text{L}/\text{min}$		<i>Avg</i> = $0.95 \pm 0.02 \mu\text{L}/\text{min}$	

**Testing the microfluidic system** The following paragraph talks about characterization of complex fluidics using AgCl precipitation chemistry to visualize flow pattern within the microchip. This is particularly important to determine flow directions in complex fluidic layouts as shown in Figure 4.13. To visualize flow path two different liquids (0,01 M solutions of KCL and AgNO<sub>3</sub>) are simultaneously pumped into the microfluidic system. The experiment consists of two parts. First KCL solution is introduced through the middle channel whereas both outer channels are filled with DI water. This step verifies that no unspecific precipitation reactions occurred, in a second

## 4 Results

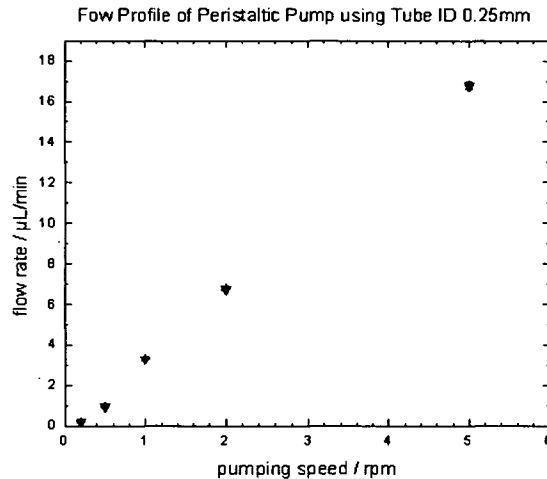


Figure 4.12: *Corresponding flow rates to turning velocity (rpm) with a peristaltic pump.*

step DI water is subsequently replaced by  $\text{AgNO}_3$  solution. At the interface of both liquids AgCl precipitates. After a certain lag of time the precipitation occurred exactly in the middle of the y-shaped channel.

Figure 4.14 shows typical behavior of parabolic flow in microchannels when large particles are centered in the middle of the channel when high flow rates are driven.

### **Adaptation of the passivation layer to experimental conditions**

During experiments using high salt concentrations irreversible damages to the epoxy resin (as can be seen in Figure 4.15). These damages might have been appeared due to undefined chemical reactions. Furthermore, SU8 resin was not suitable to handling conditions since it was ruptured after PDMS removal or easily fractionated during washing processes. Consequently we eliminate SU8 for further experimentation. The remaining passivation consisted of 100 nm  $\text{SiN}_x$  and 200 nm SOG.

### **Surface modification with APTS**

To overcome above stated problems we replaced the hydrophobic resin SU8 with APTS in an effort to create uniform surface properties. This is important in microfluidic channels because of the large surface to volume ratios. APTS (3-aminopropyltriethoxysilane) is a silane that can be covalently bonded onto glass and PDMS sur-

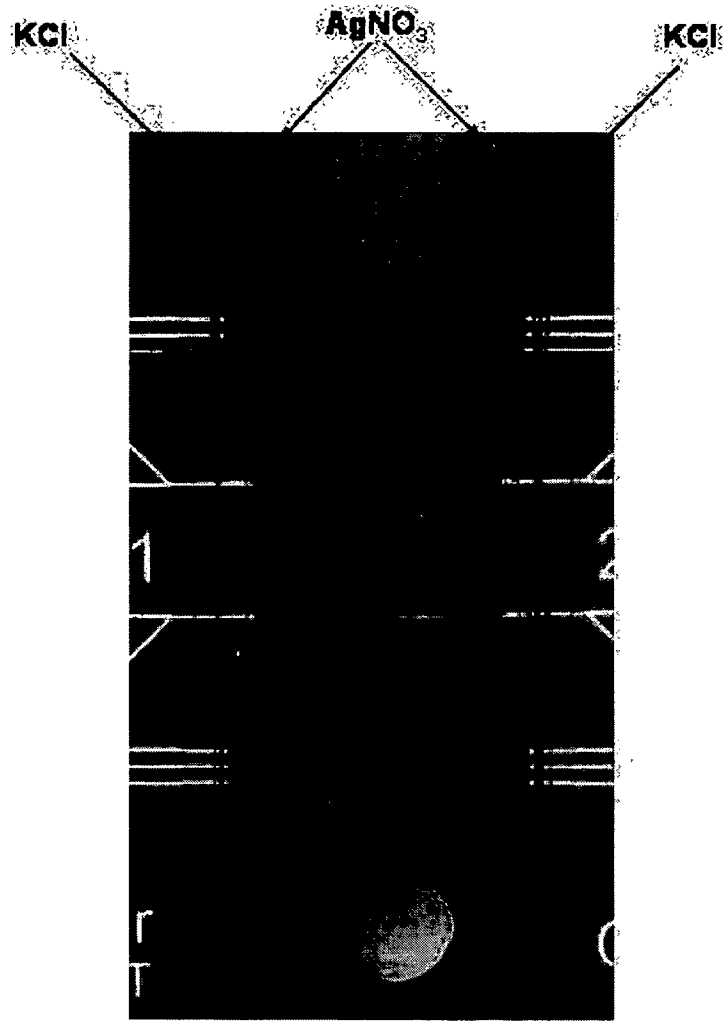


Figure 4.13: AgCl precipitation in a complex microfluidic system.

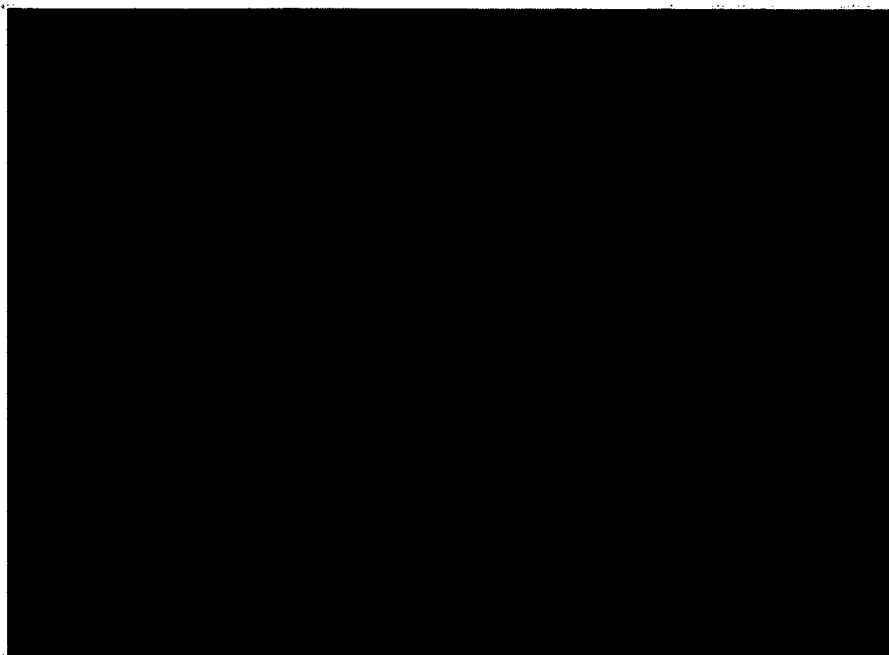


Figure 4.14: Particle transportation in a complex microfluidic channel system.

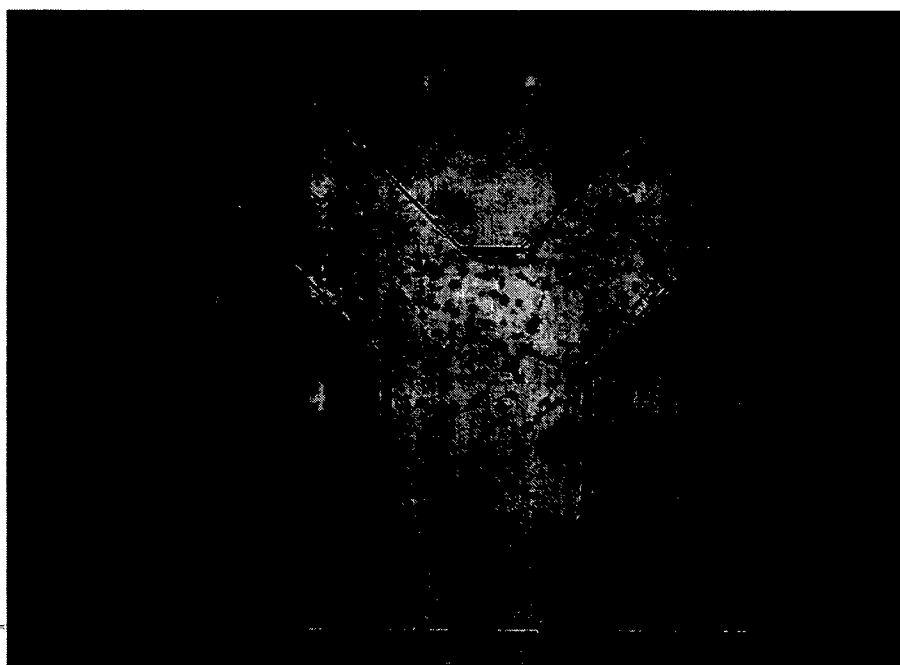


Figure 4.15: Observed damages to epoxy layer during long term experimentation

## 4 Results

faces [26] to enhance hydrophilic habits of an in general hydrophobic surface as it is on PDMS. The basic building block of silanes are monomeric silicon compounds with four substituent groups attached to the silicon atom. These substituent groups can be nearly any combination of nonreactive, inorganically reactive, or organically reactive groups. In case of this work the silane is bonded with three ethoxy groups onto the chip surface, while presenting an aminopropyl tail. It follows that high tension forces occurring between hydrophilic and hydrophobic interfaces may be overcome. This makes it easier to fill small PDMS-channels with watery solutions like cultivation media or buffers.

In this work three different modification solutions were tested. 0,5% APTS in DI-water (solution 1), 2% APTS in methanol and 0,15 M acidic acid (solution 2) and 20 mM APTS in toluol (solution 3) were used to modificate glass slides and PDMS channels. In order to modify PDMS channels, a PDMS polymeric fluidic was put on top of a microscope glass slide to form microfluidic channels. In the next step 3  $\mu$ L of each solution moved through by capillary forces, followed by intense washing. The PDMS channels were removed and the glass slides were hard baked for 30 min at 120°C in order to support covalent bonding events and to harden the APTS layer.

While solution 1 (APTS in water) is a very unstable solution, because APTS is precipitating within minutes to hours due to its sensitivity to water. Solution 3 (APTS in toluol) caused massive swelling of the PDMS. The swelling indicates that PDMS easily takes up toluol, which is toxic. Therefore it can not be guaranteed, that the solvent is entirely removed, when biological experiments are performed. In contrast solution 2 (APTS in methanol) was easiest to handle and did not show above mentioned problems.

Using solution 2 for surface modification prior surface oxidation was performed by oxygen plasma or chemical treatment. Figure 4.16 shows an APTS modified channel after chemical treatment. Figure 4.17 shows an APTS modified glass slide after oxygen plasma treatment and the corresponding height (2  $\mu$ m) of the APTS layer. APTS layers after chemically treated surfaces are much thinner than layers after oxygen plasma treatment. Therefore PDMS pieces and glass slide were chemically treated in order to oxidize surfaces. The results of contact angle measurements are presented in Figure

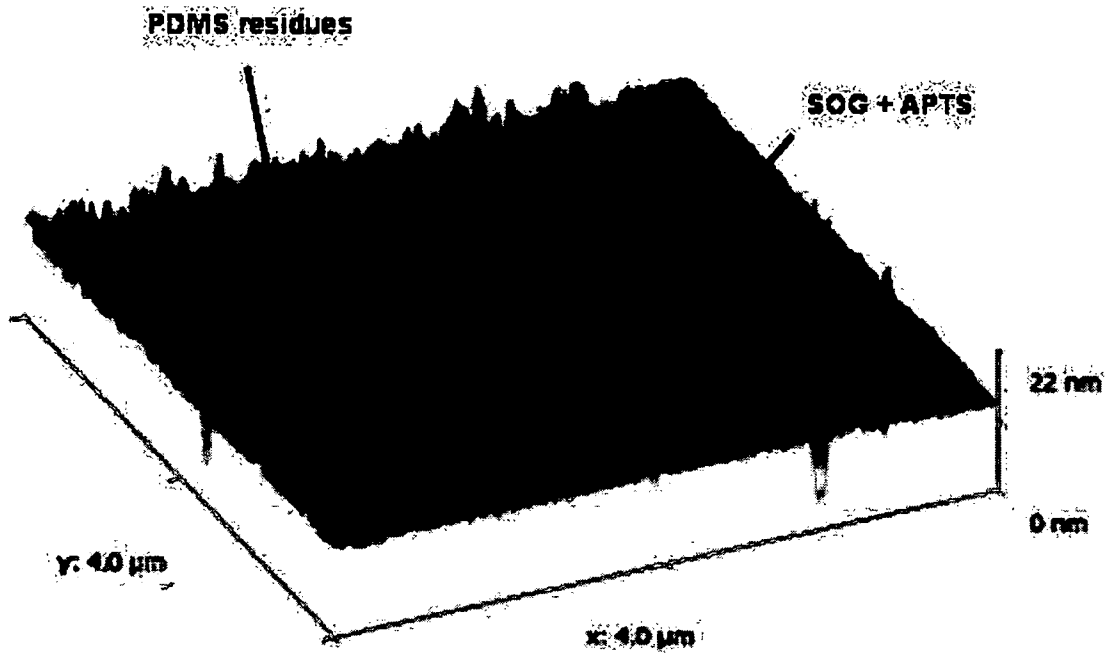


Figure 4.16: AFM image of an SOG surface after modification of an PDMS channel with APTS

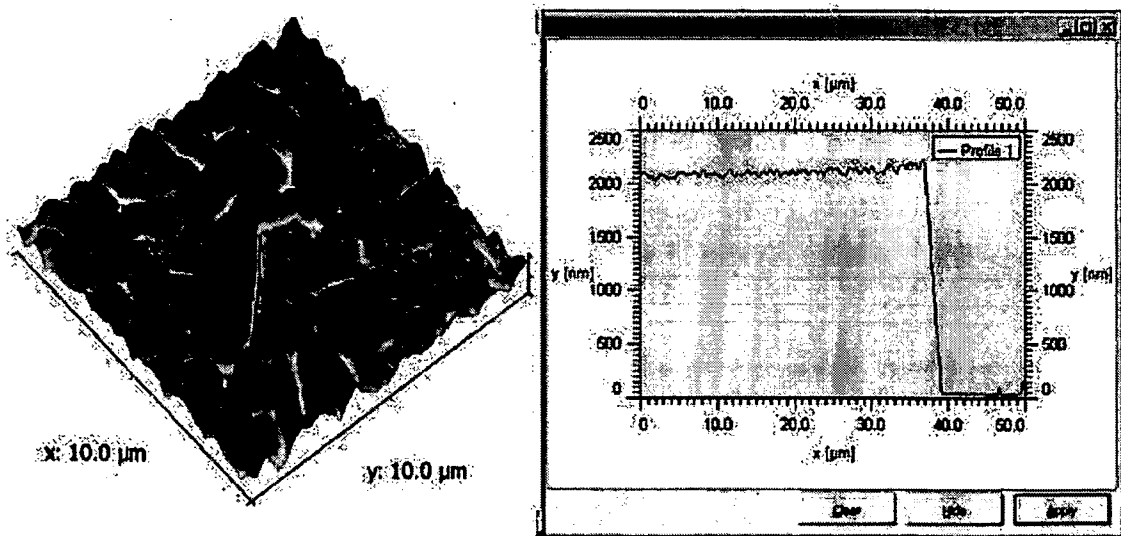


Figure 4.17: AFM image and height measurement of an APTS layer after oxygen plasma treatment of a glass surface.

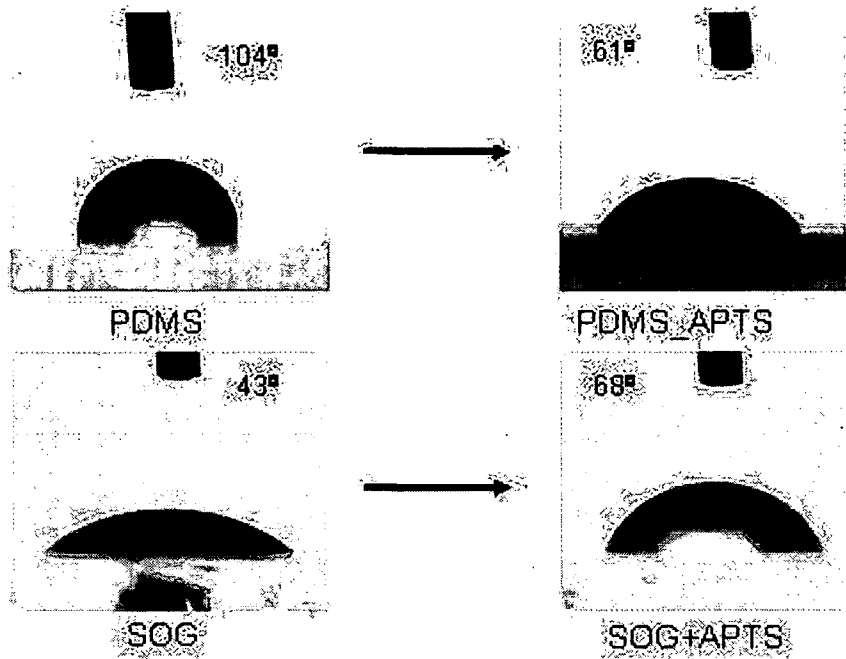


Figure 4.18: Surface wetting angles after wet chemistry surface oxidation and APTS modification.

4.18. The experiments for determination of wetting angles was performed in other Seibersdorf laboratories. The contact angle of DI water on PDMS surface changed from  $104^\circ$  to  $61^\circ$  after APTS modification, while the contact angle of water on SOG changed from  $43^\circ$  to  $68^\circ$ .

#### 4.2.1 On-chip cultivation

After performance of the setup optimization and surface modification, we started to conduct a series of experiments with yeast cells. First step was the optimization of the cell seeding. After performing some protocols including direct pipetting into the entry and/or sucking into the small and/or big waste, we decided to gravimetricly seed the cells. This means that a pipet-tip is tightly fitted into the cell seeding port and filled by pumping medium through the microfluidic system. In the next step the cells were taken from the agar plate and re-suspended in PBS at an  $OD_{600}$  equals 1. Then  $10 \mu L$  suspension is pipetted on top of the prefilled pipet-tip. Once the presence of cells in the proliferation chamber was confirmed the seeding port was closed and the

#### 4 Results

flow was turned to  $0.2 \mu\text{L}/\text{min}$ . After removing the seeding pipet-tip and closing the cell seeding ports the flow of  $0.2 \mu\text{L}/\text{min}$  was hold for 1 hour until the flow was turned to  $0.5 \mu\text{L}/\text{min}$ .

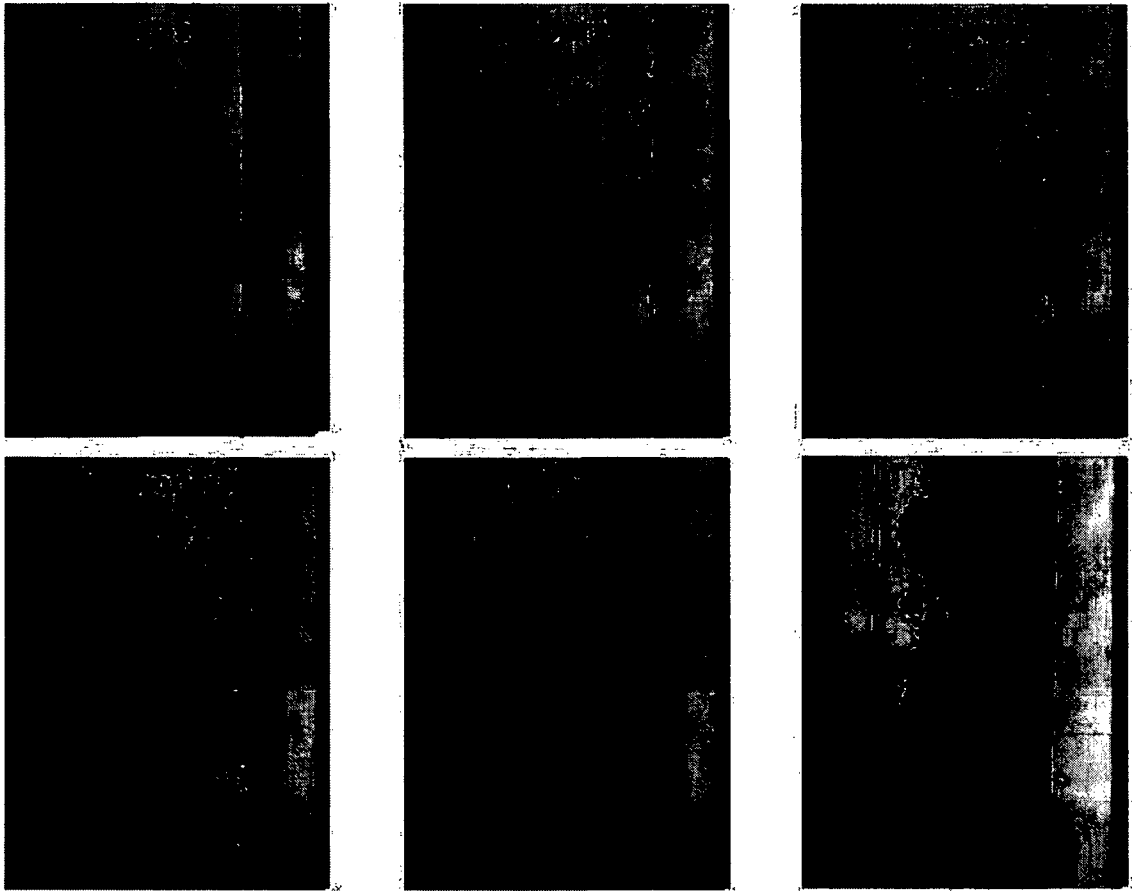


Figure 4.19: *Candida albicans* growing on chip not forming a biofilm at a flow rate of  $0.2 \mu\text{L}/\text{min}$

Yeast cells, *Candida albicans* showed different morphologies depended on the flow rate and therefore the applied shear stress. When *Candida* was cultivated on chip at a flow rate of  $0.2 \mu\text{L}/\text{min}$  single micro-colonies were established as it also observed in standard agar plate or vessel cultures (see Figure 4.19). However, at a flow rate of  $0.95 \mu\text{L}/\text{min}$  *Candida* triggered morphogenesis (see Figure 4.20). After a long period of adoption, the cells started to establish a biofilm forming pseudohyphae. During the first five hours many cells proverbial exploded and were killed, while some cells survived the high shear forces and started to build biofilm structures. It can also be observed that cells under high shear stress grow much slower than cells not building

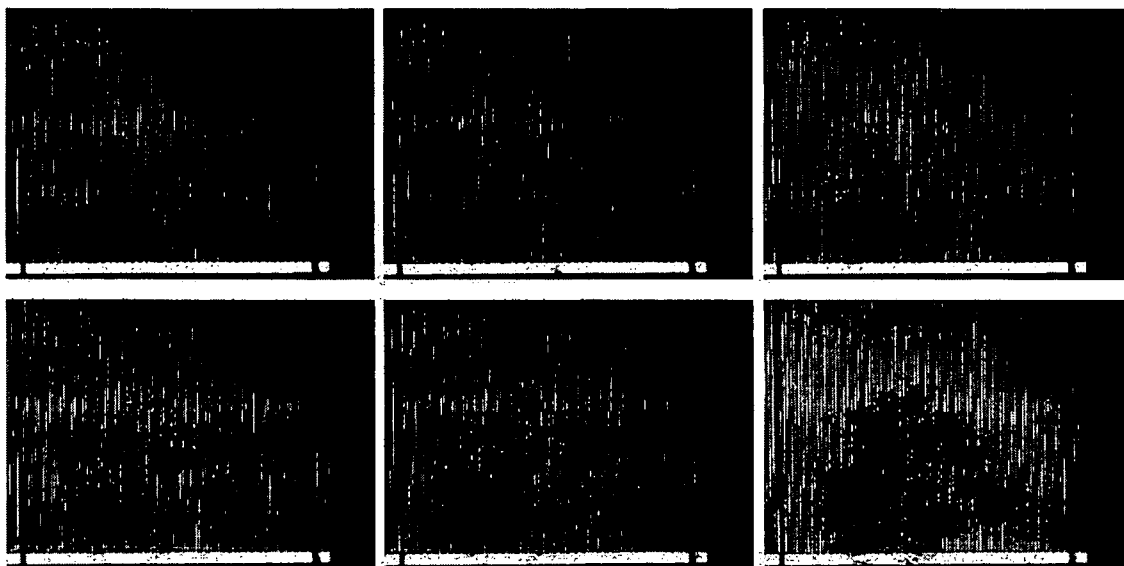


Figure 4.20: *Candida albicans* growing on chip forming a biofilm at a flow rate of  $0.95 \mu L/min$

biofilms.

#### Time laps microscopy

In this experiment the area expansion rates of yeast micro colonies were monitored in order to investigate growth characteristics of yeast cells. We accomplished this using time lapse microscopy. The area expansion rates of micro colonies in the absence and present of fluid flow ( $0, 12 \mu L/min$ ) area expansion were measured with Leica software tools. We randomly selected a number of micro colonies, that were clearly separated from each other. Colonies of approximately the same size were selected. Prior to measurement the leica software had to be calibrated using features of defined sizes such as the length and the width of the  $\mu IDES$ . Subsequently the expansion rates of six colonies over the period of  $5h$  were monitored. In the absence of continuous media supply, surface expansion rates followed known growth characteristics of liquid batch cultures. In the presence of fluid flow, however, cell growth was significantly influenced exhibiting linear growth rates (colony diameter in flow direction) of  $8.3$  and  $12.5 \mu m h^{-1}$ , respectively. Figure 4.21 shows a comparison of calculated expansion rates of *C. albicans* microcolonies in the absence and presence of fluid flow while the Figures 4.22 and 4.23 show the corresponding pictures at the beginning of the measurement

## 4 Results

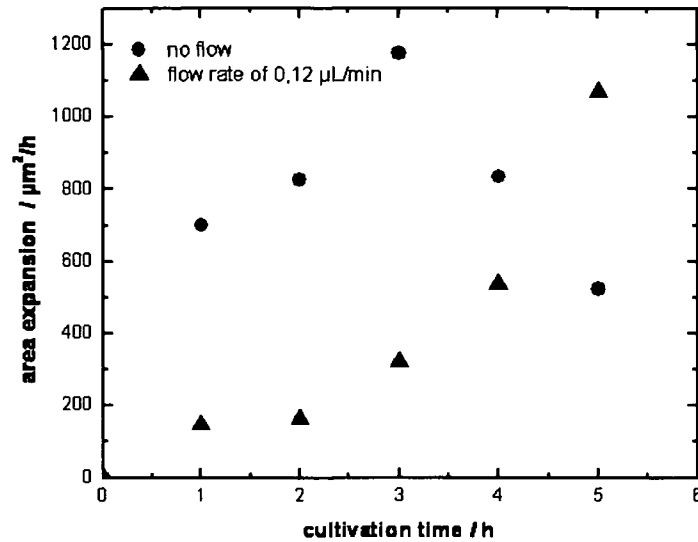


Figure 4.21: Comparison of calculated area expansion rates of *C. albicans* in the absence and presence of fluid flow

and after 5 hours.

### Bioimpedance using contact-less dielectric microsensors

Next, we showed dynamic response of surface grown yeast cultures at increasing shear forces using our contact less dielectric sensor. Impedance measurements were used to continuously monitor dynamic responses of the biofilms to shear stress following a four fold increase in flow velocities. Figures 4.24 and 4.25 show dielectric growth profiles of *P. pastoris* and *C. albicans* in the presence of alternating flow rates. Impedance values increased during measuring *P. pastoris*, while the impedance values decreased during measurements of *C. albicans*. Both graphs start at a measuring time of five hours.

Before this time the measurement was disturbed by handling processes. Following cell seeding, cell populations of both strains increased steadily over a period of 13 h for *P. pastoris* and 17 h for *C. albicans* until a flow rate increase (red arrow) from 0.12  $\mu\text{L}/\text{min}$  to 0.5  $\mu\text{L}/\text{min}$  caused an initial loss of cells. The loss of cells results in a converse signal response in both cases, thus a signal increase for *C. albicans* and a signal decrease for *P. pastoris*. However, *P. pastoris* cell population remained constant

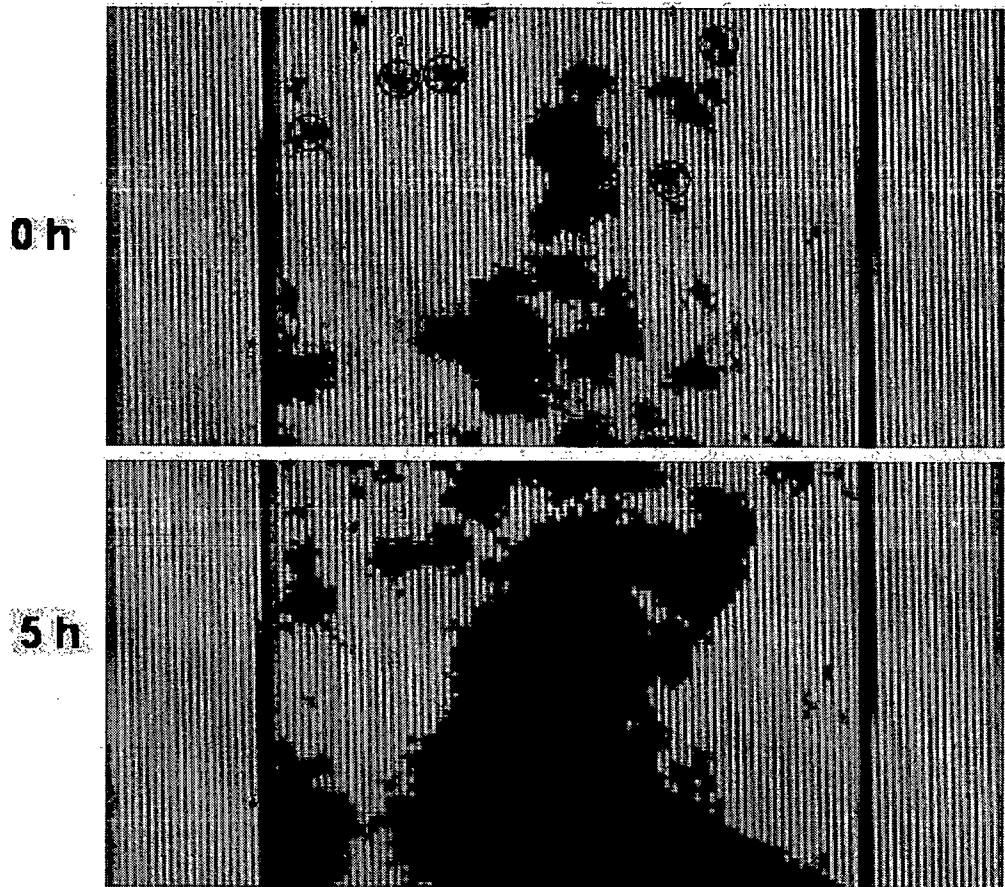


Figure 4.22: *C. albicans* micro colonies selected for time laps microscopy at the absence of fluid flow.

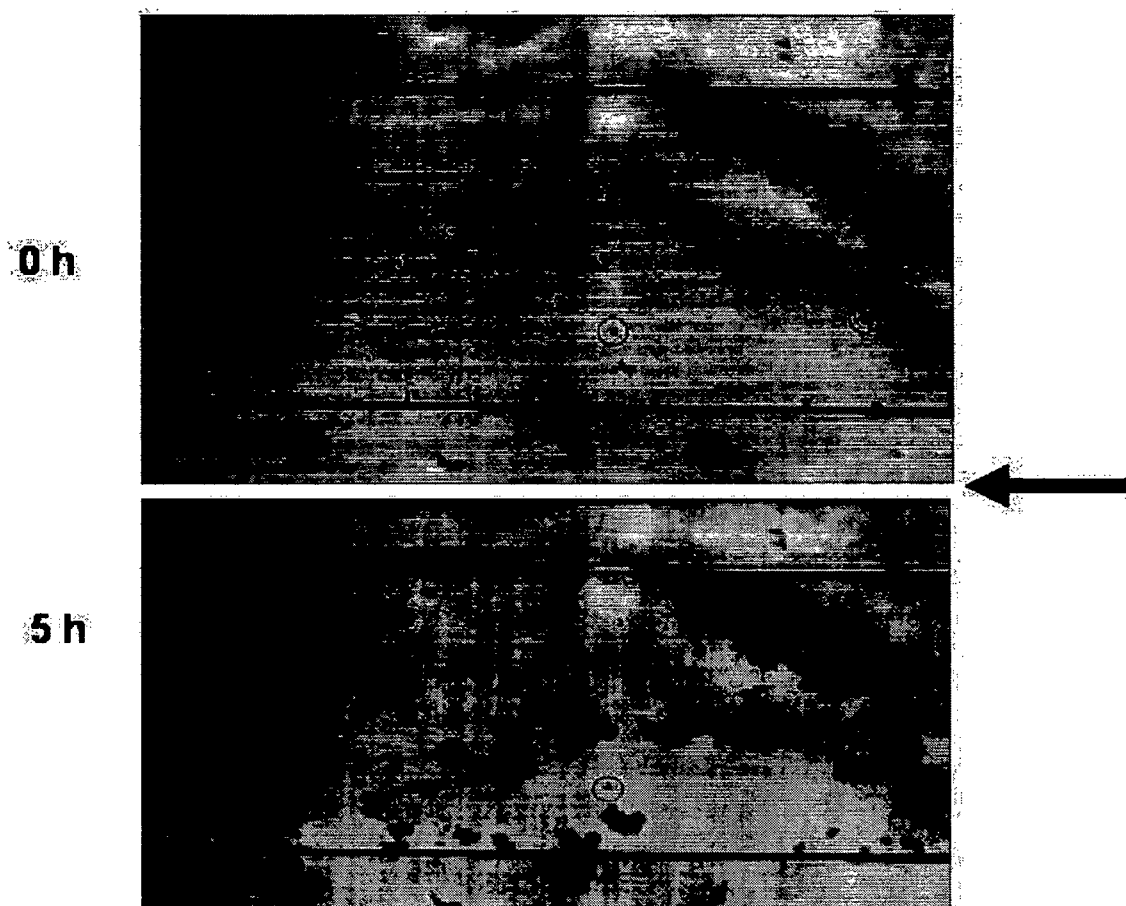


Figure 4.23: *C. albicans* microcolonies selected for time laps microscopy at the presence of fluid flow ( $0.12 \mu\text{L}/\text{min}$ ). Arrow indicates flow direction.

## 4 Results

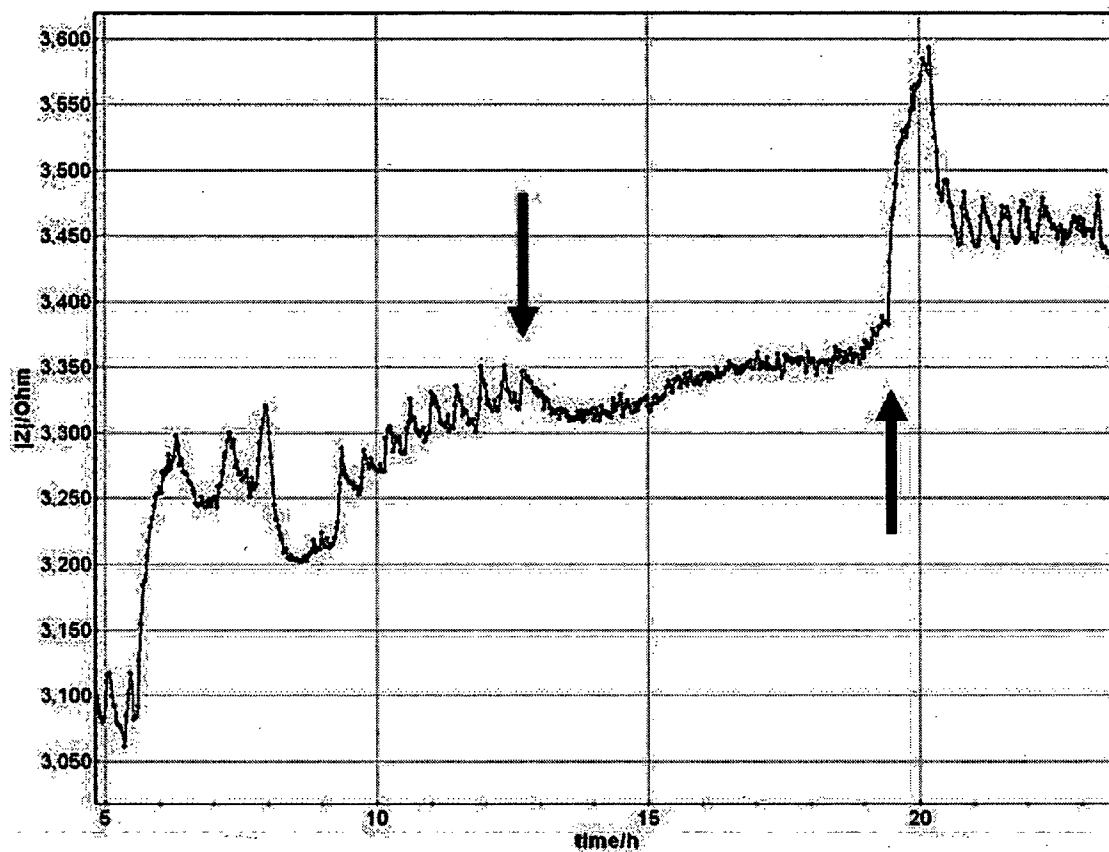


Figure 4.24: Growing profile of *P. pastoris* at alternating shear stress ( $0.12 \mu\text{L}/\text{min}$  to  $0.5 \mu\text{L}/\text{min}$  flow rate) monitored with bioimpedance using contact less micro electrodes. Red arrow indicates increase of flow rate, black arrow indicates decrease of flow rate. Impedance values increase with time and cell growth.

## 4 Results

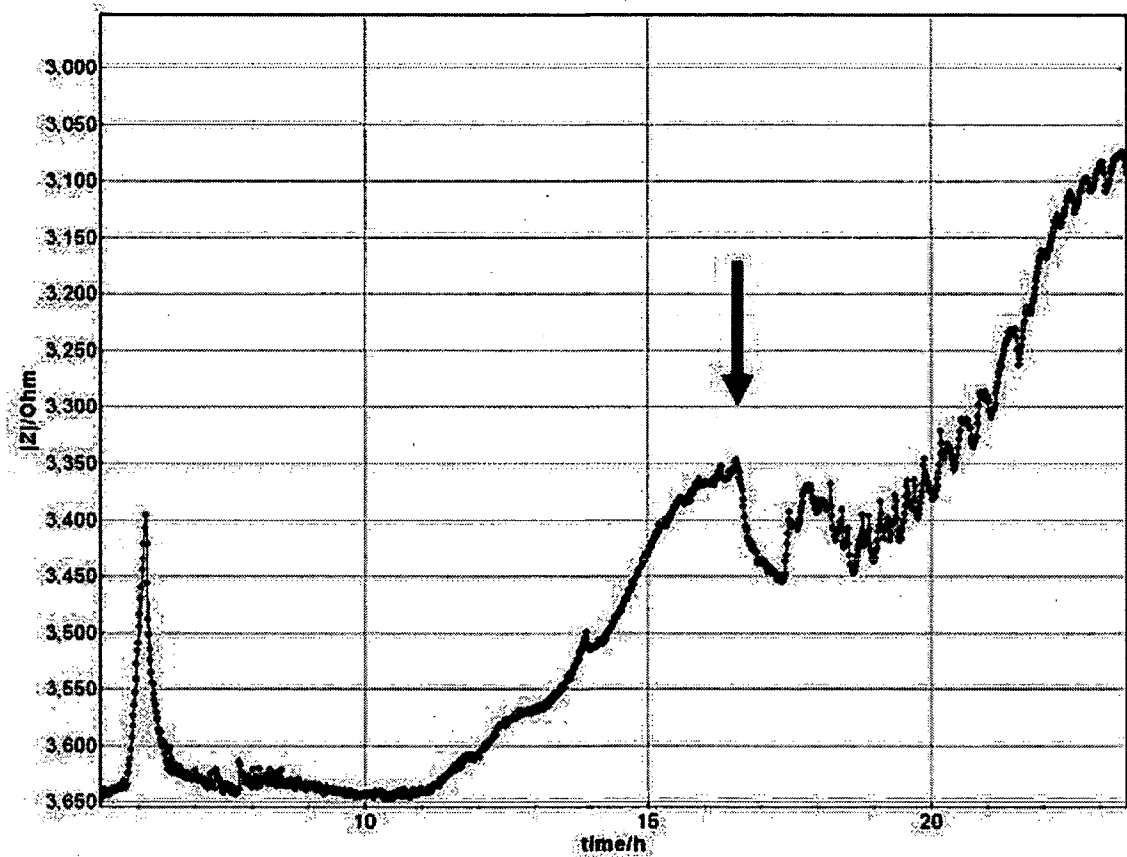


Figure 4.25: Growing profile of *C. albicans* at alternating shear stress ( $0.12 \mu\text{L}/\text{min}$  to  $0.5 \mu\text{L}/\text{min}$  flow rate) monitored with bioimpedance using contact less micro electrodes. Red arrow indicates increase of flow rate. Impedance values decrease with with time and cell growth.

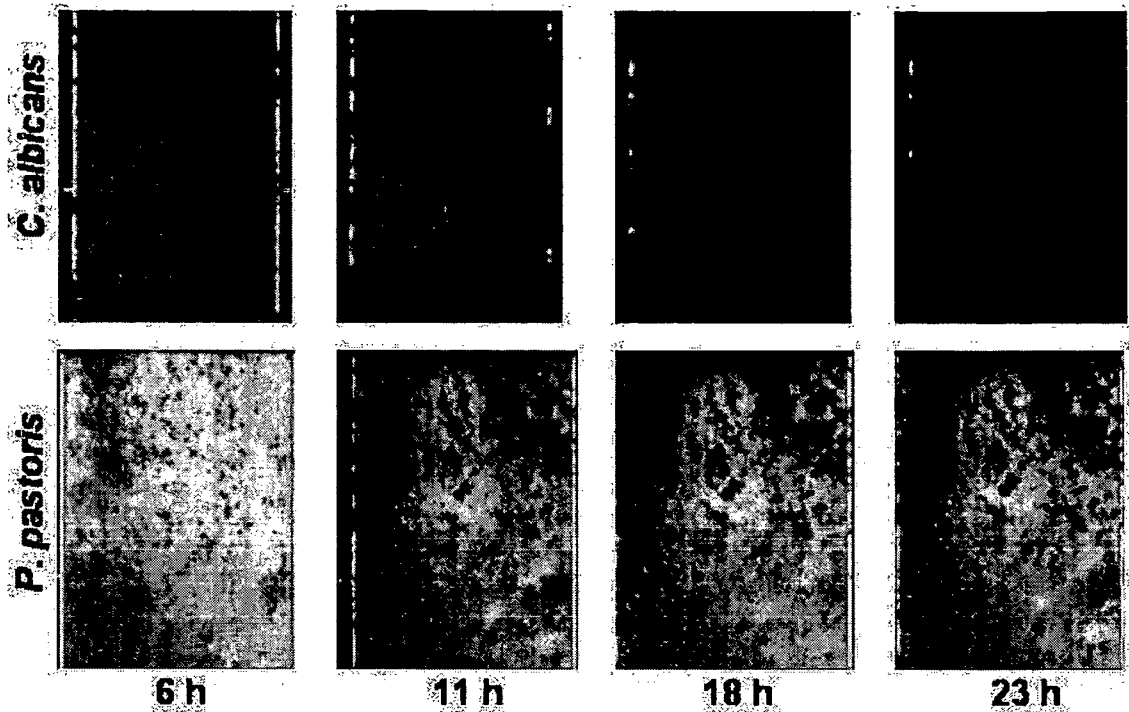


Figure 4.26: Corresponding pictures taken during the growth profile measurements of *P. pastoris* and *C. albicans*.

over a period of 6 h by washing out newly formed cells. When the flow rate was switched back to  $0.12 \mu\text{L}/\text{min}$  (black arrow) the signal rapidly increased again. In contrast *C. albicans* continued to spread after an increase in flow rate until it completely covered the proliferation chamber, which was the cause for a flattening signal in the period of 22 h to 23 h.

### 4.3 On chip monitoring of *Candida* biofilms

So far, it is possible to monitor yeast cell growth, cell death and morphology changes within cell populations. As we observed that our sensor distinguished between cells of different morphologies, like bacteria and yeast and even different yeast strains, we intent to find out if the sensor response is actually dependent on different morphological structures within cells. To do so we selected a well characterized system like Amphotericin B (AmpB) and cellular membranes. Amphotericin B is known to form channels into yeast cell membranes, what results in ion leakage. The cell is no

#### 4 Results

longer able to maintain its membrane potential and dies. Before starting an on-chip experiment we needed to find out the susceptibility of *C. albicans* to AmpB.

##### Antifungal susceptibility of Amphotericin B

To determine the antifungal susceptibility (AS) of *Candida albicans* to Amphotericin B an antibiogram is produced by using various concentrations of AmpB. AmpB dilutions were all prepared in Worth Broth (WB) in a range of 5.00 to 0.02  $\mu\text{g mL}^{-1}$ . A single colony of an 24 h incubated agar plate was harvested and re-suspended in 1 mL WB. This solution was then adjusted to an  $OD_{600} = 1$ . 10  $\mu\text{L}$  of this solution were then used to inoculate 1 mL of the AmpB dilutions in WB. The cells are incubated at 30°C and 1000 rpm for 24 h in a thermo cycler.

Table 4.4: AS of *C. albicans* to different concentrations of Amphotericin B. The minimum inhibitory concentration (MIC) is 0.059  $\mu\text{g L}^{-1}$ .

[AmpB] in $\mu\text{g L}^{-1}$	at $OD_{600}$
5.000	0.159
2.500	0.181
1.250	0.263
0.625	0.360
0.313	0.413
0.156	0.536
0.078	0.749
0.040	3.294
0.020	3.652
negative	4.094

Table 4.4 and Figure 4.27 show the resulting optical densities of *C. albicans* cultures. Between the concentrations 0.040  $\mu\text{g L}^{-1}$  and 0.078  $\mu\text{g L}^{-1}$  of AmpB a clear decrease of growth can be recognized, resulting in minimum inhibitory concentration (MIC) of 0.059  $\mu\text{g L}^{-1}$ . Additionally a slow growth can be noticed at higher concentrations what indicates a growth inhibition and not a killing mechanism by AmpB.

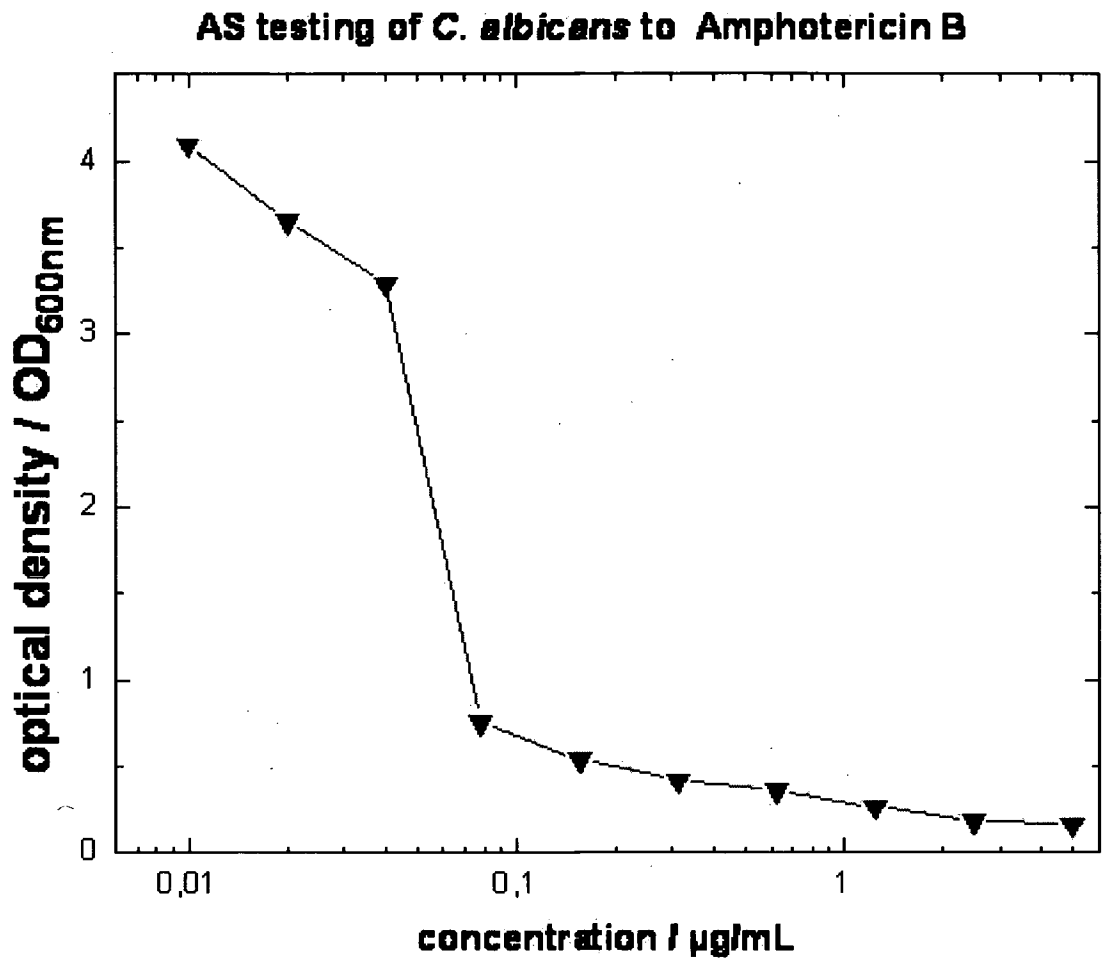


Figure 4.27: Determination of antifungal susceptibility of *C. albicans* to Amphotericin B. A clear decrease between the concentrations of  $0.040 \mu\text{gL}^{-1}$  and  $0.078 \mu\text{gL}^{-1}$  is observable. MIC is  $0.059 \mu\text{gL}^{-1}$

### AmpB on chip

In the next step it was our intention to investigate sensor performance, by studying sensor response to morphological changes in yeast cell population. Using the model compound AmpB we wanted to measure response of cell population to sub-lethal doses of this antibiotic, which was determined in the prior experiment to be  $0.5 \mu\text{g}L^{-1}$ . Figure 4.28 shows the growing behaviour and the viability of *C. albicans* when different concentrations of AmpB were administrated. It can be observed that the cells grow much slower when higher concentrations of AmpB were applied. The viabilities of the control cells and the cells exposed to  $0.5 \mu\text{m}L^{-1}$  AmpB did not remarkably differ from each other. Thus we assumed that the antibiotic was more an growth inhibiting than a destroying agent. According to these results we arranged an on-chip experiment in the next step working with AmpB at a concentration of  $0.5 \mu\text{m}L^{-1}$ . Cell growth is arrested or highly enslowed respectively at these compound concentration ( $0.5 \mu\text{g}L^{-1}$ ) and cell viability remains quite high and stable over long periods of time (5 h) as it was found out in prior experiments (see Figure 4.28). Since it is possible to maintain cell cultures on chip over even longer periods of time due to a steady supply of fresh medium, we want to continuously monitor dielectric changes induced by sub cellular morphological changes. These changes occur when AmpB was incorporated into the cell membrane in order to encourage ion leakage. To investigate the dynamic response of *C. albicans*, sub-lethal doses,  $0.5 \mu\text{g}L^{-1}$ , of the fungicide AmpB were added during on-chip cultivation. After 14 h on chip cultivation at  $30^\circ\text{C}$  in the presence of  $0.12 \mu\text{L min}^{-1}$  flow rate, the *C. albicans* cell population was perfused with medium containing  $0.5 \mu\text{g}L^{-1}$  AmpB. Figure 4.30 shows the dynamic response of the *Candida* biofilm before and after the administration of AmpB (arrow in graph). Prior to administration, the biofilm was allowed to establish over a period of 6 hours covering almost 90% of the proliferation chamber (see Figure 4.29). As it was observed in prior experiments the signal was constantly decreasing when a surface grown cell population was developed. Following the supply of media containing the fungicide, impedance signals started to increase linearly at an initial rate of  $30 \Omega h^{-1}$  along the first 2 hours followed by  $10 \Omega h^{-1}$  (at 50kHz) over a period of 10 hours suggesting a decrease in cell population. However, corresponding pictures (see Figure 4.29) taken every 30 min during the same time period

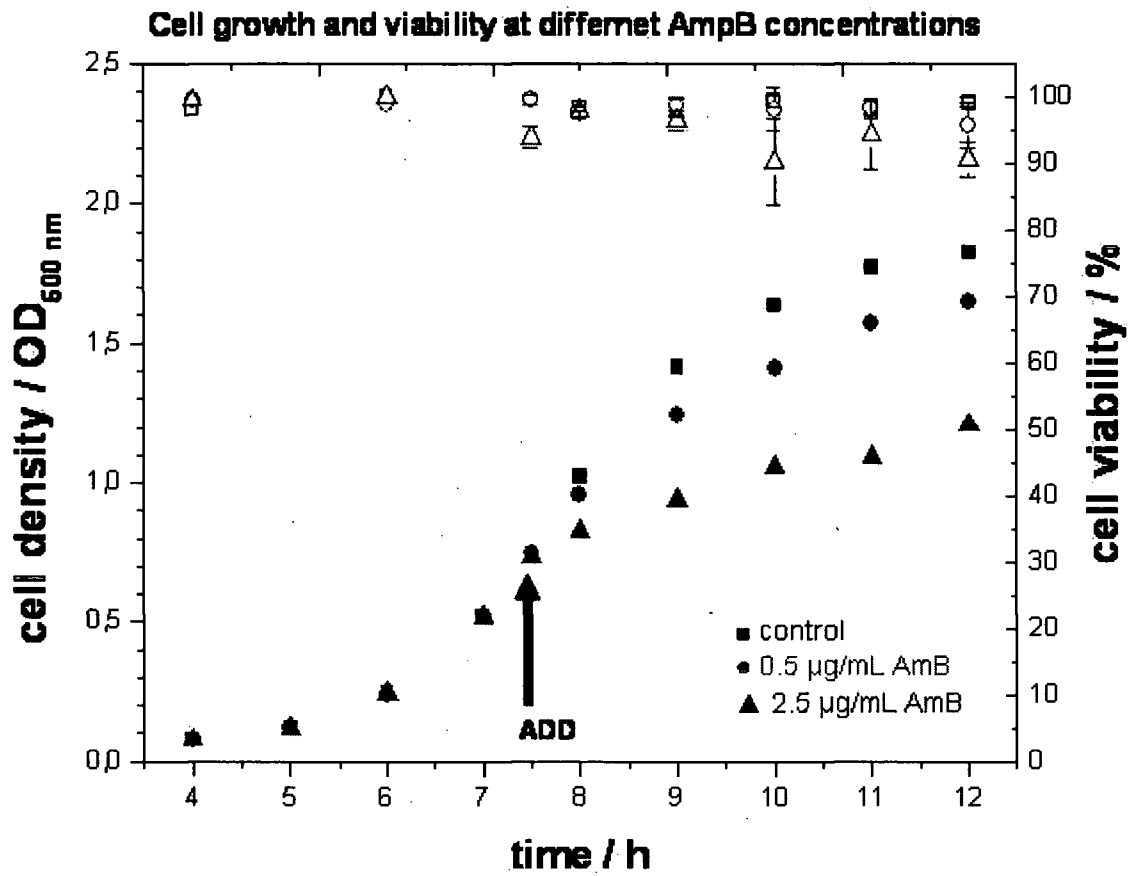


Figure 4.28: *Candida* growth curves (solid symbols correspond to left y-axis) and cell viabilities under standard cultivation conditions (shake flasks) in the absence ( $\square$ ,  $\blacksquare$ ) and presence of  $0.5 \mu\text{g mL}^{-1}$  ( $\circ$ ,  $\bullet$ ) and  $2.5 \mu\text{g mL}^{-1}$  AmpB ( $\triangle$ ,  $\blacktriangle$ ). The solid arrow shows the point of antibiotic administration.

## 4 Results

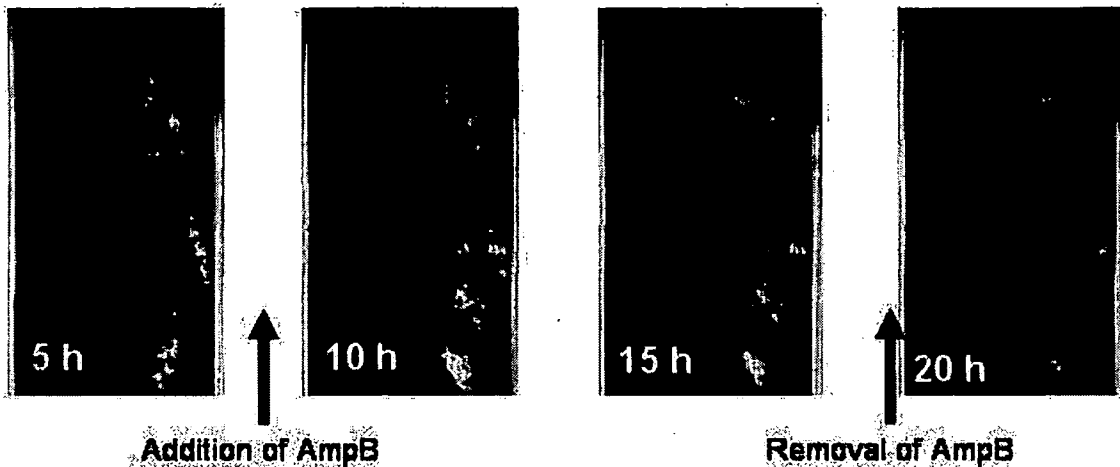


Figure 4.29: *C. albicans* cell population grown on chip under antibiotic pressure. AmpB at a concentration of  $0.5 \mu\text{gL}^{-1}$  was added after 6 hours. AmpB was removed after 20 h of cultivation.

showed that the *Candida* biofilm actually continued to spread at very low rates. Once the administration of AmpB was stopped impedance signals recovered over 3 hours. It is evident that observed signal changes were caused by the dielectric alterations within the plasma membrane due to the presence of AmpB.

### 4.4 Normalization of obtained impedance data

Since we continuously monitor cell responses over 501 frequencies data handling and frequency analysis is an important aspect in our research efforts. This slide shows a 3D plot and corresponding microscope images where cell growth is clearly visible after administration of Amphotericin B. In order to compare impedance signals between all frequencies raw data were normalized according to peak height at time 0. Although the 3D plot in Figure 4.31 shows signal changes occurring at all frequencies biggest variations are found between 20 to 145 kHz.

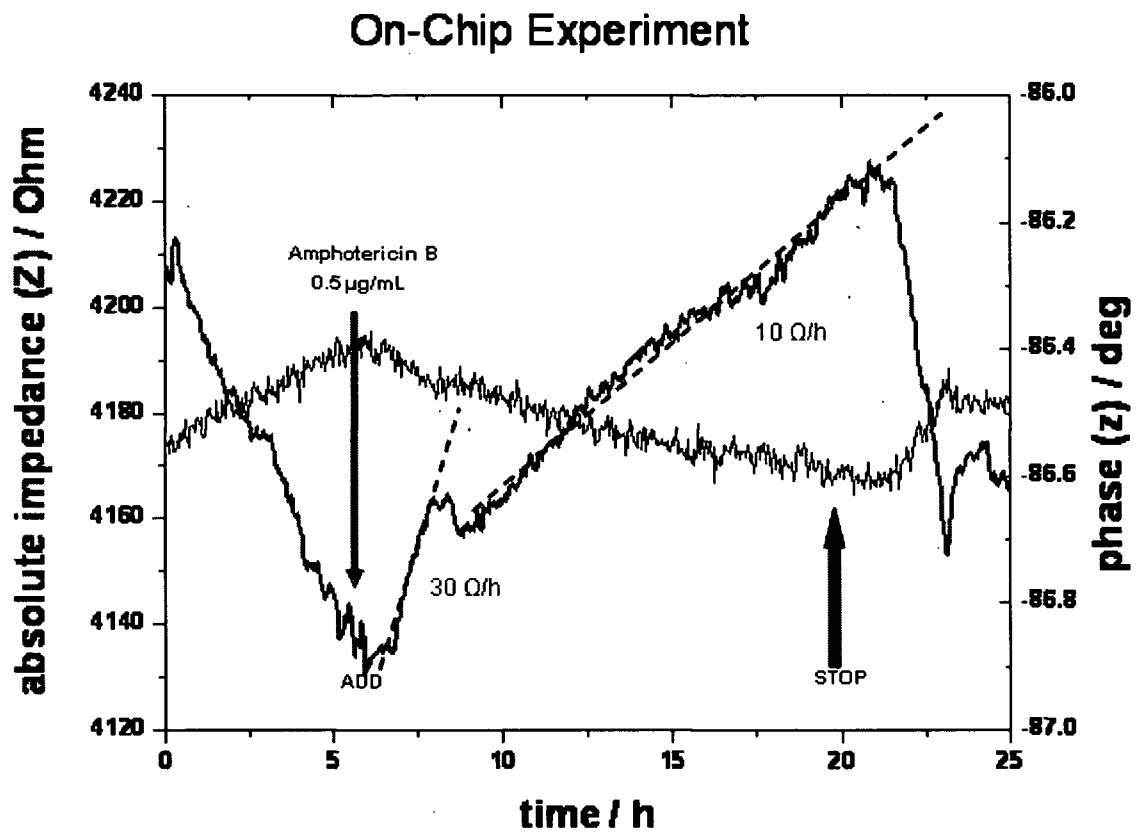


Figure 4.30: *Candida biofilm response to AmpB on chip*. After a period of biofilm establishment (first 6 h), AmpB was added to the medium (thin long arrow). The impedance signal increased with a rate of  $30 \Omega h^{-1}$  for 2 h followed by  $10 \Omega h^{-1}$  for 10 h at  $50 kHz$  until stopping AmpB administration. The signal decreased again.

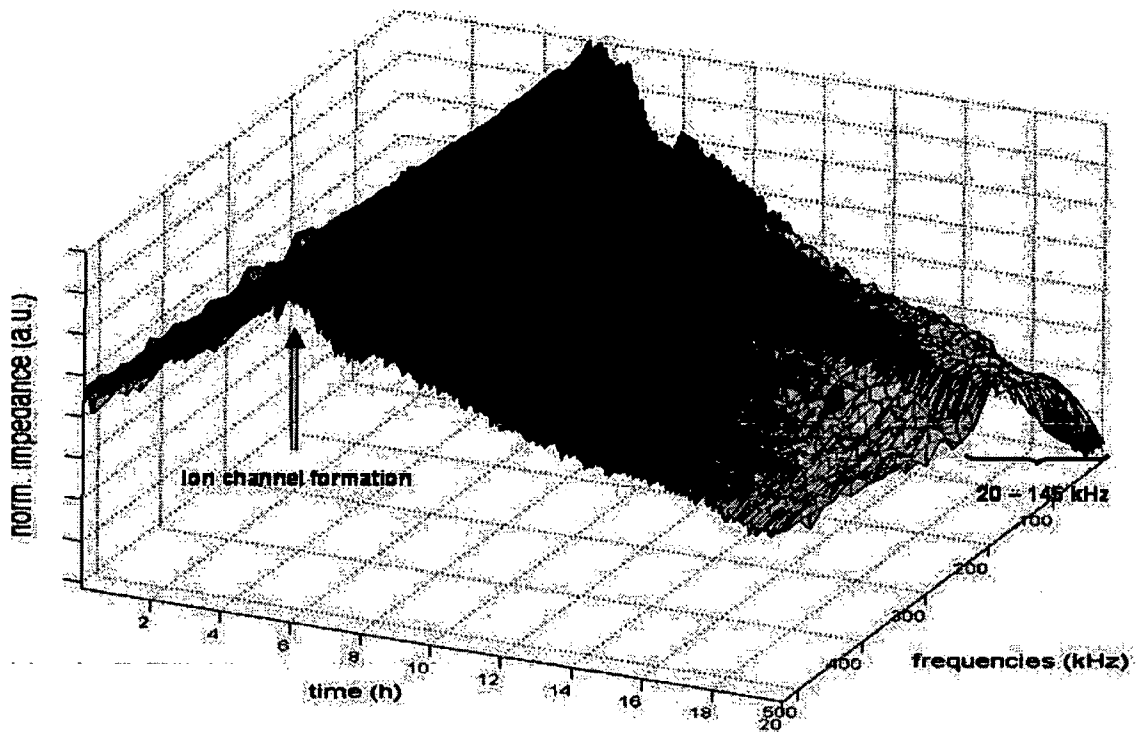


Figure 4.31: 3D plot of obtained data over a wide range of frequencies.

## 5 Discussion

We have developed, characterized and evaluated a microfluidic biochip that is capable of continuously monitoring cell growth and viability. The integrated contactless dielectric microsensor is especially sensitive towards morphological changes such as of viable and dead cells and dielectric differences of microorganisms. This new biosensor consists of high density (200 fingers of  $5\ \mu\text{m}$  width and space) interdigital electrode structures ( $\mu\text{IDES}$ ), which are insulated from the environment by a multipassivation layer consisting of a  $\text{SiN}_x$ ,  $\text{SOG}$  and a  $\text{SU8}$  resin. Calculation with FemLab software showed that 99% of the AC field are located within  $8.1\ \mu\text{m}$  above the passivation layer, so that we can assume that a single layer of yeast cells (diameter about  $5\ \mu\text{m}$ ) is monitored during experimentation. Silicon nitrate and spin-on-glass were selected as adhesion layers and to even out ripples caused by thickness of the electrodes of the  $\mu\text{IDES}$ . Deposition of silicon nitrate and spin-on-glass was also used to increase passivation and sensor stability. The passivation prevents electrode polarization, electrode fouling or bubble formation, thus leading to stable and non-drifting measurement conditions (RSD of 1.5%). The absence of ohmic currents and faradatic contributions makes the imaginary part of the impedance (capacitance) the dominating signal. Furthermore, the sensor showed stable and non drifting measurements, what is rather important for cellmonitoring over long periods of time.

Sensor insulation was tested using CV, capacitance spectroscopy and AFM to screen for optimal passivation performance. Here, optimum passivation led to high performance and elimination of background effects commonly found at bioimpedance experiments. Interferences such as changes in salt, metabolite or protein concentrations are no significant impact to detected dielectric changes occurring at the cell population level. An important feature of the sensor signal is that depending on the biological

composition signals increase or decrease with increasing cell population number. Overall, sensor signals plateau when the detection volume above the sensor is fully filled with cells.

Results of several experiments showed that the sensor discriminates biological cells based on their morphological differences rather than their size. Using chemometrics we generated pattern recognition plots in order to show distinctive groupings for different microorganisms. In theory the sensor could be used to differentiate different organisms within seconds in the absence of any sample preparation. Comparing individual spectra we observed distinct variances at different frequencies. However, further investigations have to be performed to find coherences between cellular morphological structures and applied frequencies during a CDS experiment.

The characterization of the microfluidic system showed most problems, due to cumbersome handling. Another problem posed moving aqueous fluids through a hydrophobic PDMS micro channel system. Consequently, we covalently attached an organo-silane (APTS) to the SOG surface and the PDMS channel walls to create uniform conditions within the chip. In principle a variety of organo-silanes can be used to change surface properties in such hybrid devices. This is of importance since high aspect ratios between surface to volume can effectively remove proteins from supply media.

In initial yeast culture experiments on chip we analyzed the response of *P. pastoris* and *C. albicans* to increase of fluid velocities. We showed that by controlling external parameters like flow rate, thus induced shear stress and temperature it is possible to trigger morphological states of *Candida* cells. Cells undergo a mechanism called morphogenesis, when they change their morphology from single cell state to pseudohyphae establishment. In addition it is possible to control cell numbers by controlling media flow rate and washing out newly formed cells. These findings confirm the fact that it is possible to controllably induce phenotypic switching using a microfluidic system and to dynamically monitor resulting changes in cell growth by using CDS. This platform can be used to investigate the influence of morphology on antibiotic resistance mechanism.

In order to confirm the theory that the biochip is able to monitor phenotypic changes in the presence of fungicides we monitored *C. albicans* growing under antibiotic pres-

## 5 Discussion

sure using  $0.5 \mu\text{g mL}^{-1}$  AmpB. This concentration was chosen because in reference experiments we showed that cell growth is arrested while cell viability is maintained (99%) in standard culture. Previous studies of *Candida* interaction with AmpB under standard cultivation conditions have shown concentration dependent responses leading to a range of physiological states (high/low/no viability and vitality) [95]. By investigating cell growth, membrane integrity and potential as well as intracellular ATP the study showed that in the presence of  $0.5$  to  $1.0 \mu\text{g mL}^{-1}$  AmpB *Candida* loses the ability to replicate, but maintains cell viability and is able to repair occurred membrane damage even after a period of 10 hours. We also performed viability (growing) and vitality (alive) estimations using standard *Candida* cultures. We also found out the strong growth inhibiting effect of the fungicide at  $0.5$  and  $2.5 \mu\text{g mL}^{-1}$ . However, assessment of membrane integrity performed over 6 hours after AmpB administration yielded above 95% and 90% vitality in the presence of  $0.5$  and  $2.5 \mu\text{g mL}^{-1}$ , respectively.

Prior to administration of AmpB in our system, the biofilm was allowed to establish over a period of 6 hours covering almost 90% of the proliferation chamber. After administration the signal started to increase first with a faster rate ( $30 \Omega h^{-1}$ ) followed by a slower rate ( $10 \Omega h^{-1}$ ). The biofilm continued to spread, but signal kept increasing as long as AmpB was administrated. These results are indicative that biological processes are taking place at two different rates in the cell membrane during the exposure of *C. albicans* to AmpB. In other words, the administration of  $2.5 \mu\text{g mL}^{-1}$  AmpB renders the *Candida* nearly incapable of initiating replicative processes while maintaining membrane integrity and metabolic activity (repair mechanism) over a period of 10 hours. These results clearly indicate that the on-chip monitored dielectric changes are caused by morphology changes induced by the incorporation of AmpB into the plasma membranes. Consequently, we are able to observe intracellular structures within a living cell population.

## 6 Conclusion

We have developed a novel microfabricated biofilm analysis platform that provides quantitative results of the continuous monitoring of the adaptive phenotypic changes of the entire life cycle of a cell population. The precise control of critical electrode characteristics, such as size, shape and passivation composition, as well as thickness makes microfabrication an attractive tool for the integration of electrical sensors such as contactless dielectric microsensors. An important feature of the sensor design is the application of electrical insulation making non-invasive, stable and robust measuring conditions possible. The introduction of a dielectric layer above the electrodes allows for the study of cellular dynamics in the absence of background effects. We evaluated the SiNx/SOG/SU-8 multi-passivation layer of 550 nm thickness and characterized the detector configuration utilizing various bacterial and yeast strains. We successfully demonstrated that microorganisms can be readily identified and that any morphological changes induced by external stimuli can be continuously monitored using dielectric sensors. We have also shown that induced shear stress has significant effects on biofilm formation and that, by controlling fluid flow and temperature, growth rates, cell number as well as fungal morphology can be adjusted and used for cell analysis. Using the developed technology we have monitored *Candida* biofilm dynamics and response to the antifungal agent Amphotericin B. Administration of the fungicide at physiological relevant serum concentrations triggered an immediate reaction in *Candida* leading to a stress-induced inability to replicate, while repair mechanisms cope with membrane damages. We also observed time dependent signal changes during AmB administration suggesting two different dynamic responses of *Candida*. The ability to monitor sub-cellular components with high resolution within a cell population is expected to open new insights into cellular dynamics. Extension of this work to quantify biofilm

# Bibliography

- [1] G. Storz and R. Hengge-Aronis, *Bacterial Stress Responses*. ASM Press, 2000.
- [2] A. R. M. Coates, *Dormancy and Low-Growth States in Microbial Disease*. Cambridge University Press, 2003.
- [3] D. Di Carlo, L. Y. Wu, and L. P. Lee, "Dynamic single cell culture array," *Lab Chip*, vol. 6, pp. 1445–1449, Nov 2006.
- [4] E. Odds, "Switch of phenotype as an escape mechanism of the intruder," *Mycoses*, vol. 40 Suppl 2, pp. 9–12, 1997.
- [5] J. Shuford, K. Piper, J. Steckelberg, and R. Patel, "In vitro biofilm characterization and activity of antifungal agents alone and in combination against sessile and planktonic clinical *Candida albicans* isolates," *Diagn. Microbiol. Infect. Dis.*, vol. 57, pp. 277–281, Mar 2007.
- [6] P. S. Dittrich and A. Manz, "Lab-on-a-chip: microfluidics in drug discovery," *Nat Rev Drug Discov*, vol. 5, pp. 210–218, Mar 2006.
- [7] A. Manz, N. Graber, and H. M. Widmer, "Miniaturized total chemical analysis systems: A novel concept for chemical sensing," *Sens. Actuators, B*, vol. 1, no. 1, pp. 244–248, 1990.
- [8] D. R. Reyes, D. Iossifidis, P.-A. Auroux, and A. Manz, "Micro total analysis systems. 1. Introduction, theory, and technology," *Anal Chem*, vol. 74, pp. 2623–2636, Jun 2002.
- [9] P. C. e. a. Simpson, "High-throughput genetic analysis using microfabricated 96-sample capillary array electrophoresis microplates," *PNAS*, vol. 95, pp. 2256–2261, 1998.
- [10] C. Yi, C. Li, S. Ji, and M. Yang, "Microfluidics technology for manipulation and analysis of biological cells," *Anal. Acta Chim*, vol. 560, pp. 1–23, 2006.
- [11] S. C. Terry, J. H. Jerman, and J. B. Angell, "A gas chromatographic air analyzer fabricated on a silicon wafer," *IEEE Trans. Electron Devices*, vol. 26, no. 12, pp. 1880–1886, 1975.
- [12] J. G. Smits, "Piezoelectric micropump with three valves working peristaltically," *Sens. Actuators, A*, vol. 21, no. 1, pp. 203–206, 1990.

## BIBLIOGRAPHY

- [13] F. C. M. van de Pol, H. T. G. van Lintel, M. Elwenshoek, and J. H. J. Fluitman, "A thermopneumatic micropump based on micro-engineering techniques," *Sens. Actuators, A*, vol. 21, no. 1, pp. 198–202, 1990.
- [14] S. Shoji, S. Nakagawa, and M. Esashi, "Micropump and sample-injector for integrated chemical analyzing systems," *Sens. Actuators, A*, vol. 21, no. 1, pp. 189–192, 1990.
- [15] M. Esashi, "Integrated micro flow control systems," *Sens. Actuators, A*, vol. 21, no. 1, pp. 161–167, 1990.
- [16] A. Manz, D. J. Harrison, E. M. J. Verpoorte, J. C. Fettinger, A. Paulus, H. Ludi, and H. M. Widmer, "Planar chips technology for miniaturization and integration of separation techniques into monitoring systems Capillary electrophoresis on a chip," *J. Chromatogr.*, vol. 593, no. 1, pp. 253–258, 1992.
- [17] D. J. Harrison, A. Manz, Z. H. Fan, H. Ludi, and H. M. Widmer, "Capillary Electrophoresis and Sample Injection Systems Integrated on a Planar Glass Chip," *Sensors and Actuators A-Physical*, vol. 64, pp. 1926–1932, Sep 1992.
- [18] M. A. Northrup, M. T. Ching, R. M. White, and R. T. Watson *Transducers'93*, pp. 1926–1932, 1993.
- [19] L. Bousse, R. J. McReynolds, G. Kirk, T. Dawes, P. Lam, and W. R. Bemiss *Transducers'93*, pp. 916–919, 1993.
- [20] D. Sobek, A. M. Young, M. L. Gray, and S. D. Senturia, *Micro Electro Mechanical Systems, Proceedings - An Investigation of Micro Structures, Sensors, Actuators, Machines, and Systems*. IEEE, 2003.
- [21] C. S. Effenhauser, A. Paulus, M. A., and H. M. Widmer, "High-Speed Separation of Antisense Oligonucleotides on a Micromachined Capillary Electrophoresis Device," *Anal. Chem.*, vol. 66, no. 18, pp. 2949–2953, 1994.
- [22] A. T. Woolley and R. A. Mathies, "Ultra-High-Speed DNA Fragment Separations Using Microfabricated Capillary Array Electrophoresis Chips," *PNAS*, vol. 91, no. 24, pp. 11348–11352, 1994.
- [23] G. Fan and D. J. Harrison, "Micromachining of capillary electrophoresis injectors and separators on glass chips and evaluation of flow at capillary intersections," *Anal. Chem.*, vol. 66, no. 1, pp. 177–184, 1994.
- [24] D. Sobek, A. M. Young, M. L. Gray, and S. D. Senturia, *Proceedings of Micro TOTAL Analysis Systems 1994*. Kluwer Academic Publishers, 1994.
- [25] C. D. Chin, V. Linder, and S. K. Sia, "Lab-on-a-chip devices for global health: past studies and future opportunities," *Lab Chip*, vol. 7, pp. 41–57, Jan 2007.
- [26] G. M. Whitesides, "The origins and the future of microfluidics," *Nature*, vol. 442, pp. 368–373, Jul 2006.

## BIBLIOGRAPHY

- [27] D. B. Weibel and G. M. Whitesides, "Applications of microfluidics in chemical biology," *Curr Opin Chem Biol*, vol. 10, pp. 584–591, Dec 2006.
- [28] T. Vilknor, D. Janasek, and A. Manz, "Micro total analysis systems. Recent developments," *Anal Chem*, vol. 76, pp. 3373–3385, Jun 2004.
- [29] P. S. Dittrich, K. Tachikawa, and A. Manz, "Micro total analysis systems. Latest advancements and trends," *Anal Chem*, vol. 78, pp. 3887–3908, Jun 2006.
- [30] P.-A. Auroux, D. Iossifidis, D. R. Reyes, and A. Manz, "Micro total analysis systems. 2. Analytical standard operations and applications," *Anal Chem*, vol. 74, pp. 2637–2652, Jun 2002.
- [31] P. T. Oliver Geschke, Henning Klank, *Microsystem Engineering of Lab-on-a-chip Devices*. Wiley-VCH, 2004.
- [32] P. Yager, "<http://faculty.washington.edu/yagerp/microfluidicstutorial/basicconcepts/basicconcepts.htm>," 2004.
- [33] J. El-Ali, P. K. Sorger, and K. F. Jensen, "Cells on chip," *Nature*, vol. 442, pp. 403–411, Jul 2005.
- [34] M. Berger, J. Castelino, R. Huang, M. Shah, and R. H. Austin, "Design of a microfabricated magnetic cell separator," *Electrophoresis*, vol. 22, pp. 3883–3892, Oct 2001.
- [35] M. Ozkan, M. Wang, C. Ozkan, R. Flynn, A. Birbeck, and S. Esener, "Optical Manipulation of Objects and Biological Cells in Microfluidic Devices," *Biomed. Microdevices*, vol. 5, no. 1, pp. 61–67, 2003.
- [36] H. Mohamed, L. D. McCurdy, D. H. Szarowski, S. Duva, J. N. Turner, and M. Caggana, "Development of a rare cell fractionation device: application for cancer detection," *IEEE Trans Nanobioscience*, vol. 3, pp. 251–256, Dec 2004. Evaluation Studies.
- [37] C. F. Chou, J. O. Tegenfeldt, O. Bakajin, S. S. Chan, and E. C. Cox, "Electrodeless Dielectrophoresis of Single- and Double-Stranded DNA," *Biophys. J.*, vol. 83, pp. 2170–2179, 2002.
- [38] M. J. Mahoney, R. R. Chen, J. Tan, and W. M. Saltzman, "The influence of microchannels on neurite growth and architecture," *Biomaterials*, vol. 26, pp. 771–778, Mar 2005. Evaluation Studies.
- [39] A. Tourovskaia, X. Figueroa-Masot, and A. Folch, "Differentiation-on-a-chip: a microfluidic platform for long-term cell culture studies," *Lab Chip*, vol. 5, pp. 14–19, Jan 2005.
- [40] A. Paguirigan and D. J. Beebe, "Gelatin based microfluidic devices for cell culture," *Lab Chip*, vol. 6, pp. 407–413, Mar 2006.

## BIBLIOGRAPHY

- [41] A. Khademhosseini, R. Langer, J. Borenstein, and J. P. Vacanti, "Microscale technologies for tissue engineering and biology," *Proc Natl Acad Sci U S A*, vol. 103, pp. 2480–2487, Feb 2006.
- [42] C. Prinz, J. O. Tegenfeldt, R. H. Austin, E. C. Cox, and J. C. Sturm, "Bacterial chromosome extraction and isolation," *Lab Chip*, vol. 2, pp. 207–212, 2002.
- [43] C. Yi, Q. Zhang, C.-W. Li, J. Yang, J. Zhao, and M. Yang, "Optical and electrochemical detection techniques for cell-based microfluidic systems," *Anal Bioanal Chem*, vol. 384, pp. 1259–1268, Mar 2006.
- [44] H. Salimi-Moosavi, Y. Jiang, L. Lester, G. McKinnon, and D. J. Harrison, "A multireflection cell for enhanced absorbance detection in microchip-based capillary electrophoresis devices," *Electrophoresis*, vol. 21, pp. 1291–1299, Apr 2000.
- [45] R. Davidsson, F. Genin, M. Bengtsson, T. Laurell, and J. Emneus, "Microfluidic biosensing systems. Part I. Development and optimisation of enzymatic chemiluminescent micro-biosensors based on silicon microchips," *Lab Chip*, vol. 4, pp. 481–487, Oct 2004.
- [46] H. Tani, K. Maehana, and T. Kamidate, "Chip-based bioassay using bacterial sensor strains immobilized in three-dimensional microfluidic network," *Anal Chem*, vol. 76, pp. 6693–6697, Nov 2004.
- [47] X. Y. Peng and P. C. H. Li, "A three-dimensional flow control concept for single-cell experiments on a microchip. 1. Cell selection, cell retention, cell culture, cell balancing, and cell scanning," *Anal Chem*, vol. 76, pp. 5273–5281, Sep 2004.
- [48] E. A. Schilling, A. E. Kamholz, and P. Yager, "Cell lysis and protein extraction in a microfluidic device with detection by a fluorogenic enzyme assay," *Anal Chem*, vol. 74, pp. 1798–1804, Apr 2002.
- [49] E. Tamaki, K. Sato, M. Tokeshi, K. Sato, M. Aihara, and T. Kitamori, "Single-cell analysis by a scanning thermal lens microscope with a microchip: direct monitoring of cytochrome c distribution during apoptosis process," *Anal Chem*, vol. 74, pp. 1560–1564, Apr 2002.
- [50] A. Bard, *Electrochemical Methods: Fundamentals and Applications*. Wiley, 2001.
- [51] P. T. Kissinger and W. R. Heineman, *Laboratory Techniques in Electroanalytical Chemistry*. Marcel Dekker, Inc., 1996.
- [52] K. Asami, "Characterization of biological cells by dielectric spectroscopy," *J. Non-Cryst. Solids*, vol. 305, pp. 268–277, Jul 2002.
- [53] K. Asami, T. Yonezawa, H. Wakamatsu, and N. Koyanagi, "Dielectric spectroscopy of biological cells," *Bioelectrochem. Bioenerg*, vol. 40, pp. 141–145, 1996.
- [54] J. W. Costerton, G. G. Geesey, and G. K. Cheng, "How bacteria stick.," *Sci. Am.*, vol. 238, pp. 86–95, 1978.

## BIBLIOGRAPHY

- [55] R. M. Donlan and J. W. Costerton, "Biofilms: survival mechanisms of clinically relevant microorganisms," *Clin Microbiol Rev*, vol. 15, pp. 167–193, Apr 2002.
- [56] D. G. Davies and G. G. Geesey, "Regulation of the alginate biosynthesis gene *algC* in *Pseudomonas aeruginosa* during biofilm development in continuous culture," *Appl Environ Microbiol*, vol. 61, pp. 860–867, Mar 1995.
- [57] L. J. Douglas, "Candida biofilms and their role in infection," *Trends Microbiol*, vol. 11, pp. 30–36, Jan 2003.
- [58] P. Stoodley, Z. Lewandowski, J. D. Boyle, and H. M. Lappin-Scott, "Oscillation characteristics of biofilm streamers in turbulent flowing water as related to drag and pressure drop," *Biotechnol Bioeng*, vol. 57, pp. 536–544, Mar 1998.
- [59] T. F. Mah and G. A. O'Toole, "Mechanisms of biofilm resistance to antimicrobial agents," *Trends Microbiol*, vol. 9, pp. 34–39, Jan 2001.
- [60] G. O'Toole, H. B. Kaplan, and R. Kolter, "Biofilm formation as microbial development," *Annu Rev Microbiol*, vol. 54, pp. 49–79, 2000.
- [61] J. W. Costerton, Z. Lewandowski, D. E. Caldwell, D. R. Korber, and H. M. Lappin-Scott, "Microbial biofilms," *Annu Rev Microbiol*, vol. 49, pp. 711–745, 1995.
- [62] C. G. Adair, S. P. Gorman, B. M. Feron, L. M. Byers, D. S. Jones, C. E. Goldsmith, J. E. Moore, J. R. Kerr, M. D. Curran, G. Hogg, C. H. Webb, G. J. McCarthy, and K. R. Milligan, "Implications of endotracheal tube biofilm for ventilator-associated pneumonia," *Intensive Care Med*, vol. 25, pp. 1072–1076, Oct 1999.
- [63] J. A. Crump and P. J. Collignon, "Intravascular catheter-associated infections," *Eur J Clin Microbiol Infect Dis*, vol. 19, pp. 1–8, Jan 2000.
- [64] D. G. Maki and P. A. Tambyah, "Engineering out the risk for infection with urinary catheters," *Emerg Infect Dis*, vol. 7, pp. 342–347, Mar 2001.
- [65] P. S. Stewart, "Theoretical aspects of antibiotic diffusion into microbial biofilms," *Antimicrob Agents Chemother*, vol. 40, pp. 2517–2522, Nov 1996.
- [66] M. R. Brown and J. Barker, "Unexplored reservoirs of pathogenic bacteria: protozoa and biofilms," *Trends Microbiol*, vol. 7, pp. 46–50, Jan 1999.
- [67] E. Tuomanen, R. Cozens, W. Tosch, O. Zak, and A. Tomasz, "The rate of killing of *Escherichia coli* by beta-lactam antibiotics is strictly proportional to the rate of bacterial growth," *J Gen Microbiol*, vol. 132, pp. 1297–1304, May 1986.
- [68] K. D. Xu, G. A. McFeters, and P. S. Stewart, "Biofilm resistance to antimicrobial agents," *Microbiology*, vol. 146 ( Pt 3), pp. 547–549, Mar 2000.
- [69] M. D. LaFleur, C. A. Kumamoto, and K. Lewis, "Candida albicans biofilms produce antifungal-tolerant persister cells," *Antimicrob Agents Chemother*, vol. 50, pp. 3839–3846, Nov 2006.

## BIBLIOGRAPHY

- [70] G. S. Baillie and L. J. Douglas, "Candida biofilms and their susceptibility to antifungal agents," *Methods Enzymol*, vol. 310, pp. 644–656, 1999. In Vitro.
- [71] P. Gilbert, D. G. Allison, D. J. Evans, P. S. Handley, and M. R. Brown, "Growth rate control of adherent bacterial populations," *Appl Environ Microbiol*, vol. 55, pp. 1308–1311, May 1989.
- [72] M. R. Millar, C. J. Linton, and A. Sherriff, "Use of a continuous culture system linked to a modified Robbins device or flow cell to study attachment of bacteria to surfaces," *Methods Enzymol*, vol. 337, pp. 43–62, 2001.
- [73] R. Mukhopadhyay, "When PDMS isn't the best," *Anal. Chem.*, vol. 79, pp. 3248–3253, May 2007.
- [74] B. Wang, L. Chen, Z. Abdulali-Kanji, J. H. Horton, and R. D. Oleschuk, "Aging effects on oxidized and amine-modified poly(dimethylsiloxan) surfaces studied with chemical force titration: effects on electroosmotic flow rate in microfluidic channels," *Langmuir*, vol. 19, pp. 9792–9798, 2003.
- [75] A. V. Mamishev, K. Sundara-Rajan, F. Yang, Y. Q. Du, and M. Zahn, "Interdigital sensors and transducers," *Proc. IEEE*, vol. 92, pp. 808–845, May 2004.
- [76] G. M. Whitesides, "The right size in nanobiotechnology," *Nat. Biotechnol.*, vol. 21, pp. 1161–1165, Oct 2003.
- [77] C. Ionescu-Zanetti, R. M. Shaw, J. G. Seo, Y. N. Jan, L. Y. Jan, and L. P. Lee, "Mammalian electrophysiology on a microfluidic platform," *PNAS*, vol. 102, pp. 9112–9117, Jun 2005.
- [78] G. H. Markx and C. L. Davey, "The dielectric properties of biological cells at radiofrequencies: Applications in biotechnology," *Enzyme Microb. Technol.*, vol. 25, pp. 161–171, Aug 1999.
- [79] J. Suehiro, R. Hamada, D. Noutomi, M. Shutou, and M. Hara, "Selective detection of viable bacteria using dielectrophoretic impedance measurement method," *J. Electrostat.*, vol. 57, pp. 157–168, Aug 2003.
- [80] J. H. Yeon and J.-K. Park, "Cytotoxicity test based on electrochemical impedance measurement of HepG2 cultured in microfabricated cell chip," *Anal Biochem*, vol. 341, pp. 308–315, Jun 2005.
- [81] S. M. Radke and E. C. Alocilja, "Design and fabrication of a microimpedance biosensor for bacterial detection," *IEEE Sens. J.*, vol. 4, pp. 434–440, Aug 2004.
- [82] F. K. Balagadde, L. C. You, C. L. Hansen, F. H. Arnold, and S. R. Quake, "Long-term monitoring of bacteria undergoing programmed population-control in a microchemostat," *Science*, vol. 309, pp. 137–140, Jul 2005.
- [83] J. E. Yardley, D. B. Kell, J. Barrett, and C. L. Davey, "On-line, real-time measurements of cellular biomass using dielectric spectroscopy," *Biotechnol Genet Eng Rev*, vol. 17, pp. 3–35, 2000.

## BIBLIOGRAPHY

- [84] R. Ehret, W. Baumann, M. Brischwein, A. Schwinde, and B. Wolf, "On-line control of cellular adhesion with impedance measurements using interdigitated electrode structures," *Med Biol Eng Comput*, vol. 36, pp. 365–370, May 1998.
- [85] D. Prodan, F. Mayo, J. R. Claycomb, and H. H. Miller, "Low-frequency, low-field dielectric spectroscopy of living cell suspensions," *J. Appl. Phys.*, vol. 95, pp. 3754–3756, Apr 2004.
- [86] Y. Plevaya, I. Ermolina, M. Schlesinger, B. Z. Ginzburg, and Y. Feldman, "Time domain dielectric spectroscopy study of human cells. II. Normal and malignant white blood cells," *Biochim Biophys Acta*, vol. 1419, pp. 257–271, Jul 1999. Comparative Study.
- [87] G. J. Ciambone, V. F. Liu, D. C. Lin, R. P. McGuinness, G. K. Leung, and S. Pitchford, "Cellular dielectric spectroscopy: a powerful new approach to label-free cellular analysis," *J Biomol Screen*, vol. 9, pp. 467–480, Sep 2004.
- [88] S. Takashima, *Electrical Properties of Biopolymers and Membranes*. Adam Hilger,, 1989.
- [89] K. Asami, K. Takahashi, and K. Shirahige, "Progression of cell cycle monitored by dielectric spectroscopy and flow-cytometric analysis of DNA content," *Yeast*, vol. 16, pp. 1359–1363, Nov 2000.
- [90] R. Igreja and C. J. Dias, "Analytical evaluation of the interdigital electrodes capacitance for a multi-layered structure," *Sensors and Actuators A-Physical*, vol. 112, pp. 291–301, May 2004.
- [91] P. Ertl, M. Wagner, E. Corton, and S. Mikkelsen, "Rapid identification of viable *Escherichia coli* subspecies with an electrochemical screen-printed biosensor array," *Biosens Bioelectron*, vol. 18, pp. 907–916, Jul 2003.
- [92] P. Ertl and S. Mikkelsen, "Electrochemical biosensor array for the identification of microorganisms based on lectin-lipopolysaccharide recognition," *Anal. Chem.*, vol. 73, pp. 4241–4248, Sep 2001.
- [93] R. Igreja and C. J. Dias, "Analytical evaluation of the interdigital electrodes capacitance for a multi-layered structure," *Sens. Actuators, A*, vol. 112, p. 291, 2004.
- [94] W. Huang, Z. Zhang, X. Han, J. Tang, J. Wang, S. Dong, and E. Wang, "Ion Channel Behavior of Amphotericin B in Sterol-Free and Cholesterol Ergosterol-Containing Supported Phosphatidylcholine Bilayer Model Membranes Investigated by Electrochemistry and Spectroscopy," *Biophys. J.*, vol. 83, pp. 3245–3255, 2002.
- [95] M. A. S. Alem and L. J. Douglas, "Effects of aspirin and other nonsteroidal anti-inflammatory drugs on biofilms and planktonic cells of *Candida albicans*," *Antimicrob. Agents Chemother.*, vol. 48, pp. 41–47, Jan 2004.

# Appendix

Publication of an related work in  
*Lab on a Chip* 2007, 7, 1723-1731

# Development of a microfluidic biochip for online monitoring of fungal biofilm dynamics†

Lukas Richter, Christoph Stepper, Andy Mak, Alessa Reinthaler, Rudolf Heer, Michael Kast, Hubert Brückl and Peter Ertl\*

Received 31st May 2007, Accepted 4th September 2007

First published as an Advance Article on the web 27th September 2007

DOI: 10.1039/b708236c

Microfabricated biochips are developed to continuously monitor cell population dynamics in a non-invasive manner. In the presented work we describe the novel combination of contact-less dielectric microsensors and microfluidics to promote biofilm formation for quantitative cell analysis. The cell chip consists of a polymeric fluidic (PDMS) system bonded to a glass wafer containing the electrodes while temperature and fluid flow are controlled by external heating and pumping stations. The high-density interdigitated capacitors ( $\mu$ IDES) are isolated by a 550 nm multi-passivation layer of defined dielectric property and provide stable, robust and non-drifting measurement conditions. The performance of this detector is evaluated using various bacterial and yeast strains. The high sensitivity of the developed dielectric microsensors allows direct identification of microbial strains based on morphological differences and biological composition. The novel biofilm analysis platform is used to continuously monitor the dynamic responses of *C. albicans* and *P. pastoris* biofilms to increased shear stress and antimicrobial agent concentration. While the presence of shear stress triggers significant changes in yeast growth profiles, the addition of  $0.5 \mu\text{g mL}^{-1}$  amphotericin B revealed two distinct dynamic behaviors of the *C. albicans* biofilm. Initially, impedance spectra increased linearly at  $30 \Omega \text{ h}^{-1}$  for two hours followed by  $10 \Omega \text{ h}^{-1}$  (at 50 kHz) over 10 hours while cell viability remained above 95% during fungicide administration. These results demonstrate the ability to directly monitor dielectric changes of sub-cellular components within a living cell population.

## Introduction

Understanding the complex interaction between cell populations and their environment is fundamental to medicine and biology because it provides insight into how cellular systems dynamically respond to changing conditions. Living cells can rapidly adapt<sup>1</sup> to environmental cues by altering their gene-expression pattern, protein content, membrane constitution, surface receptors *etc.*<sup>2</sup> Furthermore, cell-cell communication has a considerable influence on the cellular life cycle because the interplay of cells is known to significantly alter behavior.<sup>3</sup> As a result, the study of cellular dynamics in the context of cell populations, such as those found in a biofilm, is highly desirable because of its physiological relevance and practical application.<sup>4,5</sup>

Microbial biofilms exist in virtually all nutrient-sufficient ecosystems and are phenotypically distinct from their planktonic or free floating counterparts. Biofilms are structured microbial communities attached to a surface, sometimes embedded within a matrix of extracellular polymers, and are significantly less susceptible to antimicrobial agents.<sup>6</sup> It is also recognized that a substantial proportion of human infections

involve biofilms found on surfaces of implants or medical devices, such as catheters, joint replacements, prosthetic heart valves and others.<sup>7</sup> Although various procedures and techniques have been published that measure biofilm formation under static conditions, so far the perfused biofilm fermenter has remained one of the few systems that allows accurate control over biofilm growth rate.<sup>8</sup> The technology was developed in the late 1980s and its application demonstrated that growth rates of adherent bacterial biomass is proportional to applied medium flow rates and limiting nutrient concentration.<sup>9</sup> Here, cells are grown in a fermenter, collected by pressure filtration onto a cellulose acetate membrane and, following inversion into the modified base, membrane and microorganisms are perfused with fresh medium. Another system widely used to study biofilm growth under continuous flow is the modified Robins Device (MRD), which is comprised of a multiport sample catheter connected *via* tubing to a peristaltic pump, reservoirs and wastes.<sup>10</sup> Initially a cell suspension is pumped through the catheter to allow cell attachment on each of the 25 sampling ports. Fresh medium is subsequently pumped to control biofilm growth rates.<sup>11</sup> However, both existing biofilm analysis methods cannot monitor cellular responses in real time.

The interrelated and complex nature of cellular dynamics within biofilms requires the creation of an analysis technology capable of continuously monitoring phenotypic changes such as adaptation, aging *etc.* throughout the entire life cycle. We have therefore developed a microfluidic biochip capable of

Division of Nano-System-Technologies, Austrian Research Centers GmbH-ARC, Donau-City-Street 1, 1220 Vienna, Austria.  
E-mail: peter.ertl@arcs.ac.at; Fax: +43 (0) 50550 4399;  
Tel: +43 (0) 50550 4305

† Electronic supplementary information (ESI) available: Supplementary figures Fig. 1–3. See DOI: 10.1039/b708236c

detecting morphological changes continuously in a non-invasive manner while maintaining physiological conditions throughout the experiment. Microchip technology is ideally suited to address biofilm requirements because it allows the creation of biological niches by providing relevant fluidic conditions such as physiological flow velocities and low fluid-to-cell volume ratios, and by maintaining stable temperature profiles over long periods of time.<sup>12–16</sup> Precise control of the above parameters is vital because they determine stress-related cellular signaling levels known to influence cellular behavior.<sup>17</sup> The developed biofilm analysis platform described here is thus specifically designed to offer a large surface to facilitate microbial adhesion (biofilm chamber width 1 mm, length 3 mm, and height 20  $\mu\text{m}$ ) and adequate nutrient supply. Additionally, external heating and pumping stations allow exact control over environmental conditions, while the integrated reference arm provides an interference-free detection setting by eliminating background signals and interferences. Furthermore, since microfluidic devices are generally compatible with imaging and microscopy techniques, an optical window has been implemented to visually follow cell growth throughout experimentation.

The technique employed to continuously measure cell viability and morphology changes is cellular dielectric spectroscopy (CDS). Dielectric spectroscopy makes use of the electrical properties of cells exposed to a small magnitude ( $\pm 15$  mV) radio-frequency electrical field.<sup>18</sup> Dielectric spectroscopy has proven useful for analyzing biological cell suspensions to study cell sedimentation, cell aggregation, cell division and growth rates of low density liquid cultures (volume fraction below 0.15).<sup>19–23</sup> The main advantage of dielectric spectroscopy is its ability to perform non-invasive measurements with high precision over a wide time and frequency range.<sup>18,24,25</sup> At the applied frequencies (5 to 500 kHz) the reorientation of the dielectric dipoles and the polarization of the surface charge accumulated on the cell membranes (membrane potential) can be continuously monitored, thus allowing the investigation of cell structure and electrical properties of cellular components.<sup>20,47</sup>

In contrast to existing bioimpedance methods implemented for cell analysis,<sup>26–30</sup> the dielectric microsensors applied in this study are completely insulated and physically removed from the liquid sensing environment using defined multi-passivation layers of distinct size and composition. Complete sensor isolation results not only in the absence of ohmic currents or faradaic contributions, but also eliminates electrode polarization events, fouling or bubble formation. CDS was integrated into the microfluidic biochips using interdigitated electrode structures ( $\mu\text{IDES}$ ) because interdigital capacitors exhibit improved performance over standard two electrode systems.<sup>31</sup> Additionally, dielectrometry measurements using fringing quasi-static electric fields above interdigitated electrodes has been extensively described in industrial applications (e.g. curing processes, electrical insulation, moisture sensing etc.) as a non-destructive means of measuring dielectric changes induced by alterations of physical, chemical and structural properties of polymeric materials.<sup>32</sup> In the context of cell analysis, high-density interdigital capacitors are ideal dielectric sensors due to their large active surface area and ability to tune

electric field distribution.<sup>33</sup> It is known from the literature that the penetration depth of the generated periodic electric field is proportional to the spacing between the sensing and driving electrodes and is independent of frequency.<sup>32</sup> Precise control over sensor geometry, such as the ratio between space, widths and thickness of the individual fingers, is therefore crucial for the development of a high performance sensor and is achieved using MEMS (micro-electromechanical-systems) technology.<sup>12–15,34</sup>

One practical application of the developed cellular analysis platform is the investigation of fungal biofilms. Although the role of bacterial biofilm in disease has been intensively studied in the past decade,<sup>10,35</sup> little is known about the behavior and dynamics of fungal biofilms.<sup>36</sup> The genus *Candida* is of particular interest because it is distributed worldwide and is recognized as a major source of hospital-acquired infections causing superficial and deep-seated mycoses. We examined *Candida albicans* because it is the principal pathogen of the genus and can grow either as oval budding yeasts, as continuous septate hyphae or as pseudohyphae.<sup>6</sup> Furthermore, previous studies suggest that phenotypic switching from uni-cellular to the filamentous form of *Candida albicans* may play a role in its virulence and multi-drug resistance.<sup>37</sup> Since increased resistance (up to 10 times) of *Candida* biofilms has been reported, the application of standard antimicrobial susceptibility tests performed with planktonic *Candida* (cell suspensions) may be particularly misleading.<sup>38</sup> We therefore applied the newly developed biofilm chip to assess the dynamic response of invasive *C. albicans* infections at relevant clinical peak serum concentrations of amphotericin B (0.2–0.5  $\mu\text{g mL}^{-1}$ ).

## Experimental

### Biofilm chip design and fabrication

The complete lab-on-a-chip system consists of the biochip embedded in an aluminium block containing the water based temperature control system and a polycarbonate top fixture containing the fluidic inputs and exits, as well as the electronic connectors. Constant temperature is maintained by externally heating the aluminium block connected *via* tubing to a water bath (Haake 10, Thermo Electron Coop.) while flow velocities are adjusted using an infusion pump (KdScientific, KDS 250). Furthermore, an optical window is implemented to allow the application of optical microscopy (Leica MZ16).

The microfluidic biochip layout shown in Fig. 1(A) consists of two substrates (a) 20  $\times$  20 mm<sup>2</sup> quartz glass housing the electrodes and (b) fluidic channels in polymer. Microbial cells are injected into the proliferation chamber through the cell seeding port located in the centre of the biochip. Additionally, a reference arm has been integrated to provide a low noise detection environment during cell analysis. Fig. 1(B) shows pictures of dielectric microsensors ( $\mu\text{IDES}$ ) located in the biofilm growth and reference chambers.

Fabrication of biochips commenced by using dry baked and primed (TI-Prime, MicroChemicals<sup>®</sup>) glass substrates (170  $^{\circ}\text{C}$  for 5 min). An initial resist layer is formed by spinning the non-photosensitive resist (LOR 3A, MicroChem<sup>®</sup>) on the wafer at 3000 rpm for 35 s. A second layer using the photo resist

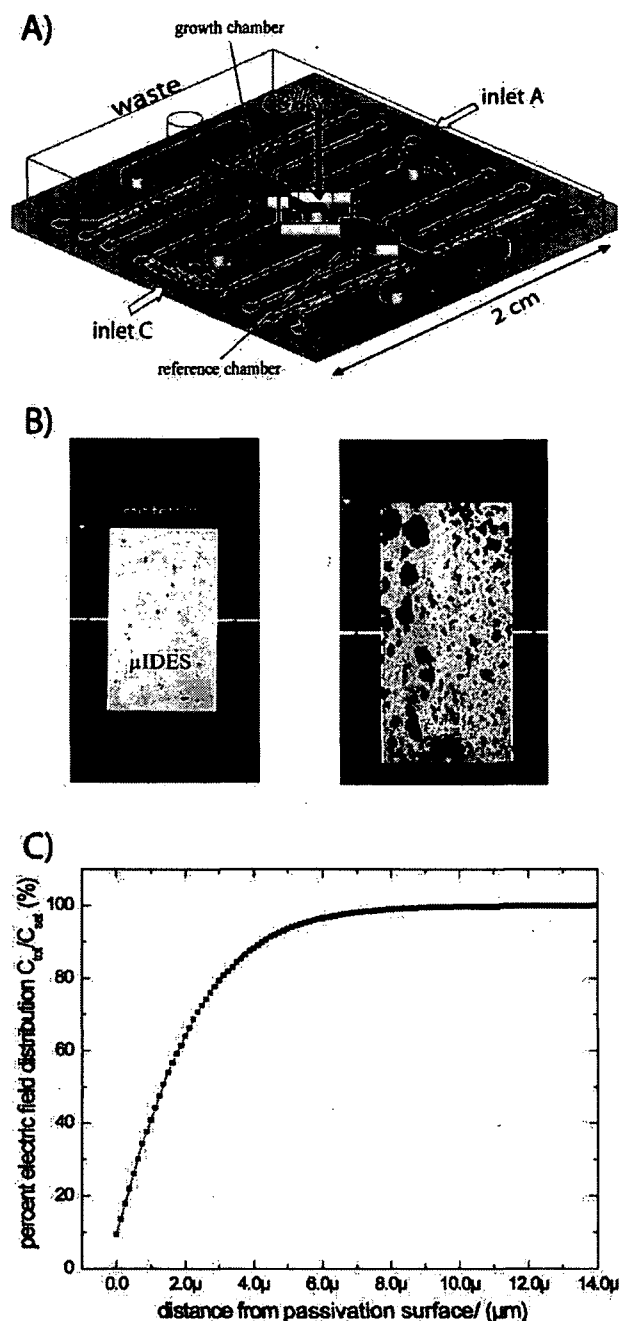


**Fig. 1** (A) Schematic representation of the microfluidic biochip. (B) Photos of dielectric microsensors located in the reference and proliferation chambers containing *P. pastoris* microcolonies (10 hour cultivation). (C) Calculation of electric field distribution (z-direction) in air using 200 nm thick interdigitated electrodes of 5  $\mu\text{m}$  width, 1000  $\mu\text{m}$  length separated by 5  $\mu\text{m}$  gap.

(positive resist AZ<sup>®</sup>MIRTM 701) is applied and soft baked at 110 °C, 60 s. The resist is patterned using a MJB 3 mask aligner from SUESS Microtec (350 W mercury lamp, exposure time 6.35 s), developed for 25 s (AZ<sup>®</sup>MIF 726). Electrodes, leads, as well as contact pads, are fabricated by sputtering a 10 nm titanium seed layer and 200 nm platinum onto the

pre-patterned glass substrates and placing the glass substrates into a solution of NMP (1-methyl-2-pyrrolidinon) at a temperature of 70–80 °C for at least 60 min. The micro-dielectric sensors are further embedded underneath a multi passivation layer deposited on top of the interdigitated electrode structures ( $\mu\text{IDES}$ ). First a thin layer of silicon nitride (100 nm) is deposited *via* low temperature plasma enhanced chemical vapour deposition (PECVD, Oxford Plasmalab 80). A layer of spin-on-glass (SOG P84F, Filmtronics Inc.) is subsequently spun at 3000 rpm for 15 s (100 nm) onto the silicon nitride. After a soft bake, ramped from 80 °C to 200 °C on a hot plate, the chips are annealed for 1 hour at 70 °C in a furnace. Curing of the layer takes place in a rapid thermal process (RTP) oven at 425 °C for 1 hour under nitrogen atmosphere. A final 350 nm layer of SU-8 negative photoresist is used to cover the SOG surface thus creating a multi-passivation layer with a total thickness of 550 nm.

The microfluidic system is formed in a PDMS layer as an imprint of silicon master molds fabricated by KOH silicon etching using a 750 nm silicon oxide layer as hard mask and buffered HF (14 min). After stripping the photo resist (MIR 701 positive photo resist) the substrate is etched in a 40% KOH solution at a constant temperature of 80 °C for 25 minutes resulting in an etch depth of 20  $\mu\text{m}$ . Reaction chambers and channels are formed by pouring PDMS (10 : 1 Sylgard 184) silicone elastomer base to curing agent over the silicon master molds. After baking at 80 °C for 12 hours the PDMS fluidics is removed from the master molds, cleaned, aligned under a microscope and put in contact with the sensor substrate using alignment marks. Fluidic access ports (three inputs and two wastes) are created by punching 0.5 mm holes through the PDMS.

#### Cultivation of microorganisms

The bacterial strains *E. coli* K12 ATCC 23716, *B. subtilis* ATCC 6501, *S. fonticola*, and *S. xylois* are cultivated aerobically in an incubation shaker (Grant GLS 400) at 37 °C and 200 rpm using Miller Hinton (MH, Merck) media, while yeast strains *P. pastoris* ATCC 28485 and *C. albicans* ATCC 10231 are cultured at 30 °C using malt extract bouillon (YPD, Merck) and Worth broth (WB, Sifin), respectively. Optical density of buffered samples is measured at 600 nm using a UV-visible spectrophotometer (Evolution 100, Thermo Electron Coop.). Colony forming units ( $\text{cfu mL}^{-1}$ ) are determined after biological samples are subjected to a series of 10-fold dilutions, and samples (100  $\mu\text{L}$ ) of  $10^{-6}$ ,  $10^{-7}$  and  $10^{-8}$  dilutions are spread onto agar plates. The colony forming units are counted for each individual strain after overnight incubation at 30 °C at 300 rpm using an Eppendorf shaker (Thermomixer, Eppendorf).

#### Dielectrometry measurements

Absolute impedance ( $|Z|$ ) and phase angle ( $\theta$ ) values are measured continuously over a frequency range of 5–500 kHz. Unless otherwise noted, 1  $\mu\text{L}$  of cell suspension ( $\text{OD}_{600} < 1.0$ ) is injected into the open fluidic access port (cell seeding) located in the center of the pre-filled biochip. Any excess fluid is carefully removed and the reservoir is sealed using a thin

piece of PDMS. Activation of microfluidic flow through inputs A and/or C to the waste compartment causes cells to freely move into the proliferation chamber due to the establishment of a negative pressure within the cell seeding port. Cell growth, viability and morphology changes are continuously measured and compared to signals obtained from the reference chamber also filled with media using a multichannel potentiostat (VMP3/P-01, Princeton Applied Research). The working and reference micro-dielectric sensors are addressed simultaneously by continuously scanning 501 frequencies applying  $\pm 15$  mV between the interdigitated electrode structures ( $\mu$ IDES).

#### Chemometric data analysis

Dielectric spectroscopy data obtained for five replicate runs with each cell culture is used to generate the matrix for principal component analysis (PCA). Each column in the data matrix consists of 501 signals for one replicate measurement with each of the six microbial strains. The matrix was converted into a Lotus file for incorporation into MATLAB (Version 7.01). Factor analysis was performed using the Chemometric Toolbox for Matlab (Version 3.02), and involved the generation of reduced eigenvectors, examination of the resulting residual plots for randomness of noise, and the generation of scores for the first three principal components.<sup>39</sup> The obtained scores are plotted to determine qualitative groupings of individual data sets.<sup>40</sup>

#### Calculation of sensor geometry

One benefit of using interdigitated electrode structures ( $\mu$ IDES) is their adaptability because the electric field distribution ( $H$ ) can be adjusted by controlling the ratio between space ( $G$ ) and width ( $w$ ) of the individual fingers ( $H = w + G$ ).<sup>32</sup> Our current  $\mu$ IDES design consists of 200 fingers each 5  $\mu$ m in width and 1000  $\mu$ m in length that are separated by a 5  $\mu$ m gap from each other. This means that the generated electric field protrudes up to 10  $\mu$ m in the half spaces above and below the  $\mu$ IDES containing an intrinsic capacitance (offset) within the glass substrate and passivation layers.<sup>41</sup> To estimate the percentage of electric field distribution over the distance from the passivation surface, the capacity of the interdigitated electrode structures were calculated using the conformal mapping technique described elsewhere.<sup>33</sup> In brief, the total capacitance of a  $\mu$ IDES sandwiched between arbitrary multi-layers is evaluated analytically by conformal transformations using the partial capacitance method. In the first step, the planar comb-shaped electrodes are replaced by an equivalent circuit consisting of partial capacitances individually mapped onto parallel plate capacitor geometry for which capacitance values are calculated (see Fig. 1(C)).

#### Antifungal susceptibility and viability testing

Minimum inhibitory concentration (MIC) is determined by the broth dilution method. *C. albicans* is incubated in growth medium containing various concentrations of amphotericin B (Sigma). A stock solution of amphotericin B with a final concentration of 1 mg ml<sup>-1</sup> in DMSO is used to prepare a series of dilutions ranging from 5 to 0.02  $\mu$ g ml<sup>-1</sup> in yeast

growth media. Next, an agar plate colony of *C. albicans* is removed, re-suspended into buffer solution and adjusted to OD<sub>600</sub> of 1.0. An inoculum of 10  $\mu$ L cell suspension was added to each Eppendorf tube (2 mL) containing the growth media and the fungicide. Four blank cultures (no fungicide) are included to ensure viability. Cell cultures are incubated overnight at 30 °C using an Eppendorf shaker and OD<sub>600</sub> values are recorded for each culture. Trypan blue (Sigma) staining method is used to assess cell viability by counting the ratio between total cells over dead cells (stained). On average 150 to 200 cells are visually inspected every hour using a hemocytometer for each antimicrobial agent concentration.

#### Time-lapse microscopy

The average microcolony expansion rate of yeast cells is determined by measuring the increase in surface area covered by newly formed colonies every 30 min. Microcolonies are imaged with a phase contrast microscope and expansion rates are calculated by approximating colony areas using the toolbox of Leica imaging software.

## Results and discussion

#### Cell chip characterization

The aim of this research is the development and characterization of technology capable of continuously monitoring cell growth, viability and morphology changes with high sensitivity. An important feature of the newly developed detection technology is the complete isolation of the  $\mu$ IDES to guarantee non-invasive monitoring conditions. Consequently, only passivation materials with reported dielectric constants ( $\epsilon$ ) below 10 and amenable to standard lithography processes were selected for this study. In total, single, bi- and multi-layer passivation strategies using epoxy (350 nm), spin-on-glass (100 nm), and silicon nitride (100 nm), and a combination thereof, were investigated. Since polymeric surfaces promote fungal biofilm formation, epoxy was used as the top layer,<sup>7</sup> while silicon nitride and spin-on-glass were selected as adhesion layers and to even out ripples caused by thickness of the electrodes. Deposition of silicon nitride and spin-on-glass was also used to increase passivation and sensor stability.

The application of single passivation layers using epoxy resin (SU-8 photoresist) or spin-on-glass (SOG) showed significant leakage following electrochemical investigation. AFM studies (data not shown) confirmed the presence of passivation losses and pin holes caused by poor epoxy adhesion, uneven layer distribution and droplet formation along finger electrodes. The 50 to 70 nm diameter pin holes found throughout the SOG layer are believed to be formed during the curing process of the precursor substrates at 425 °C. A direct comparison of oxidation currents using unpassivated sensors ( $-62$   $\mu$ A) with single passivation layers using epoxy and SOG yielded  $-28$   $\mu$ A and  $-8$   $\mu$ A in the presence of the electro-active compound ferrocyanide (10 mM). Although the application of bi-layers sufficiently insulated the dielectric sensors ( $-2$  nA) any degradation during chip cleaning, assembly or re-use resulted in massive drifts. A 100 nm SiN<sub>x</sub> layer is added to the passivation strategy and characterized

using impedance spectroscopy to further increase sensor stability. Detection limit and baseline stability was determined over 20 hours continuous flow measurement in saline buffer solution (flow rate  $0.5 \mu\text{L min}^{-1}$ ) and yielded a relative standard deviation of 1.5% or  $\pm 15 \Omega$  (at 100 kHz). Therefore, the elimination of interaction between electro-active ion species and electrodes (e.g. electrode polarization), or the prevention of electrode fouling events or bubble formation has led to non-drifting conditions.

Passivation materials can significantly influence electric field distribution and is therefore important to determine their effect on sensor sensitivity. For instance, calculations (conformal mapping technique) of electric field distribution (Fig. 1(C)) for  $\text{SiN}_x/\text{SOG}/\text{SU-8}$  multi-passivation layer in the presence of air indicated that 50%, 95% and 99% of the electric field is located within a height of 3.13, 5.51 and  $8.1 \mu\text{m}$ , respectively. This means that dielectric changes occurring at  $8.1 \mu\text{m}$  distance from the passivation surface, for example, contribute only 1% to the overall signal, while the 550 nm thick multi-passivation layer is responsible for a 9% sensitivity loss (offset in Fig. 1(C)). Furthermore, calculations using an electromagnetic finite element method software (Comsol Multiphysics 3.3a) in the presence of water ( $\epsilon_r = 80$ ) above a 550 nm passivation layer ( $\epsilon_r = 8.7$ ) has shown that two thirds of the voltage drops off in the passivation region directly above the electrodes.

Next, sensor sensitivity to extracellular matrix changes using increasing concentrations of gelatin and protein solutions as model systems was investigated. Fig. 2 shows the growth profile of *C. albicans* cultivated in a shake flask under standard conditions where cell free media extract harvested every hour was injected into the biochip. It is evident that the dielectric microsensor is remarkably insensitive towards media alterations induced by metabolic activity of the yeast strain. Real and imaginary parts of the impedance in the presence of increasing concentrations of gelatin and BSA solutions are listed in Table 1. Results of this study show that 0.01% (w/v) gelatin and approximately  $1 \text{ mg mL}^{-1}$  BSA is needed before significant dielectric changes can be detected.

Sensor performance in the presence of biological samples was evaluated using two Gram-negative, two Gram-positive

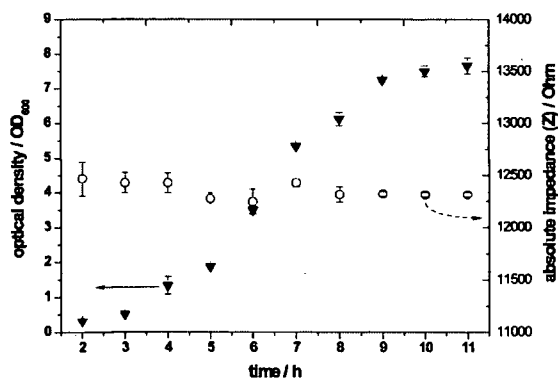


Fig. 2 Growth profile ( $\text{OD}_{600}$ ) of *Candida albicans* (▼) obtained under standard cultivation conditions and corresponding averaged impedance data ( $|Z|$  at 50 kHz) of triplicate measurements from cell-free media extracts.

Table 1 Dielectric microsensor response to increasing protein and gelatin concentrations

	Concentration	Real part of impedance/ $\Omega$	Imaginary part of impedance/ $\Omega$
BSA solution	$1 \mu\text{g mL}^{-1}$	$14873 \pm 503$	$35721 \pm 1618$
	$10 \mu\text{g mL}^{-1}$	$14941 \pm 136$	$36629 \pm 680$
	$100 \mu\text{g mL}^{-1}$	$15696 \pm 60$	$32322 \pm 533$
	$1000 \mu\text{g mL}^{-1}$	$6419 \pm 82$	$17597 \pm 130$
Gelatin solution	0.01 w/v%	$2599 \pm 12$	$14133 \pm 30$
	0.1 w/v%	$967 \pm 15$	$12368 \pm 14$
	1.0 w/v%	$704 \pm 16$	$12010 \pm 17$

<sup>a</sup> Averaged impedance values ( $n = 3$ ) at 50 kHz.

bacteria and two yeast strains. Microbial strains were selected based on their differences in size and morphological composition. For instance, Gram-negative bacterial cell walls consist of a second outer membrane of different complexities while yeast cells are 5 to 10 times bigger than bacteria. In a series of experiments, cells cultivated using an incubator shaker were harvested in the exponential phase, centrifuged and re-suspended in saline buffer prior to use. Aliquots of  $1 \mu\text{L}$  buffered sample solutions were injected into the proliferation chamber (90 nL volume) and impedance data were recorded after cells were allowed to settle for 20 min prior to measurement. Fig. 3(A) shows impedance values from three microbial strains where absolute impedance signals increased/decreased rapidly as soon as cell concentrations reached a minimum detectable level and plateaued following complete coverage of the entire sensing volume ( $\sim 16 \text{ nL}$ ). In all cases microbial concentrations above  $1000 \text{ cfu } \mu\text{L}^{-1}$  showed significant signal changes, with decreasing impedance values for *E. coli* K12 (Gram-negative), *S. fonticola* (Gram-negative) and *C. albicans* (yeast) and increasing signals in the presence of *B. subtilis* (Gram-positive), *S. xyloso* (Gram-positive) and *P. pastoris* (yeast) strains. Table 2 lists results of all six strains in the presence of low and high cell concentrations. Although the much larger yeast cells yielded measurable signals at low concentrations, highest signal changes are obtained with the smaller bacteria *S. xyloso* and *B. subtilis*. These results contrast existing and commercially available dielectric sensors where measured relative permittivity ( $\Delta\epsilon_r$ ) is directly proportional to cell radius, capacitance of the cell wall and volume fraction.<sup>26</sup>

The above findings led us to investigate the ability of the contact-less dielectric microsensors to directly distinguish and identify individual strains in a nanovolume setting in the absence of any labels or indicators. In a series of similar experiments, five microbial strains were cultivated in shake flasks, harvested in the exponential phase and the untreated cell suspension (pure culture) was directly injected into the biochip. As indicated in the above section (see Table 2), cell concentrations above  $10^8 \text{ cfu mL}^{-1}$  were used to guarantee saturation of the sensing region. Next, chemometric PCA was applied to dielectric spectra of untreated samples in order to apply pattern recognition methods to classify microbial strains. Fig. 3(B) shows score plots using raw data (phase angle) of four replicate measurements of five microbial strains. Results show that variances between microorganisms appear high enough to allow classification, while replicate measurements possess enough similarities to cluster together.

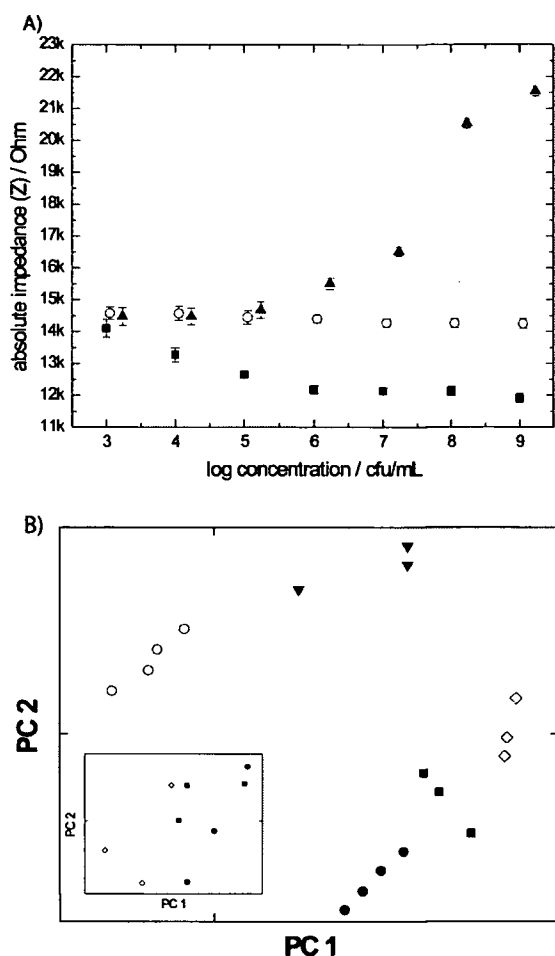


**Fig. 3** (A) Averaged impedance signals ( $|Z|$  at 50 kHz) of increasing concentrations ( $n = 3$ ) of ( $\blacktriangle$ ) *B. subtilis*, ( $\circ$ ) *E. coli* K12 and ( $\blacksquare$ ) *S. fonticola*. (B) Pattern recognition plot generated from dielectric spectra (5–500 kHz) obtained in the presence of *S. fonticola* ( $\blacktriangledown$ ), *S. xylosois* ( $\circ$ ), *E. coli* K12 ( $\diamond$ ), *B. subtilis* ( $\blacksquare$ ), and *C. albicans* ( $\bullet$ ). Inset shows pattern recognition plot of cell free media extract of exponential phase cultivations.

In comparison, generated pattern recognition plots of cell free media extracts showed only random distribution as seen in the inset of Fig. 3(B). These results clearly indicate that the identification of organisms is not affected by media components or metabolites generated during microbial cultivation.

**Table 2** Dielectric microsensor response to increasing microbial concentrations

Strain	Averaged background subtracted impedance values (at 50 kHz) <sup>a</sup>	
	At $10^4$ cfu mL <sup>-1</sup>	At $10^8$ cfu mL <sup>-1</sup>
<i>E. coli</i> K12 (Gram-neg)	$-25 \pm 10 \Omega$	$-325 \pm 50 \Omega$
<i>S. fonticola</i> (Gram-neg)	$-476 \pm 65 \Omega$	$-1838 \pm 105 \Omega$
<i>B. subtilis</i> (Gram-pos)	$72 \pm 22 \Omega$	$6143 \pm 352 \Omega$
<i>S. xylosois</i> (Gram-pos)	$900 \pm 110 \Omega$	$12152 \pm 260 \Omega$
<i>C. albicans</i> (yeast)	$-1150 \pm 145 \Omega$	$-2368 \pm 378 \Omega$
<i>P. pastors</i> (yeast)	$1962 \pm 250 \Omega$	$2653 \pm 350 \Omega$

<sup>a</sup> Triplicate measurements.

**Table 3** Comparison between live, dead and plasma membrane disrupted yeast strains using cellular dielectric spectroscopy

Treatment	<i>C. albicans</i>		<i>P. pastoris</i>	
	Background subtracted impedance signals in $\Omega$ and corresponding phase angle values ( $\theta$ ) measured at 50 kHz ( $n = 3$ ) <sup>a</sup>			
Untreated	$-210 \pm 28$	$-74^\circ$	$372 \pm 16$	$-76^\circ$
Amphotericin B ( $5 \mu\text{g mL}^{-1}$ )	$1651 \pm 43$	$-80^\circ$	$1105 \pm 38$	$-78^\circ$
Sonication	$2160 \pm 9$	$-81^\circ$	$1999 \pm 28$	$-82^\circ$

<sup>a</sup> Average of triplicate measurements.

Overall, impedance signals and phase angle values of 501 frequencies were recorded during each measurement and used to generate pattern recognition plots. In principle, not all frequencies are necessary for the clear distinction between microbial species. Analysis of impedance and phase angle data using bacterial strains show highest standard deviations between 72–75 kHz and 19–21 kHz, respectively. In turn, highest variances between *C. albicans* and *P. pastoris* are found at frequencies of 74 and 75 kHz using impedance signals and between 20–26 kHz, at 32 and 75 kHz using phase angle values. However, further investigation needs to be conducted to link the above listed frequencies to specific morphological differences of microbial cells.

The effects of cell morphology changes on sensor performance were further investigated using *C. albicans* and *P. pastoris*. Both strains were grown under standard conditions and harvested in the exponential phase. Aliquots of in-buffer re-suspended cell suspensions were either exposed to the plasma membrane disrupter amphotericin B ( $5 \mu\text{g mL}^{-1}$  for 4 hours at  $37^\circ\text{C}$ ) or subjected to sonication treatment (2 hours). Results of this study are listed in Table 3 including impedance and phase angle values of live, dead and plasma membrane disrupted cells. It is evident that a brief exposure to the antimicrobial agent amphotericin B can be readily detected using the present sensor geometry. Additionally, pre-treated cell suspensions were also plated on agar plates confirming the high killing efficiency of the sonication treatment, while significant cell growth was observed with samples of amphotericin B treated yeast samples. The demonstrated ability of the contact-less dielectric microsensors to rapidly detect differences and alterations in cell morphologies is fundamental for a high-sensitivity, real-time cellular dynamics detection technology. While complete cell coverage of the sensing layer can be used for identification, introducing a small number of cells into the proliferation chamber, in turn, allows for a continuous and non-invasive monitoring of cell growth, viability and morphology changes.

#### Effects of microfluidics on fungal biofilm growth

Initially we assessed the effects of fluid shear stress on biofilm growth rates and dynamic responses using *C. albicans* and *P. pastoris*, because of their importance in medicine and biotechnology. Growth rates were initially determined by calculating area expansion rates of individual colonies over a 5 hour period using time-lapse microscopy.<sup>42</sup> Fig. 4(A) shows a comparison of calculated expansion rates of *C. albicans*

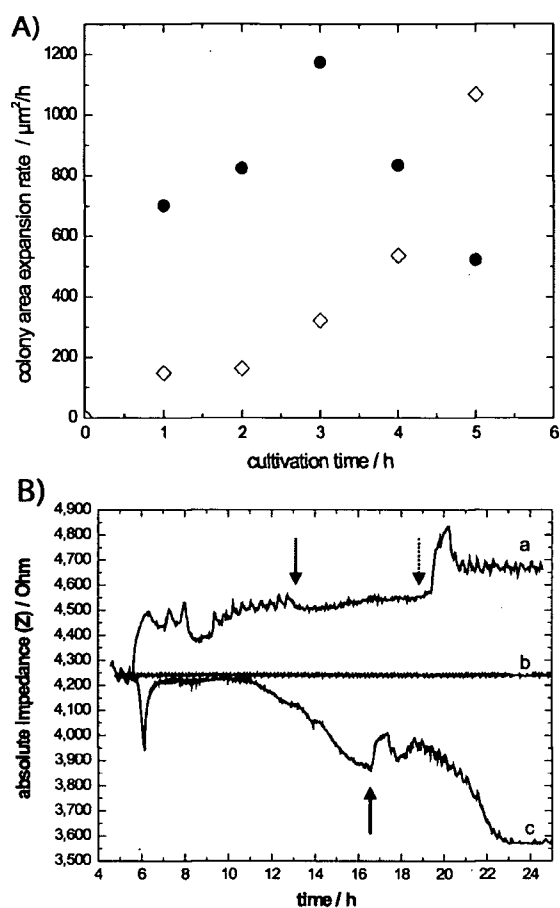


**Fig. 4** (A) Calculated colony area expansion rates using time-lapse microscopy of single *C. albicans* microcolonies grown in proliferation chamber in the absence (●) and presence (◇) of  $0.12 \mu\text{L min}^{-1}$  fluid flow. (B) Growth profiles ( $|Z|$  at 75 kHz) of (a) *P. pastoris*, (b) cell-free growth media and (c) *C. albicans* before and after shear stress increase (solid arrow) and subsequent decrease (dashed arrow) from  $0.12$  to  $0.5 \mu\text{L min}^{-1}$  to  $0.12 \mu\text{L min}^{-1}$ .

microcolonies in the absence and presence of fluid flow ( $0.12 \mu\text{L min}^{-1}$ ). In the absence of continuous media supply, surface expansion rates followed known growth characteristics of liquid batch cultures. In the presence of fluid flow, however, cell growth was significantly influenced exhibiting linear growth rates (colony diameter in flow direction) of  $8.3$  and  $12.5 \mu\text{m h}^{-1}$ , respectively (see ESI†). Furthermore, *Candida* colonies exhibited no difference in expansion rates (data not shown) in the absence and presence of an applied  $\pm 15$  mV AC field.

Dielectrometry measurements were then used to continuously monitor dynamic responses of the biofilms to shear stress following a four fold increase in flow velocities. Fig. 4(B) shows growth profiles of *C. albicans* and *P. pastoris* in the presence of alternating flow rates. Following cell seeding, cell populations of both strains increased steadily over a period of 8 hours until a flow rate increase (solid arrow) from  $0.12 \mu\text{L min}^{-1}$  to  $0.5 \mu\text{L min}^{-1}$  caused an initial loss of cells. However, while with *Pichia* cell population remained constant over a period of 6 hours by washing out newly formed cells

*C. albicans* continued to spread until it completely covered the proliferation chamber. Furthermore, visual inspection showed the establishment of filaments and hyphae of *C. albicans* (see ESI†). This phenomena is also observed in standard shake flask cultures where increased agitation leads to *Candida* biofilm formation. It is known from the literature that to infect host tissue, the usual unicellular yeast-like form of *C. albicans* reacts to environmental cues and switches into an invasive, multicellular filamentous form.<sup>43</sup> Consequently, *C. albicans* undergoes a process called phenotypic switching or morphogenesis, in which different cellular morphologies are generated in response to increased shear stress.<sup>44</sup> The ability to fine-tune growth characteristics represents an important tool for complex cell analysis where external stimuli such as toxins, activators, receptors, carbon sources *etc.* are introduced to a specific phenotype.

#### On-chip monitoring of fungal biofilm dynamics

To further investigate the dynamic response of *C. albicans*, sub-lethal doses of the fungicide amphotericin B were added during on-chip cultivation. Amphotericin B is a polyene macrolide antibiotic that is widely used for its antifungal activity and acts by forming ion channels in the presence of sterols (cholesterol or ergosterol) in the membrane.<sup>45</sup> Initial experimentation involved the study of sub-minimum inhibitory concentration (MIC) effects on biofilm growth rate and morphogenesis. After 14 hours on chip cultivation at  $30^\circ\text{C}$  in the presence of  $0.12 \mu\text{L min}^{-1}$  flow rate, the *Candida* cell population was perfused with medium containing  $0.05 \mu\text{g mL}^{-1}$  amphotericin B. No change in apparent growth rate, morphogenesis or long-time effects was found in the presence of sub-MIC ( $0.07 \mu\text{g mL}^{-1}$ ) concentrations (data not shown). Consequently, temperature setting, flow rates and antifungal concentration were increased in subsequent experiments. Visual inspection confirmed the presence of hyphae and filament formation throughout the *Candida* biofilm at  $37^\circ\text{C}$  and  $500 \text{ nL min}^{-1}$  flow rate culture conditions. Fig. 5(A) shows the dynamic response of the *Candida* biofilm before and after the administration of  $0.5 \mu\text{g mL}^{-1}$  amphotericin B (arrow in graph). Prior to administration, the biofilm was allowed to establish over a period of 6 hours covering almost 90% of the proliferation chamber. Following the supply of media containing the fungicide impedance signals started to increase linearly at an initial rate of  $30 \Omega \text{ h}^{-1}$  (first 2 hours) followed by  $10 \Omega \text{ h}^{-1}$  (at 50 kHz) over a period of 10 hours suggesting a decrease in cell population (see ESI†). However, corresponding pictures taken every 30 min during the same time period showed that the *Candida* biofilm actually continued to spread at very low rates.

Previous studies of *Candida* interaction with amphotericin B under standard cultivation conditions have shown concentration dependent responses leading to a range of physiological states (high/low/no viability and vitality).<sup>46</sup> By investigating cell growth, membrane integrity and potential as well as intracellular ATP the study showed that in the presence of  $0.5$  to  $1.0 \mu\text{g mL}^{-1}$  AmB *Candida* loses the ability to replicate, but maintains the ability to repair occurred membrane damage after a period of 10 hours. Our results indicated that biological

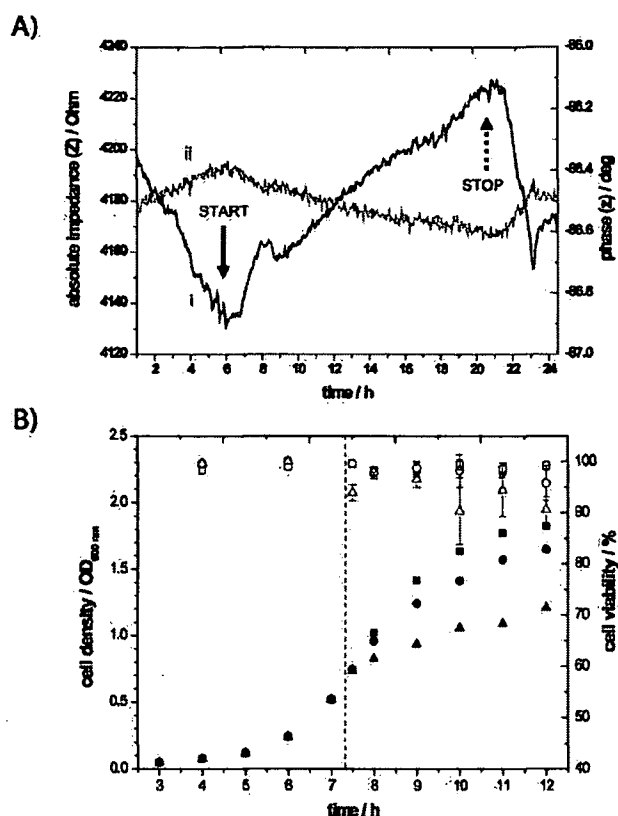


Fig. 5 (A) *Candida* biofilm response to addition of 0.5 μg mL<sup>-1</sup> amphotericin B where (i) impedance signals and (ii) phase angle values obtained at 50 kHz are plotted against cultivation time. (B) *Candida* growth curves (solid symbols correspond to left y-axis) and cell viabilities under standard cultivation conditions (shake flasks) in the absence (■, □) and presence of (●, ○) 0.5 μg mL<sup>-1</sup> and (▲, △) 2.5 μg mL<sup>-1</sup> amphotericin B.

processes are taking place at two different rates in the cell membrane during the exposure of *C. albicans* to AmB. We also performed viability (growing) and vitality (alive) estimations using standard *Candida* cultures. Fig. 5(B) shows optical density and membrane staining measurements confirming the strong growth inhibiting effect of the fungicide at 0.5 and 2.5 μg mL<sup>-1</sup>. However, assessment of membrane integrity performed over 6 hours after Am B administration yielded above 95% and 90% vitality in the presence of 0.5 and 2.5 μg mL<sup>-1</sup>, respectively. In other words, the administration of 2.5 μg mL<sup>-1</sup> AmB renders the *Candida* nearly incapable of initiating replicative processes while maintaining membrane integrity and metabolic activity (repair mechanism) over a period of 6 hours. These results clearly indicate that the on-chip monitored dielectric changes are caused by morphology changes induced by the incorporation of amphotericin B into the plasma membranes.

## Conclusion

We have developed a novel microfabricated biofilm analysis platform that provides quantitative results of the continuous monitoring of the adaptive phenotypic changes of the entire

life cycle of a cell population. The precise control of critical electrode characteristics, such as size, shape and passivation composition, as well as thickness makes microfabrication an attractive tool for the development of contact-less dielectric microsensors. An important feature of the sensor design is the application of electrical insulation making non-invasive, stable and robust measuring conditions possible. The introduction of a dielectric layer above the electrodes allows for the study of cellular dynamics in the absence of background effects. We evaluated the SiN<sub>x</sub>/SOG/SU-8 multi-passivation layer of 550 nm thickness and characterized the detector configuration utilizing various bacterial and yeast strains. Additionally, obtained phase angles (θ) of -84° in the presence of saline buffer indicate that the system behaves almost like an ideal capacitor (θ of -90°). We successfully demonstrated that microorganisms can be readily identified and that any morphological changes induced by external stimuli can be continuously monitored using dielectric sensors. We have also shown that induced shear stress has significant effects on biofilm formation and that, by controlling fluid flow and temperature, growth rates as well as fungal phenotypes can be adjusted and used for cell analysis. Using the developed technology we have monitored *Candida* biofilm dynamics and response to the antifungal agent amphotericin B. Administration of the fungicide at physiological relevant serum concentrations triggered an immediate reaction in *Candida* leading to a stress-induced inability to replicate, while repair mechanisms cope with membrane damages. We also observed time dependent signal changes during AmB administration suggesting two different dynamic responses of *Candida*. The ability to monitor sub-cellular components with high resolution within a cell population is expected to open new insights into cellular dynamics. Extension of this work to quantify biofilm dynamics and its application to a wide range of external stimuli is underway.

## Abbreviations

CDS	Cellular dielectric spectroscopy
μIDES	Microfabricated-Interdigitated electrode structures
MRD	Modified Robins Device
MIC	Minimum inhibitory concentration
MEMS	Micro-electromechanical-systems
PCA	Principal component analysis
SOG	Spin-on-glass
AmB	Amphotericin B

## Acknowledgements

The authors thank Astrit Shoshi for his valuable technical assistance and the Department of Applied Microbiology at the University of Life Sciences, Vienna for providing the bacterial strains *S. xylosum* and *S. foniticola*. Microfabrication was carried out in clean rooms of the Center for Micro- and Nanostructures, Vienna University of Technology.

## References

- 1 G. Storz and R. Hengge-Aronis, *Bacterial Stress Responses*, ASM Press, Washington D.C., 2000.

- 2 A. R. M. Coates, *Dormancy and Low-Growth States in Microbial Disease*, Cambridge University Press, Cambridge, 2003.
- 3 D. N. Breslauer, P. J. Lee and L. P. Lee, *Mol. BioSyst.*, 2006, **2**, 97.
- 4 D. J. Weatherall, *Nat. Rev. Genet.*, 2001, **2**, 245.
- 5 M. Hirota, *J. Biochem. Mol. Biol.*, 2004, **37**, 83.
- 6 L. J. Douglas, *Trends Microbiol.*, 2003, **11**, 30.
- 7 F. K. Balagadde, L. You, C. L. Hansen, F. H. Arnold and S. R. Quake, *Science*, 2005, **309**, 137.
- 8 G. S. Baillie and L. J. Douglas, *Methods Enzymol.*, 1999, **310**, 644.
- 9 P. Gilbert, D. G. Allison, D. J. Evans, P. S. Handy and M. R. Brown, *Appl. Environ. Microbiol.*, 1989, **55**, 1308.
- 10 M. R. Millar, C. J. Linton and A. Sheriff, Use of a continuous culture system linked to a modified Robbins device or flow cell to study attachment of bacteria to surfaces, in *Microbial Growth in Biofilms, Part B*, 2001, vol. 337, pp. 43.
- 11 M. A. Al-Fattani and L. J. Julia Douglas, *J. Med. Microbiol.*, 2006, **55**, 999–1008.
- 12 T. Vilknær, D. Janasek and A. Manz, *Anal. Chem.*, 2004, **76**, 3373.
- 13 P.-A. Auroux, D. Iossifidis, D. R. Reyes and A. Manz, *Anal. Chem.*, 2002, **74**, 2637.
- 14 G. M. Whitesides, *Nat. Biotechnol.*, 2003, **21**, 1161.
- 15 C. Ionescu-Zanetti, R. M. Shaw, J. Seo, Y. Jan, L. Y. Jan and L. P. Lee, *Proc. Natl. Acad. Sci. U. S. A.*, 2005, **102**, 9112.
- 16 P. S. Dittrich and A. Manz, *Nature*, 2006, **5**, 210.
- 17 T. H. Park and M. L. Shuler, *Biotechnol. Prog.*, 2003, **19**, 243.
- 18 J. E. Yardley, D. B. Kell, J. Barrett and C. L. Davey, *Biotechnol. Genet. Eng. Rev.*, 2000, **17**, 3.
- 19 R. Ehret, W. Baumann, M. Brischwein, A. Schwinde and B. Wolf, *Med. Biol. Eng. Comput.*, 1998, **36**, 365.
- 20 D. Prodan, F. Mayo, J. R. Claycomb and H. H. Miller, *J. Appl. Phys.*, 2004, **95**, 3754.
- 21 K. Asami, *J. Non-Cryst. Solids*, 2002, **305**, 268.
- 22 Y. Plevaya, I. Ermolina, M. Schlesinger, B. Z. Ginzburg and Y. Felman, *Biochim. Biophys. Acta*, 1999, **1419**, 257.
- 23 G. J. Ciambone, V. F. Liu, D. C. Lin, R. P. McGuinness, G. K. Leung and S. Pitchford, *J. Biomol. Screen.*, 2004, **9**, 467.
- 24 A. J. Bard and L. R. Faulkner, *Electrochemical Methods*, 2nd edn., John Wiley & Sons, New York, 2001.
- 25 S. Takashima, *Electrical Properties of Biopolymers and Membranes*, Adam Hilger, Bristol, 1989.
- 26 G. H. Markx and C. L. Davey, *Enzyme Microb. Technol.*, 1999, **25**, 161.
- 27 J. Suehiro, R. Hamada, m. D. Noutomi, M. Shutou and M. Hara, *J. Electroanal. Chem.*, 2003, **57**, 157.
- 28 S. Arndt, J. Seebach, K. Psathaki, H.-J. Galla and J. Wegener, *Biosens. Bioelectron.*, 2004, **19**, 583.
- 29 R. Gomez, D. T. Morissette and R. Bashir, *IEEE Micromech. Syst.*, 2005, **14**, 829.
- 30 J. H. Yeon and J.-K. Park, *Anal. Biochem.*, 2005, **341**, 308.
- 31 P. V. Gerwen, W. Laureyn, W. Laureys, G. Huyberechts, M. O. De Beeck, K. Baert, J. Suls, W. Sansen, P. Jacobs, L. Hermans and R. Mertens, *Sens. Actuators, B*, 1998, **49**, 73.
- 32 A. Mamihev, K. Sundara-Rajan, F. Yang, Y. Du and M. Zahn, *Proc. IEEE*, 2004, **92**, 808.
- 33 R. Igrėja and C. J. Dias, *Sens. Actuators, A*, 2004, **112**, 291.
- 34 D. J. Harrison, A. Manz, Z. Fan, H. Luedi and H. M. Widmer, *Anal. Chem.*, 1992, **64**, 1926.
- 35 C. Sternberg, B. B. Christensen, T. Johansen, A. T. Nielsen, J. B. Andersen, M. Givskov and S. Molin, *Appl. Environ. Microbiol.*, 1999, **65**, 4108.
- 36 D. G. Allison, P. Gilbert, H. M. Lappin-Scott and M. Wilson, *Community Structure and Co-operation in Biofilms*, Cambridge University Press, Cambridge, 2000.
- 37 E. C. Odds, *Mycoses*, 1997, **40**.
- 38 J. A. Shuford, K. E. Piper, J. M. Steckelberg and R. Patel, *Diagnostic Microbiology and Infectious Disease*, 2007, **57**, 277.
- 39 P. Ertl, M. Wagner, E. Corton and S. R. Mikkelsen, *Biosens. Bioelectron.*, 2003, **18**, 907.
- 40 P. Ertl and S. R. Mikkelsen, *Anal. Chem.*, 2001, **73**, 4241.
- 41 M. S. Radke and E. C. Alocilja, *IEEE Sensors J.*, 2004, **4**, 434.
- 42 N. Q. Balaban, J. Merrin, R. Chait, L. Kowalik and S. Leibler, *Science*, 2004, **305**, 1622.
- 43 K. J. Ryan and C. G. Ray, *Sherris Medical Microbiology: An Introduction to Infectious Diseases*, 4th edn., McGraw Hill, London, 2004.
- 44 M. A. S. Alem and L. J. Douglas, *Antimicrob. Agents Chemother.*, 2004, **48**, 41.
- 45 S. Yilma, N. Liu, A. Samoylov, T. Lo, C. J. Brinker and V. Vodyanoy, *Biosens. Bioelectron.*, 2006, **22**, 1605.
- 46 R. S. Liao, R. P. Rennie and J. A. Talbot, *Antimicrob. Agents Chemother.*, 1999, **43**, 1034.
- 47 K. Asami, K. Takashashi and K. Shirahige, *Yeast*, 2000.